A UNIFORMLY CONVERGENT NUMERICAL SCHEME FOR SINGULARLY PERTURBED NON-LINEAR EIGENVALUE PROBLEM UNDER CONSTRAINTS

CHAI MING HUANG

(B.Sc.(Hons.), NUS)

A THESIS SUBMITTED

FOR THE DEGREE OF MASTER OF SCIENCE

DEPARTMENT OF MATHEMATICS

NATIONAL UNIVERSITY OF SINGAPORE

2006

Acknowledgments

First and foremost, I would like to thank my supervisor, Associate Professor Bao Weizhu for his patience, guidance and invaluable advice. He had been extremely patient with me throughout my studies and was always ready to guide me in my research.

It is also my pleasure to express my appreciation and thanks to my fellow post-graduates Yang Li, Lim Fong Yin and especially my seniors Dr. Wang Hanquan and Dr. Zhang Yanzhi. They provided immense help especially with the Mathematical derivation and programming. This dissertation would not be completed smoothly without their kind assistance and heartfelt encouragement.

Lastly, I would like to dedicate this work with love to my wife, my parents and my family for being always there for me.

Chai Ming Huang

Dec 2006

Contents

Summary

The time-independent Gross-Pitaevskii equation (GPE) in the semiclassical regime is used to describe the equilibrium properties of Bose-Einstein Condensate at extremely low temperature. In this regime, the GPE is a singular perturbed nonlinear eigenvalue problem.

The aim of this thesis is to present a uniformly convergent numerical scheme to solve the singularly perturbed nonlinear eigenvalue problem. The adaptive numerical scheme proposed is based on a piecewise uniform mesh. The scheme is found to be able to treat the interior layers or boundary layers inherent in solutions of singularly perturbed nonlinear eigenvalue problems.

A comparison of the new proposed scheme based on piecewise uniform mesh is made against the classical numerical scheme based on uniform mesh. We found that the numerical accuracy of the new numerical scheme proposed is greatly improved over the classical numerical scheme.

An extension of the new numerical scheme is made to two dimensions. The scheme is then applied to solve the singular perturbed nonlinear eigenvalue problem in two dimensions.

Chapter 1

Introduction

1.1 Brief history of Bose-Einstein condensation

In 1925, Indian physicist Satyendra Nath Bose published a paper devoted to the statistical description of the quanta of light. Based on Bose's results, Albert Einstein [13] predicted that a phase transition in a gas of noninteracting atoms could occur due to quantum statistical effects. During this phase of transition period, a Bose-Einstein Condensate (BEC) will be formed when a macroscopic number of non-interacting bosons simultaneously occupy the single quantum state of the lowest energy [31].

For many years, there was no practical application of BEC. In 1938, after superfluditiy was discovered in liquid helium, F. London theorized that the superfluidity could be a manifestation of BEC. However in 1955, experiments on superfluid helium showed that only a small fraction of condensate is found. In the 1970s, experimental studies on dilute atomic gases were developed. The first of these studies focused on spin-polarized hydrogen. This gas was chosen as it has a very light mass and is thus likely to achieve BEC. After numerous attempts, BEC was almost achieved but it was not pure [44].

In the 1980s, there was remarkable progress made in the application of laser-based cooling techniques and magneto-optical trapping. In 1995, a historical milestone was achieved when the experimental teams of Cornell and Wieman at Boulder of JILA and of Ketterle at MIT succeeded in reaching the ultra low temperature and densities required to observe BEC in vapors of ^{87}Rb [2] and ^{23}Na [22]. Later in the same year, occurrence of BEC in vapors of ^{7}Li was also reported [15]. For their achievement, the Nobel Prize of Physics was awarded to the first three researchers who created this fifth state of matter in the laboratory. After realizing BEC in dilute bosonic atomic gases, BEC was also reached in other atomic matter, including the spin-polarized hydrogen, metastable ^{4}He and ^{41}K [28].

Since all the particles occupy the same state in the BEC at ultra low temperature, the condensate is characterized by a complex-valued wave function $\psi(\vec{x}, t)$, whose time evolution is governed by the time-dependent Gross-Pitaevskii equation (GPE) [20, 37]. It is impossible to solve the GPE analytically except for the simplest cases of GPE. Various numerical methods are used to solve the GPE instead. When the problems involve the static properties of the condensate, the numerical solutions of the time-independent GPE are of interest.

Over the last several years, there were extensive progress made towards developing innovative approaches and algorithms in solving both time-dependent and time-independent GPE. We will survey some of the more important recent research papers written in the field, with more emphasis of the numerical methodology in solving the time-independent GPE, which is the main subject of interest in this dissertation.

1.2 Review of existing numerical methods

The earliest attempts to solve the GPE might be started by Edwards and Burnetts [27]. They developed a Runge-Kutta method based on finite-difference to solve the time-independent GPE for spherical condensates. Edwards [26] also designed a basis set approach to solve GPE. For the solving of time-independent GPE in ground state and the vortex states in anisotropic traps, a finite-difference based imaginary time method was developed by Dalfovo and Stringari [21]. Adhikari [1] used a finite-difference based approach to solve the two-dimensional time-independent GPE. Cerimele, together with his coworkers [17], developed a finite-difference and imaginary-time approach for solving the time-independent GPE. Schneider and Feder [48] used a discrete variable representation that is coupled with a Gaussian quadrature integration scheme, to attain the ground and the excited states of GPE in three dimensions. Recently, Bao and Tang [11] used a different approach for obtaining the ground state of GPE. They did this by directly minimizing the corresponding energy functional with a finite element discretization. Utilizing the harmonic oscillator as the basis set, Dion and Cancés [23] proposed a Gauss-Hermite quadrature integration scheme to solve both the time-dependent and time-independent GPE. More recently, Bao and Du [4] developed a novel method called the gradient flow with discrete normalization to find the ground state of the GPE. This numerical method is perhaps one of the most efficient ways to solve the time-independent GPE [4, 5, 9, 17, 19, 21].

1.3 The problem

However, there are numerical difficulties when the time-independent GPE is in a semiclassical regime, i.e. BEC is a strong repulsively interacting condensate. In such a regime, the GPE is reduced into a singularly perturbed non-linear eigenvalue

problem under a constraint as shown

$$\mu\phi(\vec{x}) = -\frac{\varepsilon^2}{2}\nabla^2\phi(\vec{x}) + V(\vec{x})\phi(\vec{x}) + |\phi(\vec{x})|^2\phi(\vec{x}), \qquad \vec{x} \in \Omega, \tag{1.1}$$

$$\phi(\vec{x})|_{\partial\Omega} = 0, \tag{1.2}$$

under the normalization condition

$$||\phi||^2 = \int_\Omega |\phi(\vec{x})|^2 d\vec{x} = 1, \tag{1.3}$$

where $\phi(\vec{x})$ is a real function, $\vec{x} \in \Omega \subseteq \mathbb{R}^d$, $V(\vec{x})$ is an external potential, $\mu > 0$ and $0 < \varepsilon \ll 1$. When ε goes to zero, the solutions of the problem have boundary layers or interior layers [8]. The classical numerical scheme based on uniform mesh to discretize the gradient flow would be difficult to track these layers [24]. In order to obtain a reliable numerical solution for (1.1) when $\varepsilon \ll 1$, it is desirable to use an adaptive mesh that concentrates nodes in the boundary layers or interior layers. Ideally, the mesh should be generated by adapting it to the features of the computed solution. There has been a great deal of research done on the use of adaptive methods for steady and unsteady partial differential equations recently [16, 18, 29, 42, 41, 34, 33, 35, 45, 46]. Among which, Shishkin [49] in 1990 proposed an upwind scheme based on a piecewise uniform mesh to solve the two-point boundary layer problems—fine in the boundary and coarse in the rest of the domain. This scheme is useful and has been demonstrated to be ε-uniform convergenct by Miller et al. [42, 41]. It has also been shown that the scheme is uniformly convergent near the boundary layer and it has been pointed out that uniform convergence cannot be obtained at all interior mesh points unless the mesh is specially tailored to the solution of the problem.

In this thesis, we aim to design a uniformly convergent numerical scheme based on piecewise uniform mesh for discretizing the gradient flow so that we can treat problems with complicated boundary layer or interior layers effectively.

1.4 The organization of the thesis

This thesis is organized as follows.

In Chapter 2, starting from the time-dependent GPE, we first rescale it to a dimensionless form and then reduce the time-dependent GPE from three dimensions into lower dimensions. We next describe how to obtain the stationary states of BEC and the time-independent GPE in a semiclassical regime, i.e., the ground state and excited states.

In Chapter 3, we arrive at the singularly perturbed nonlinear eigenvalue problem under a constraint to be solved. For the sake of comparison with numerical approximation later, we present some analytical approximations for the ground and excited states in BEC with box potential in one dimension (1D). We also present some analytical approximations for the first excited states in BEC with harmonic potential in 1D. We demonstrate that there are boundary layers or interior layers in these solutions.

In Chapter 4, we describe the numerical methods for solving such singularly perturbed nonlinear eigenvalue problem under a constraint. We apply one of the most efficient numerical technique–the gradient flow with discrete normalization to solve the singularly perturbed and constrained nonlinear eigenvalue problem. We first show a classical numerical scheme based on uniform mesh to discretize the gradient flow. We then analyze the shortcomings of the scheme and introduce the detailed algorithm of our newly proposed numerical scheme based on piecewise uniform mesh to discretize the gradient flow to treat boundary layers or interior layers. Finally we provide numerical error analysis for both uniform mesh and piecewise uniform mesh. The limitations of uniform mesh are shown and the advantages from using piecewise uniform mesh are presented. Comparisons between solutions obtained by our proposed piecewise uniform mesh and solutions generated with the classical uniform

mesh are shown in more details.

In Chapter 5, we apply our new proposed scheme based on piecewise uniform mesh to calculate the ground state, first, third, and ninth excited states of BEC with box potential in 1D and the first excited state of BEC with harmonic potential in 1D. We compare the numerical results with those asymptotic approximation shown in Chapter 3. We then extend our numerical scheme based on piecewise uniform mesh to find numerical solutions of the singularly perturbed and constrained nonlinear eigenvalue problem in two dimensions (2D), for example, ground state and excited states of BEC in three different potentials, box potential, harmonic potential and harmonic plus optical potential. This is to illustrate the capability of the proposed piecewise uniform scheme in solving the time-independent GPE under different potentials and conditions, more specifically, to treat the boundary layers or interior layers in two dimensions.

Finally in Chapter 6, some conclusions on our results are drawn and possible future works are highlighted.

Chapter 2

The Gross-Pitaevskii equation

In this chapter, we derive the time-independent GPE from the well-known time-dependent GPE. As preparatory steps, we introduce the time-dependent GPE with two kinds of external potentials, i.e., the harmonic oscillator potential and the box potential. The GPE is then non-dimensionalized, rescaled and reduced into lower-dimensional formulations. Finally the solutions of the time-independent GPE, ground state and excited states are summarized.

2.1 The time-dependent GPE

At temperatures T much lower than the critical temperature T_c, the BEC is well described by the macroscopic wave function $\psi = \psi(\vec{x}, t)$. The evolution of this wave function is governed by a self-consistent nonlinear Schrödinger equation known as the Gross-Pitaevskii equation [32, 43]

$$i\hbar\frac{\partial\psi(\vec{x},t)}{\partial t} = -\frac{\hbar^2}{2m}\nabla^2\psi(\vec{x},t) + V(\vec{x})\psi(\vec{x},t) + NU_0\left|\psi(\vec{x},t)\right|^2\psi(\vec{x},t), \tag{2.1}$$

where $\vec{x} = (x, y, z)^T$ is the spatial coordinate vector, $\hbar$ is the Planck constant, m is the atomic mass, N is number of atoms in the condensate, $U_0 = 4\pi\hbar^2 a_s/m$ describes the interactions between atoms in the condensate with a_s the atomic scattering

length (positive for repulsive interaction and negative for attractive interaction), $V(\vec{x})$ is an external trapping potential.

Two important invariants of (2.1) are the normalization of the wave function

$$||\psi(\cdot,t)||^2 = \int_{\mathbb{R}^3} |\psi(\vec{x},t)|^2 \, d\vec{x} = 1, \tag{2.2}$$

and the energy

$$E(\psi) = \int_{\mathbb{R}^3} \left[\frac{\hbar^2}{2m} |\nabla\psi(\vec{x},t)|^2 + V(\vec{x})|\psi(\vec{x},t)|^2 + \frac{NU_0}{2}|\psi(\vec{x},t)|^4 \right] d\vec{x}. \tag{2.3}$$

There are two typical external potentials $V(\vec{x})$ considered in this dissertation:

1. The box potential:

$$V_{\text{box}}(\vec{x}) = \begin{cases} 0, & 0 < x, y, z < L, \\ \infty, & \text{otherwise.} \end{cases} \tag{2.4}$$

2. The harmonic oscillator potential:

$$V_{\text{ho}}(\vec{x}) = V_{\text{ho}}(x) + V_{\text{ho}}(y) + V_{\text{ho}}(z), \qquad \vec{x} \in \mathbb{R}^3, \tag{2.5}$$

$$V_{\text{ho}}(\tau) = \frac{m}{2}\omega_\tau^2 \tau^2, \qquad \tau = x, y, z, \tag{2.6}$$

where ω_τ is the trap frequency in $\tau-$direction.

2.2 Non-dimensionalization of GPE

We introduce the following parameters in order to scale (2.1) under the normalization (2.2) [8]

$$\tilde{t} = \frac{t}{t_s}, \quad \tilde{\vec{x}} = \frac{\vec{x}}{x_s}, \quad \tilde{\psi}(\tilde{\vec{x}}, \tilde{t}) = x_s^{3/2}\psi(\vec{x}, t), \tag{2.7}$$

where t_s and x_s are the dimensionless time and length units. Substituting (2.7) into (2.1), multiplying throughout by $\frac{t_s^2}{m\sqrt{x_s}}$, then removing all $\tilde{}$, we obtain a dimensionless GPE under the normalization (2.2) in three dimensions (3D):

$$i\frac{\partial\psi(\vec{x},t)}{\partial t} = -\frac{1}{2}\nabla^2\psi(\vec{x},t) + V(\vec{x})\psi(\vec{x},t) + \beta\,|\psi(\vec{x},t)|^2\,\psi(\vec{x},t), \tag{2.8}$$

and the dimensionless energy functional $E(\psi)$ is defined as follows:

$$E(\psi) = \int_{\mathbb{R}^3} \left[\frac{1}{2} |\nabla \psi(\vec{x}, t)|^2 + V(\vec{x}) |\psi(\vec{x}, t)|^2 + \frac{\beta}{2} |\psi(\vec{x}, t)|^4 \right] d\vec{x}, \tag{2.9}$$

where the interaction parameter $\beta = \frac{4\pi a_s N}{x_s}$. The choices used for the scaling parameters, t_s and x_s for the two different dimensionless potential $V(\vec{x})$ are:

1. The box potential:

$$t_s = \frac{mL^2}{\hbar}, \qquad x_s = L, \tag{2.10}$$

$$V(\vec{x}) = \begin{cases} 0, & 0 < x, y, z < 1, \\ \infty, & \text{otherwise.} \end{cases} \tag{2.11}$$

2. The harmonic oscillator potential:

$$t_s = \frac{1}{\omega_x}, \qquad x_s = \sqrt{\frac{\hbar}{m\omega_x}}, \tag{2.12}$$

$$V(\vec{x}) = \frac{1}{2}(x^2 + \gamma_y^2 y^2 + \gamma_z^2 z^2), \tag{2.13}$$

where $\gamma_y = \frac{\omega_y}{\omega_x}$ and $\gamma_z = \frac{\omega_z}{\omega_x}$.

2.3 Reduction of the GPE to lower dimensions

In order to illustrate dimension reduction of the GPE in 3D to two dimensions (2D) or one dimension (1D), we first consider the dimensionless GPE with the harmonic potential. The dimensionless GPE with its normalization is given by:

$$i\frac{\partial \psi(\vec{x}, t)}{\partial t} = -\frac{1}{2}\nabla^2 \psi(\vec{x}, t) + \frac{1}{2}(x^2 + \gamma_y^2 y^2 + \gamma_z^2 z^2)\psi(\vec{x}, t) + \beta \left|\psi(\vec{x}, t)\right|^2 \psi(\vec{x}, t), \tag{2.14}$$

where $\beta = \frac{NU_0}{x_s^3 \hbar \omega_x} = \frac{4\pi a_s N}{x_s}$.

In a disk-shaped condensation with parameters $\omega_x \approx \omega_y$ and $\omega_z \gg \omega_x$ ($\Longleftrightarrow$ $\gamma_y \approx 1$ and $\gamma_z \gg 1$), the three-dimensional GPE (2.14) can be reduced to a two-dimensional GPE by assuming that the time evolution does not cause excitations

along the z-axis, since the excitations along the z-axis have large energy (of order $\hbar\omega_z$) compared to that along the x- and y-axis with energies of order $\hbar\omega_x$. Thus we may assume that the condensation wave function along the z-axis is always well described by the ground state wave function and set

$$\psi(x, y, z, t) = \psi_2(x, y, t)\phi_3(z), \tag{2.15}$$

where $\phi_3(z) \approx \phi_{\rm ho}(z) = (\gamma_z/\pi)^{1/4}\, e^{-\gamma_z z^2/2}$. Plugging (2.15) into (2.14), then multiplying by $\bar{\phi}_3(z)$ (the conjugate of $\phi_3(z)$), integrating with respect to z over $(-\infty, \infty)$, we get the two-dimensional GPE with $\vec{x} = (x, y)^T$

$$i\,\frac{\partial\psi_2(\vec{x}, t)}{\partial t} = -\frac{1}{2}\nabla^2\psi_2 + \frac{1}{2}\left(x^2 + \gamma_y^2 y^2 + C\right)\psi_2 + \beta_2|\psi_2|^2\psi_2, \tag{2.16}$$

where

$$\begin{aligned} C &= \gamma_z^2\int_{-\infty}^{\infty} z^2|\phi_3(z)|^2\, dz + \int_{-\infty}^{\infty}\left|\frac{d\phi_3(z)}{dz}\right|^2 dz, \\ \beta_2 &= \beta\int_{-\infty}^{\infty}|\phi_3(z)|^4\, dz \approx \beta\int_{-\infty}^{\infty}|\phi_{\rm ho}(z)|^4\, dz = \beta\sqrt{\gamma_z/2\pi}. \end{aligned} \tag{2.17}$$

Since this GPE is time-transverse invariant, we can replace $\psi_2 \to \psi e^{-iCt/2}$ which drops the constant C in the trapping potential and obtain:

$$i\,\frac{\partial\psi(\vec{x}, t)}{\partial t} = -\frac{1}{2}\nabla^2\psi + V_2(\vec{x})\psi + \beta_2|\psi|^2\psi, \tag{2.18}$$

where $V_2(\vec{x}) = \frac{1}{2}\left(x^2 + \gamma_y^2 y^2\right)$.

In a cigar-shaped condensation where the energies along x-axis is much smaller than energies along y- and z-axis, i.e. $\omega_y \gg \omega_x$ and $\omega_z \gg \omega_x$, and there is almost no excitation along the y- and z-axis as time evolves, we can obtain a one-dimensional GPE. In fact, for any fixed $\beta \geq 0$ and when $\gamma_y \gg 1$ and $\gamma_z \gg 1$, we set

$$\psi(\vec{x}, t) = \psi_1(x, t)\phi_{23}(y, z), \tag{2.19}$$

$$\phi_{23}(y, z) \approx \phi_{23}^{\rm ho}(y, z) = \frac{(\gamma_y\gamma_z)^{\frac{1}{4}}}{\sqrt{\pi}} e^{-(\gamma_y y^2 + \gamma_z z^2)/2}. \tag{2.20}$$

Substituting (2.19) into (2.8), multiplying both sides by $\bar{\phi}_{23}^{\text{ho}}(y,z)$ (the conjugate of $\phi_{23}^{\text{ho}}(y,z)$), and integrating both sides in the yz-plane over $\mathbb{R}^2$, we get:

$$i\frac{\partial\psi_1}{\partial t} = -\frac{1}{2}\frac{\partial^2\psi_1}{\partial x^2} + \frac{1}{2}(x^2+C)\psi_1 + \left(\beta\int_{\mathbb{R}^2}|\phi_{23}(y,z)|^4 dydz\right)|\psi_1|^2\psi_1, \tag{2.21}$$

where

$$C = \int_{\mathbb{R}^2}|\nabla\phi_{23}(y,z)|^2 dydz + \int_{\mathbb{R}^2}(\gamma_y^2y^2+\gamma_z^2z^2)|\phi_{23}(y,z)|^2 dydz. \tag{2.22}$$

Since (2.21) is time-transverse invariant, we let $\psi_1 \to \psi e^{-i\frac{Ct}{2}}$. This will remove the term containing the constant C and we obtain the GPE in 1D as:

$$i\frac{\partial}{\partial t}\psi(x,t) = -\frac{1}{2}\frac{\partial^2}{\partial x^2}\psi(x,t) + V_1(x)\psi(x,t) + \beta_1|\psi(x,t)|^2\psi(x,t), \tag{2.23}$$

where $V_1(x) = \frac{1}{2}x^2$ and $\beta_1 = \beta\int_{\mathbb{R}^2}|\phi_{23}(y,z)|^4\ dydz \approx \beta\int_{\mathbb{R}^2}|\phi_{23}^{\text{ho}}(y,z)|^4\ dydz = \beta\sqrt{\gamma_y\gamma_z}/2\pi$.

Thus here we consider the dimensionless GPE with the harmonic potential in d-dimensions ($d = 1, 2, 3$):

$$i\ \frac{\partial\psi(\vec{x},t)}{\partial t} = -\frac{1}{2}\nabla^2\psi + V_d(\vec{x})\psi + \beta_d|\psi|^2\psi, \quad \vec{x}\in\mathbb{R}^d, \quad t\geq 0, \tag{2.24}$$

where

$$\beta_d = \beta\begin{cases}\sqrt{\gamma_y\gamma_z}/2\pi, \\ \sqrt{\gamma_z/2\pi}, \\ 1,\end{cases} \qquad V_d(\vec{x}) = \begin{cases}x^2/2, & d=1, \\ (x^2+\gamma_y^2y^2)/2, & d=2, \\ (x^2+\gamma_y^2y^2+\gamma_z^2z^2)/2, & d=3.\end{cases}$$

Similarly, we can obtain the GPE with the box potential in d-dimensions:

$$i\frac{\partial}{\partial t}\psi(\vec{x},t) = -\frac{1}{2}\nabla^2\psi(\vec{x},t) + V_d(\vec{x})\psi(\vec{x},t) + \beta_d|\psi(\vec{x},t)|^2\psi(\vec{x},t), \tag{2.25}$$

where the box potential

$$V_d(\vec{x}) = \begin{cases}0, & \vec{x}\in[0,1]^d, \quad d=1,2,3, \\ \infty, & \text{otherwise.}\end{cases}$$

Hence, a general d-dimensional (d=1,2,3) GPE will be as follows:

$$i\partial_t\psi(\vec{x},t) = -\frac{1}{2}\nabla^2\psi(\vec{x},t) + V_d(\vec{x})\psi(\vec{x},t) + \beta_d|\psi(\vec{x},t)|^2\psi(\vec{x},t), \quad \vec{x}\in\Omega, \tag{2.26}$$
$$\psi(\vec{x},t) = 0, \quad \vec{x}\in\partial\Omega,$$

where Ω is a bounded domain in $\mathbb{R}^d$. Two important invariants of (2.26) are the normalization of the wave function

$$N(\psi) = \int_\Omega |\psi(\vec{x},t)|^2\, d\vec{x} \equiv \int_\Omega |\psi(\vec{x},0)|^2\, d\vec{x} = 1, \quad t\geq 0, \tag{2.27}$$

and the energy

$$E_\beta(\psi) = \int_\Omega \left[\frac{1}{2}|\nabla\psi(\vec{x},t)|^2 + V_d(\vec{x})|\psi(\vec{x},t)|^2 + \frac{\beta_d}{2}|\psi(\vec{x},t)|^4\right] d\vec{x} = E_\beta(\psi(\vec{x},0)), \quad t\geq 0. \tag{2.28}$$

2.4 Stationary states of GPE

In order to find stationary state of (2.26), we let

$$\psi(\vec{x},t) = e^{-i\mu t}\phi(\vec{x}), \tag{2.29}$$

where $\phi(\vec{x})$ is a function independent of time t and μ is the chemical potential of the condensate. Substitute (2.29) into (2.26), we get

$$\mu\phi(\vec{x}) = -\frac{1}{2}\nabla^2\phi(\vec{x}) + V_d(\vec{x})\phi(\vec{x}) + \beta_d|\phi(\vec{x})|^2\phi(\vec{x}), \quad \vec{x}\in\Omega, \tag{2.30}$$
$$\phi(\vec{x}) = 0, \quad \vec{x}\in\partial\Omega, \tag{2.31}$$

under the normalization condition

$$||\phi(\vec{x})||^2 = \int_\Omega |\phi(\vec{x})|^2 d\vec{x} = 1. \tag{2.32}$$

This is a nonlinear eigenvalue problem with a constraint and the eigenvalue μ can be calculated from the corresponding eignfunction $\phi(\vec{x})$ by

$$\begin{aligned} \mu &= \mu_\beta(\phi) = \int_\Omega \left[\frac{1}{2}|\nabla\phi(\vec{x})|^2 + V_d(\vec{x})|\phi(\vec{x})|^2 + \beta_d|\phi(\vec{x})|^4\right] d\vec{x} \\ &= E_\beta(\phi) + \int_\Omega \frac{\beta_d}{2}|\phi(\vec{x})|^4 d\vec{x}. \end{aligned} \tag{2.33}$$

2.4.1 Ground state

The ground state wave function $\phi^g := \phi^g(\vec{x})$ of a BEC is found by minimizing the energy functional $E_\beta(\phi)$ over the unit sphere $S = \{\phi(\vec{x}) | \quad ||\phi(\vec{x})|| = 1, E(\phi) < \infty\}$, i.e., find $(\mu^g, \phi^g \in S)$ such that

$$E^g := E_\beta(\phi^g) = \min_{\phi\in S} E_\beta(\phi), \quad \mu^g := \mu_\beta(\phi^g). \tag{2.34}$$

We can easily show that the ground state ϕ^g is an eigenfunction of the nonlinear eigenvalue problem (2.30) under the constraint (2.32).

2.4.2 Excited states

Any eigenfunction $\phi(\vec{x})$ of (2.30) under the constraint (2.32) whose energy $E_\beta(\phi) > E_\beta(\phi^g)$ is usually called as an excited state in the physics literature.

Suppose the eigenfunctions of the eigenvalue problem (2.30) under the constraint (2.32) are

$$\pm\phi^g(\vec{x}), \pm\phi_1(\vec{x}), \pm\phi_2(\vec{x}), \cdots, \tag{2.35}$$

whose energies satisfy

$$E_\beta(\phi^g) < E_\beta(\phi_1) < E_\beta(\phi_2) < \cdots. \tag{2.36}$$

Then $\phi_j(\vec{x})$, $j = 1, 2, 3, \cdots$, is called as the j-th excited state solution.

Chapter 3

The singularly perturbed nonlinear eigenvalue problem

In this chapter, we derive the singularly perturbed nonlinear eigenvalue problem from the time-independent GPE (2.30). When $\beta_d \gg 1$, the time-independent GPE, in the bounded domain or whole space, is then rescaled and reduced into semiclassical formulations. We finally obtain the singularly perturbed nonlinear eigenvalue problem under a constraint in a general form.

3.1 The singularly perturbed nonlinear eigenvalue problem

When $\beta_d \gg 1$, i.e. the time-independent GPE (2.30) is in a strongly repulsive interacting condensation or in the semiclassical regime, we need another scaling for the GPE.

3.1.1 For bounded domain $\Omega = [0,1]^d$

When $\Omega = [0,1]^d$, the GPE (2.30) with box potential is

$$\mu\phi(\vec{x}) = -\frac{1}{2}\nabla^2\phi(\vec{x}) + \beta_d|\phi(\vec{x})|^2\phi(\vec{x}), \qquad \vec{x} \in \Omega = [0,1]^d, \tag{3.1}$$

$$\phi(\vec{x}) = 0, \quad \vec{x} \in \partial\Omega. \tag{3.2}$$

We let $\varepsilon = \frac{1}{\sqrt{\beta_d}}$ and μ represent μ/ε^2. Divided by β_d at both sides, the equation (2.30) with the box potential reduces to the singularly perturbed nonlinear eigenvalue problem

$$\mu\phi(\vec{x}) = -\frac{\varepsilon^2}{2}\nabla^2\phi(\vec{x}) + |\phi(\vec{x})|^2\phi(\vec{x}), \qquad \vec{x} \in [0,1]^d, \tag{3.3}$$

and the normalization as

$$||\phi||^2 = \int_{[0,1]^d} |\phi(\vec{x})|^2 d\vec{x} = 1. \tag{3.4}$$

The chemical potential μ in (3.3) can be computed from its corresponding eigenfunction ϕ by

$$\begin{aligned} \mu &= \mu_\varepsilon(\phi) = \int_{[0,1]^d} \left[\frac{\varepsilon^2}{2}|\nabla\phi(\vec{x})|^2 + |\phi(\vec{x})|^4\right] d\vec{x} \\ &= E_\varepsilon(\phi) + \int_{[0,1]^d} \left[\frac{1}{2}|\phi(\vec{x})|^4\right] d\vec{x}, \end{aligned}$$

and the energy functional reduces to

$$E_\varepsilon(\phi) = \int_{[0,1]^d} \left[\frac{\varepsilon^2}{2}|\nabla\phi(\vec{x})|^2 + \frac{1}{2}|\phi(\vec{x})|^4\right] d\vec{x}.$$

3.1.2 For the whole space $\Omega = \mathbb{R}^d$

When $\Omega = \mathbb{R}^d$ is the whole space, the time-independent GPE (2.30) with the harmonic potential is as follows,

$$\mu\phi(\vec{x}) = -\frac{1}{2}\nabla^2\phi(\vec{x}) + V_d(\vec{x})\phi(\vec{x}) + \beta_d|\phi(\vec{x})|^2\phi(\vec{x}), \quad \vec{x} \in \Omega = \mathbb{R}^d, \tag{3.5}$$

$$\phi(\vec{x}) \longrightarrow 0, \quad |\vec{x}| \longrightarrow \infty. \tag{3.6}$$

In order to rescale the GPE, We let

$$\vec{x} = \varepsilon^{1/2}\widetilde{\vec{x}}, \quad \phi = \varepsilon^{d/4}\widetilde{\phi}, \quad \mu = \varepsilon\widetilde{\mu}, \quad \varepsilon = \beta_d^{-d/d+2}. \tag{3.7}$$

Substituting the above scaling parameters into (2.30), and rearranging the variables, we have the singularly perturbed nonlinear eigenvalue problem

$$\mu\phi(\vec{x}) = -\frac{\varepsilon^2}{2}\nabla^2\phi(\vec{x}) + V_d(\vec{x})\phi(\vec{x}) + |\phi(\vec{x})|^2\phi(\vec{x}), \tag{3.8}$$

with the constraint

$$\int_{\mathbb{R}^d} |\phi(\vec{x})|^2 \, d\vec{x} = 1.$$

Again, the chemical potential μ in (3.8) can be computed from its corresponding eigenfunction ϕ by

$$\begin{aligned} \mu = \mu_\varepsilon(\phi) &= \int_{\mathbb{R}^d} \left[\frac{\varepsilon^2}{2}|\nabla\phi(\vec{x})|^2 + V_d|\phi(\vec{x})|^2 + |\phi(\vec{x})|^4\right] d\vec{x}. \\ &= E_\varepsilon(\phi) + \int_{\mathbb{R}^d} \left[\frac{1}{2}|\phi(\vec{x})|^4\right] d\vec{x}, \end{aligned}$$

and the energy functional becomes

$$E_\varepsilon(\phi) = \int_{\mathbb{R}^d} \left[\frac{\varepsilon^2}{2}|\nabla\phi(\vec{x})|^2 + V_d|\phi(\vec{x})|^2 + \frac{1}{2}|\phi(\vec{x})|^4\right] d\vec{x}.$$

3.1.3 General formulation

In conclusion, we have the following singularly perturbed nonlinear eigenvalue problem whatever the potentials $V_d(\vec{x})$ as

$$\mu\phi(\vec{x}) = -\frac{\varepsilon^2}{2}\nabla^2\phi(\vec{x}) + V_d(\vec{x})\phi(\vec{x}) + |\phi(\vec{x})|^2\phi(\vec{x}), \qquad \vec{x} \in \Omega, \tag{3.9}$$

$$\phi(\vec{x}) = 0, \quad \vec{x} \in \partial\Omega, \tag{3.10}$$

with the normalization as

$$||\phi||^2 = \int_\Omega |\phi(\vec{x})|^2 d\vec{x} = 1. \tag{3.11}$$

The chemical potential μ in (3.9) can be computed from its corresponding eigenfunction by

$$\begin{aligned} \mu = \mu_\varepsilon(\phi) &= \int_\Omega \left[\frac{\varepsilon^2}{2} |\nabla \phi(\vec{x})|^2 + V_d |\phi(\vec{x})|^2 + |\phi(\vec{x})|^4 \right] d\vec{x}, \\ &= E_\varepsilon + \frac{1}{2} \int_\Omega |\phi(\vec{x})|^4 d\vec{x}, \end{aligned} \tag{3.12}$$

and the energy functional is

$$\begin{aligned} E_\varepsilon(\phi) &= \int_\Omega \left[\frac{\varepsilon^2}{2} |\nabla \phi(\vec{x})|^2 + V_d |\phi(\vec{x})|^2 + \frac{1}{2} |\phi(\vec{x})|^4 \right] d\vec{x}, \\ &= E_{\text{kin}}(\phi) + E_{\text{pot}}(\phi) + E_{\text{int}}(\phi), \end{aligned} \tag{3.13}$$

where E_{kin}, E_{pot} and E_{int} are the kinetic energy, potential energy and interaction energy respectively. They are defined as

$$E_{\text{kin}}(\phi) = \frac{\varepsilon^2}{2} \int_\Omega |\nabla \phi(\vec{x})|^2 d\vec{x}, \tag{3.14}$$

$$E_{\text{pot}}(\phi) = \int_\Omega V_d |\phi(\vec{x})|^2 d\vec{x}, \tag{3.15}$$

$$E_{\text{int}}(\phi) = \frac{1}{2} \int_\Omega |\phi(\vec{x})|^4 d\vec{x}. \tag{3.16}$$

In addition, the chemical potential μ can also be given by

$$\mu_\varepsilon(\phi) = E_{\text{kin}}(\phi) + E_{\text{pot}}(\phi) + 2E_{\text{int}}(\phi). \tag{3.17}$$

The equation (3.9) with the constraint (3.11) is a singularly perturbed nonlinear eigenvalue problem and its solutions are of main interest in this thesis. In the next section, some approximated solutions for the problem in 1D, which have boundary layer or interior layer for small ε, are summarized.

3.2 Approximations in 1D box potential

In this section, we present the matched asymptotic approximations for the ground state and excited states of BEC confined in a 1D box potential, i.e., $V_1(x) = 0$, for

$0 \le x \le 1$; $V_1(x) = \infty$, otherwise. We truncate the eigenvalue problem into $[0, 1]$ with homogeneous Dirichlet boundary condition in this case.

3.2.1 Thomas-Fermi approximation for ground state

We first consider (3.9) with box potential in 1D. Since $0 < \varepsilon \ll 1$, we can drop the first term on the right side and obtain the ground state approximation as:

$$\mu_g^{\mathrm{TF}} \phi_g^{\mathrm{TF}}(x) \;=\; |\phi_g^{\mathrm{TF}}|^2 \phi_g^{\mathrm{TF}}(x), \qquad x \in [0, 1],$$

which implies

$$\phi_g^{\mathrm{TF}} \;=\; \sqrt{\mu_g^{\mathrm{TF}}}, \quad 0 < x < 1. \tag{3.18}$$

Substituting (3.18) into the normalization condition (3.11), we get:

$$\int_0^1 |\phi^{\mathrm{TF}}(x)|^2 dx = \int_0^1 \mu_g^{\mathrm{TF}} dx = \mu_g^{\mathrm{TF}} = 1. \tag{3.19}$$

Hence, the Thomas-Fermi approximation for ground state is given by

$$\phi_g(x) \approx \phi_g^{\mathrm{TF}}(x) = 1, \qquad 0 < x < 1. \tag{3.20}$$

However, the approximation for the ground state does not satisfy the zero boundary condition (3.10). This suggests the existence of two boundary layers in the region near $x = 0$ and near $x = 1$ in the ground state of BEC with box potential when we remove the diffusion term in (3.3).

3.2.2 Matched asymptotic approximations for ground state

Since the layers exist at the two boundaries $x = 0$ and $x = 1$ when $0 < \varepsilon \ll 1$, we solve (3.8) near $x = 0$ and $x = 1$, respectively. Let us suppose the boundary layer is of width δ $(0 < \delta < 1)$. We do a rescaling in the region of $x \in [0, \delta]$ and let

$$x = \delta X, \quad \phi(x) = \phi_s \Phi(X). \tag{3.21}$$

We substitute (3.21) into (3.8) and obtain

$$\mu\Phi(X) = -\frac{\varepsilon^2}{2\delta^2}\Phi_{XX}(X) + \phi_s^2\Phi^3(X), \qquad X \in (0,1), \tag{3.22}$$

$$\Phi(0) = 0, \qquad \Phi(1) = 1. \tag{3.23}$$

In order to solve the above equation, we need to rescale all the terms to O(1). We choose $\delta = \varepsilon/\sqrt{\mu}$ and $\phi_s = \sqrt{\mu}$ in (3.21), the above equation reduces to

$$\Phi(X) = -\frac{1}{2}\Phi_{XX}(X) + \Phi^3(X), \qquad X \in (0,1), \tag{3.24}$$

$$\Phi(0) = 0, \qquad \Phi(1) = 1. \tag{3.25}$$

All the terms in the equation are now O(1). Solving the above equation, we obtain

$$\Phi(X) = \tanh(X), \quad X \in (0,1). \tag{3.26}$$

Since $\mu \approx \mu^{\mathrm{TF}} = 1$ for the ground state, we can conclude that the width of boundary layer near $x = 0$ is O(ε). Thus finally we have

$$\phi_g(x) \approx \sqrt{\mu_g}\tanh\left(\frac{\sqrt{\mu_g}}{\varepsilon}x\right), \quad x \in (0,\delta). \tag{3.27}$$

Repeating the similar procedure, we can obtain the approximation near $x = 1$

$$\phi_g(x) \approx \sqrt{\mu_g}\tanh\left(\frac{\sqrt{\mu_g}}{\varepsilon}(1-x)\right), \quad x \in (1-\delta,1). \tag{3.28}$$

Finally, using the matched asymptotic technique, an approximation for the ground state with the box potential in 1D can be given by

$$\begin{aligned}\phi_g \approx \phi_g^{\mathrm{MA}} &= \sqrt{\mu_g^{\mathrm{MA}}}\left[\tanh\left(\frac{\sqrt{\mu_g^{\mathrm{MA}}}}{\varepsilon}x\right) + \tanh\left(\frac{\sqrt{\mu_g^{\mathrm{MA}}}}{\varepsilon}(1-x)\right)\right.\\ &- \left.\tanh\left(\frac{\sqrt{\mu_g^{\mathrm{MA}}}}{\varepsilon}\right)\right], \quad 0 \le x \le 1.\end{aligned} \tag{3.29}$$

Using the normalization condition (3.11), we find

$$
\begin{aligned}
1 &= \int_0^1 |\phi_g^{\mathrm{MA}}(x)|^2\, dx \\
&= \mu_g^{\mathrm{MA}} \Bigg[\int_0^1 \tanh^2\left(\sqrt{\mu_g^{\mathrm{MA}}}x/\varepsilon\right)\, dx + \int_0^1 \tanh^2\left(\sqrt{\mu_g^{\mathrm{MA}}}(1-x)/\varepsilon\right)\, dx \\
&\quad -2\tanh\left(\sqrt{\mu_g^{\mathrm{MA}}}/\varepsilon\right) \int_0^1 \left[\tanh\left(\sqrt{\mu_g^{\mathrm{MA}}}x/\varepsilon\right) + \tanh\left(\sqrt{\mu_g^{\mathrm{MA}}}(1-x)/\varepsilon\right)\right]\, dx \\
&\quad +2\int_0^1 \tanh\left(\sqrt{\mu_g^{\mathrm{MA}}}x/\varepsilon\right)\tanh\left(\sqrt{\mu_g^{\mathrm{MA}}}(1-x)/\varepsilon\right)\, dx + \int_0^1 \tanh^2\left(\sqrt{\mu_g^{\mathrm{MA}}}/\varepsilon\right)\, dx \Bigg] \\
&= \mu_g^{\mathrm{MA}} \Big[2\left(1-\varepsilon\tanh\left(\sqrt{\mu_g^{\mathrm{MA}}}/\varepsilon\right)/\sqrt{\mu_g^{\mathrm{MA}}}\right) \\
&\quad -4\varepsilon\tanh\left(\sqrt{\mu_g^{\mathrm{MA}}}/\varepsilon\right)\ln\left(\cosh(\sqrt{\mu_g^{\mathrm{MA}}}/\varepsilon)\right)/\sqrt{\mu_g^{\mathrm{MA}}} \\
&\quad +2\left(-1+2\varepsilon\mathrm{coth}(\sqrt{\mu_g^{\mathrm{MA}}}/\varepsilon)\ln\left(\cosh\left(\sqrt{\mu_g^{\mathrm{MA}}}/\varepsilon\right)\right)/\sqrt{\mu_g^{\mathrm{MA}}}\right) + \tanh^2(\sqrt{\mu_g^{\mathrm{MA}}}/\varepsilon)\Big] \\
&\approx \mu_g^{\mathrm{MA}} \left[2\left(1-\frac{\varepsilon}{\sqrt{\mu_g^{\mathrm{MA}}}}\right) - 4\frac{\sqrt{\mu_g^{\mathrm{MA}}}-\varepsilon\ln 2}{\sqrt{\mu_g^{\mathrm{MA}}}} + 2\left(-1+2\frac{\sqrt{\mu_g^{\mathrm{MA}}}-\varepsilon\ln 2}{\sqrt{\mu_g^{\mathrm{MA}}}}\right) + 1\right] \\
&= \mu_g^{\mathrm{MA}} - 2\varepsilon\sqrt{\mu_g^{\mathrm{MA}}}.
\end{aligned} \tag{3.30}
$$

Solving it, we obtain the chemical potential

$$
\mu_g^{\mathrm{MA}} \approx 1 + 2\varepsilon\sqrt{1+\varepsilon^2} + 2\varepsilon^2, \quad 0 < \varepsilon \ll 1. \tag{3.31}
$$

Moreover, we can obtain

$$
\begin{aligned}
E_{\mathrm{kin,g}}^{\mathrm{MA}} &= E_{\mathrm{kin}}(\phi_g^{\mathrm{MA}}) = \frac{\varepsilon^2}{2}\int_0^1 \left|\left[\phi_g^{\mathrm{MA}}(x)\right]'\right|^2\, dx \\
&= \frac{1}{2}\left(\mu_g^{\mathrm{MA}}\right)^2 \int_0^1 \left[\mathrm{sech}^2\left(\sqrt{\mu_g^{\mathrm{MA}}}x/\varepsilon\right) - \mathrm{sech}^2\left(\sqrt{\mu_g^{\mathrm{MA}}}(1-x)/\varepsilon\right)\right]^2\, dx \\
&\approx \frac{2}{3}\mu_g^{\mathrm{MA}}\sqrt{\mu_g^{\mathrm{MA}}}\varepsilon.
\end{aligned} \tag{3.32}
$$

Substitute (3.31) into (3.32), we can get the kinetic potential as

$$
E_{\mathrm{kin,g}}^{\mathrm{MA}} = \frac{2}{3}\varepsilon\sqrt{1+\varepsilon^2} + 2\varepsilon^2. \tag{3.33}
$$

Note that $E_{\mathrm{int,g}}^{\mathrm{MA}} = \frac{1}{2}\left(\mu_g^{\mathrm{MA}} - E_{\mathrm{kin,g}}^{\mathrm{MA}}\right)$ we can obtain

$$
E_{\mathrm{int,g}}^{\mathrm{MA}} = \frac{1}{2} + \frac{2}{3}\varepsilon\sqrt{1+\varepsilon^2}, \tag{3.34}
$$

and

$$\begin{aligned} E_{\mathrm{g}}^{\mathrm{MA}} &= E_{\mathrm{kin,g}}^{\mathrm{MA}} + E_{\mathrm{int,g}}^{\mathrm{MA}} \\ &= \frac{1}{2} + \frac{4}{3}\varepsilon\sqrt{1+\varepsilon^2} + 2\varepsilon^2. \end{aligned} \tag{3.35}$$

3.2.3 Matched asymptotic approximations for excited states

For the BEC in 1D box potential, when $0 < \varepsilon \ll 1$, the kth ($k \in \mathbb{N}$) excited state not only has boundary layers near $x = 0$ and $x = 1$, but also has k interior layers at

$$x = \frac{j}{k+1}, \qquad j = 1, 2, \ldots, k. \tag{3.36}$$

Using the matched asymptotic method described in the previous subsection, we can obtain an approximation for ϕ_k^{MA}, i.e., the kth ($k \in \mathbb{N}$) excited states as

$$\begin{aligned} \phi_k \;\approx\; \phi_k^{\mathrm{MA}} = \sqrt{\mu_k^{\mathrm{MA}}}\Bigg\{ & \sum_{j=0}^{[(k+1)/2]} \tanh\left(\frac{\sqrt{\mu_k^{\mathrm{MA}}}}{\varepsilon}(x - \frac{2j}{k+1})\right) \\ + & \sum_{j=0}^{[k/2]} \tanh\left(\frac{\sqrt{\mu_k^{\mathrm{MA}}}}{\varepsilon}(\frac{2j+1}{k+1} - x)\right) - C_k \tanh\left(\frac{\sqrt{\mu_k^{\mathrm{MA}}}}{\varepsilon}\right)\Bigg\}, \end{aligned} \tag{3.37}$$

where $[\tau]$ takes the integer part of the real number τ and the constant $C_k = 1$ when k is odd and $C_k = 0$ when k is even. Plugging equation (3.37) into the normalization condition (3.11), we have

$$1 = \int_0^1 |\phi_k^{\mathrm{MA}}(x)|^2 dx \approx \mu_k^{\mathrm{MA}} \left[1 - \frac{2(k+1)\varepsilon}{\sqrt{\mu_k^{\mathrm{MA}}}}\right].$$

Solving it, we obtain

$$\mu_k \approx \mu_k^{\mathrm{MA}} = 1 + 2(k+1)\varepsilon\sqrt{1+(k+1)^2\varepsilon^2} + 2(k+1)^2\varepsilon^2, \quad k \in \mathbb{N}, \tag{3.38}$$

where $0 < \varepsilon \ll 1$. Similarly, we can obtain

$$E_{\mathrm{kin,k}}^{\mathrm{MA}} = \frac{2}{3}(k+1)\varepsilon\sqrt{1+(k+1)^2\varepsilon^2} + 2(k+1)^2\varepsilon^2, \tag{3.39}$$

$$\begin{aligned} E^{\mathrm{MA}}_{\mathrm{int,k}} &= \frac{1}{2}\left(\mu^{\mathrm{MA}}_{k} - E^{\mathrm{MA}}_{\mathrm{kin,k}}\right) \\ &\approx \frac{1}{2} + \frac{2}{3}(k+1)\varepsilon\sqrt{1+(k+1)^2\varepsilon^2}, \end{aligned} \tag{3.40}$$

and

$$\begin{aligned} E^{\mathrm{MA}}_{\mathrm{k}} &= E^{\mathrm{MA}}_{\mathrm{kin,k}} + E^{\mathrm{MA}}_{\mathrm{int,k}} \\ &\approx \frac{1}{2} + \frac{4}{3}(k+1)\varepsilon\sqrt{1+(k+1)^2\varepsilon^2} + 2(k+1)^2\varepsilon^2. \end{aligned} \tag{3.41}$$

Based on the above analytical results, we make the following observations for the ground state and excited states of BEC with box potential:

1. Boundary layers are observed at $x = 0$ and $x = 1$ for all ground state and excited states when $0 < \varepsilon \ll 1$. The width of these layers are of $\mathrm{O}(\varepsilon)$.

2. For k-th excited states, interior layers are also observed at $x = \frac{j}{k+1}$, $(j = 1, \ldots, k)$ when $0 < \varepsilon \ll 1$. The widths of these interior layers are twice the size of widths at the boundary layers.

Similarly, we can extend the above asymptotic approximations to ground state and excited states of BEC with box potential in higher dimensions. These approximate results will be useful since they tell us the locations and width of the boundary and interior layers of the solutions. These results also help us in choosing the piecewise uniform mesh more effectively, which we will discuss in next chapter.

3.3 Approximations for 1D harmonic potential

In this section, we present some approximations for both ground state and the first excited states of BEC with 1D harmonic potential, i.e., $V_1(x) = \frac{1}{2}x^2$.

3.3.1 Thomas-Fermi approximation for ground state

We first consider the Thomas-Fermi (TF) approximation for 1D harmonic oscillator potential. From (3.9), we drop the first term on the right side because $0 < \varepsilon \ll 1$ and obtain

$$\mu_g^{\mathrm{TF}}\phi_g^{\mathrm{TF}}(x) = \frac{x^2}{2}\phi_g^{\mathrm{TF}}(x) + |\phi_g^{\mathrm{TF}}(x)|^2\phi_g^{\mathrm{TF}}(x), \quad x \in \mathbb{R}, \tag{3.42}$$

which results in the TF approximation for ground state as

$$\phi_g(x) \approx \phi_g^{\mathrm{TF}} = \begin{cases} \sqrt{\mu_g^{\mathrm{TF}} - \frac{x^2}{2}}, & \mu_g^{\mathrm{TF}} > \frac{x^2}{2}, \\ 0, & \text{otherwise.} \end{cases} \tag{3.43}$$

Plugging (3.43) into (3.11), we get

$$1 = \int_{x^2<2\mu_g^{\mathrm{TF}}} |\phi_g^{\mathrm{TF}}(x)|^2\, dx = \int_{-\sqrt{2\mu_g^{\mathrm{TF}}}}^{\sqrt{2\mu_g^{\mathrm{TF}}}} \left(\mu_g^{\mathrm{TF}} - \frac{x^2}{2}\right) dx. \tag{3.44}$$

Solving it, we obtain the TF approximation of the chemical potential in ground state as

$$\mu_g^{\mathrm{TF}} = \frac{1}{2}\left(\frac{3}{2}\right)^{2/3}. \tag{3.45}$$

We also obtain the potential energy

$$\begin{aligned} E_{\mathrm{pot},g}^{\mathrm{TF}} &= \int_{|x|<\sqrt{2\mu_g^{\mathrm{TF}}(x)}} \frac{x^2}{2}|\phi_g^{\mathrm{TF}}(x)|^2\, dx \\ &= \int_{-\sqrt{2\mu_g^{\mathrm{TF}}(x)}}^{\sqrt{2\mu_g^{\mathrm{TF}}(x)}} \left(\mu_g^{\mathrm{TF}}\frac{x^2}{2} - \frac{x^4}{4}\right)\, dx \\ &= \frac{4\sqrt{2}}{15}\left(\mu_g^{\mathrm{TF}}\right)^{5/2} \\ &= \frac{1}{10}\left(\frac{3}{2}\right)^{2/3}, \end{aligned} \tag{3.46}$$

the interaction energy

$$E_{\mathrm{int},g}^{\mathrm{TF}} = \frac{1}{2}\int_{|x|<\sqrt{2\mu_g^{\mathrm{TF}}}} |\phi_g^{\mathrm{TF}}|^4\, dx$$

$$
\begin{aligned}
&= \frac{1}{2}\int_{-\sqrt{2\mu_g^{\mathrm{TF}}(x)}}^{\sqrt{2\mu_g^{\mathrm{TF}}(x)}} \left(\mu_g^{\mathrm{TF}} - \frac{x^2}{2}\right)^2 dx \\
&= \frac{8\sqrt{2}}{15}\left(\mu_g^{\mathrm{TF}}\right)^{5/2} \\
&= \frac{1}{5}\left(\frac{3}{2}\right)^{2/3}, \qquad (3.47)
\end{aligned}
$$

and the ground state energy

$$E_g^{\mathrm{TF}} = \mu_g^{\mathrm{TF}} - E_{\mathrm{int},g}^{\mathrm{TF}} = \frac{3}{10}\left(\frac{3}{2}\right)^{2/3}. \qquad (3.48)$$

3.3.2 Thomas-Fermi approximation for the first excited state

Similarly, using the same approach in the derivation of the TF approximation for the ground state, we can obtain the TF approximation for the 1st excited state,

$$\phi_1(x) \approx \phi_1^{\mathrm{TF}}(x) = \begin{cases} \sqrt{\mu_1^{\mathrm{TF}} - \frac{x^2}{2}}, & 0 < x < \sqrt{2\mu_1^{\mathrm{TF}}}, \\ -\sqrt{\mu_1^{\mathrm{TF}} - \frac{x^2}{2}}, & -\sqrt{2\mu_1^{\mathrm{TF}}} < x < 0, \\ 0, & \text{otherwise.} \end{cases} \qquad (3.49)$$

Plugging (3.49) into (3.11), we get

$$1 = \int_{x^2<2\mu_1^{\mathrm{TF}}} |\phi_1^{\mathrm{TF}}(x)|^2\, dx = \int_{-\sqrt{2\mu_1^{\mathrm{TF}}}}^{\sqrt{2\mu_1^{\mathrm{TF}}}} \left(\mu_1^{\mathrm{TF}} - \frac{x^2}{2}\right) dx. \qquad (3.50)$$

Solving it, we obtain the approximation of the chemical potential in the first excited state as

$$\mu_1^{\mathrm{TF}} = \frac{1}{2}\left(\frac{3}{2}\right)^{2/3}. \qquad (3.51)$$

We will then obtain the same potential energy as the ground state

$$
\begin{aligned}
E_{\mathrm{pot},1}^{\mathrm{TF}} &= \int_{|x|<\sqrt{2\mu_1^{\mathrm{TF}}(x)}} \frac{x^2}{2}|\phi_1^{\mathrm{TF}}(x)|^2\, dx \\
&= \int_{-\sqrt{2\mu_1^{\mathrm{TF}}(x)}}^{\sqrt{2\mu_1^{\mathrm{TF}}(x)}} \left(\mu_1^{\mathrm{TF}}\frac{x^2}{2} - \frac{x^4}{4}\right) dx \\
&= \frac{4\sqrt{2}}{15}\left(\mu_1^{\mathrm{TF}}\right)^{5/2} \\
&= \frac{1}{10}\left(\frac{3}{2}\right)^{2/3}, \qquad (3.52)
\end{aligned}
$$

the interaction energy

$$\begin{aligned} E_{\text{int},1}^{\text{TF}} &= \frac{1}{2}\int_{|x|<\sqrt{2\mu_1^{\text{TF}}}} |\phi_1^{\text{TF}}|^4\, dx \\ &= \frac{1}{2}\int_{-\sqrt{2\mu_1^{\text{TF}}(x)}}^{\sqrt{2\mu_1^{\text{TF}}(x)}} \left(\mu_1^{\text{TF}} - \frac{x^2}{2}\right)^2 dx \\ &= \frac{8\sqrt{2}}{15}\left(\mu_1^{\text{TF}}\right)^{5/2} \\ &= \frac{1}{5}\left(\frac{3}{2}\right)^{2/3}, \end{aligned} \tag{3.53}$$

and the first excited state energy

$$E_1^{\text{TF}} = \mu_1^{\text{TF}} - E_{\text{int},1}^{\text{TF}} = \frac{3}{10}\left(\frac{3}{2}\right)^{2/3}. \tag{3.54}$$

3.3.3 Matched asymptotic approximations for the first excited state

Since $\mu_1^{\text{TF}} > 0$, we can deduce that an interior layer exists at $x = 0$. In order to find the width of this interior layer, we suppose the width of the layer is δ and rescale the equation in the region of $x \in (-\delta, \delta)$ by setting

$$x = \delta X, \quad \phi(x) = \phi_s \Phi(X). \tag{3.55}$$

Substituting (3.55) into (3.9), we obtain

$$\mu\Phi(X) = -\frac{\varepsilon^2}{2\delta^2}\Phi_{XX}(X) + \frac{\delta^2 X^2}{2}\Phi(x) + \phi_s^2\Phi^3(X), \quad X \in (-1,1), \tag{3.56}$$

Since δ is small, we can drop the second term on the right hand side of the equation (3.56) and get

$$\mu\Phi(X) = -\frac{\varepsilon^2}{2\delta^2}\Phi_{XX}(X) + \phi_s^2\Phi^3(X), \quad X \in (-1,1). \tag{3.57}$$

The equation above is similar to the equation (3.22) obtained for the box potential and the first excited state is an odd function. In order to solve the above equation

for $0 \leq X < 1$, we need to rescale all the terms to O(1). By choosing $\delta = \varepsilon/\sqrt{\mu}$ and $\phi_s = \sqrt{\mu}$, the equation becomes

$$\begin{aligned} &\Phi(X) = -\frac{1}{2}\Phi_{XX}(X) + \Phi^3(X), \quad 0 < X < 1, \\ &\Phi(0) = 0, \quad \Phi(1) = 1. \end{aligned} \tag{3.58}$$

Solving the above equation, we obtain

$$\Phi(X) = \tanh(X), \quad X \in (-1, 1). \tag{3.59}$$

Thus we have

$$\phi_1(x) = \sqrt{\mu_1}\tanh(\frac{\sqrt{\mu_1}}{\varepsilon}x), \quad x \in (-\delta, \delta). \tag{3.60}$$

From (3.60), we can conclude that the width of the interior layer near $x = 0$ is O(ε). In fact the first excited solution of the equation from $x = 0$ can be approximated by (3.49).

Similarly, using the matched asymptotic method, we can get an approximate solution for the first excited state in BEC with 1D harmonic potential

$$\phi_1 \approx \phi_1^{\mathrm{MA}} = \begin{cases} \sqrt{\mu_1^{\mathrm{MA}}}\tanh\left(\frac{\sqrt{\mu_1^{\mathrm{MA}}}}{\varepsilon}x\right) + \sqrt{\mu_1^{\mathrm{MA}} - \frac{x^2}{2}} - \sqrt{\mu_1^{\mathrm{MA}}}, & 0 < x < \sqrt{2\mu_1^{\mathrm{MA}}}, \\ \sqrt{\mu_1^{\mathrm{MA}}}\tanh\left(\frac{\sqrt{\mu_1^{\mathrm{MA}}}}{\varepsilon}x\right) - \sqrt{\mu_1^{\mathrm{MA}} - \frac{x^2}{2}} + \sqrt{\mu_1^{\mathrm{MA}}}, & -\sqrt{2\mu_1^{\mathrm{MA}}} < x < 0, \\ 0, & \text{otherwise}, \end{cases} \tag{3.61}$$

where μ_1^{MA} can be determined by the normalization condition (3.11).

Based on the analytical results obtained, we make the following observations for the ground state and first excited state of BEC with harmonic potential:

1. No boundary layer or interior layer is observed for ground state solutions.

2. For the 1st excited states, an interior layer is observed at $x = 0$. The width of the interior layer is O(ε).

Similar to the box potential, we can extend these observations accordingly to higher dimensions. These observations will be useful on how we choose the piecewise uniform mesh when we numerically solve the 2D eigenvalue problem (3.8) in the subsequent chapters.

Chapter 4

Numerical Methods for Singularly Perturbed Eigenvalue Problems

In this chapter, we apply the gradient flow with discrete normalization to solve the singularly perturbed nonlinear eigenvalue problem (3.8) under the constraint (3.9). The efficiency and mathematical justification of this numerical method to solve the problem can be found in [4]. The ground state and excited states of BEC under a box or harmonic potential are difficult to solve due to the presence of boundary and interior layers. In order to overcome this difficulty, we discretize the gradient flow with a new numerical scheme based on a piecewise uniform mesh also known as "Shishkin" mesh [49].

4.1 Gradient flow with discrete normalization

The gradient flow with discrete normalization (GFDN) is one of the most popular techniques for dealing with the normalization constraint (3.9). The key idea of the method is as follows: (i) apply the steepest decent method to an unconstrained minimization problem; (ii) project the solution back to the unit sphere S. For

simplification of notation, we only consider the following GFDN in 1D as extension of the method to higher dimension is straightforward:

$$\frac{\partial}{\partial t}\phi(x,t) = \frac{\varepsilon^2}{2}\frac{\partial^2}{\partial x^2}\phi(x,t) - V_1(x)\phi(x,t) - |\phi(x,t)|^2\phi(x,t), \tag{4.1}$$

$$x \in \Omega = (a,b), \quad t_n \le t \le t_{n+1},$$

$$\phi(x,t_{n+1}) = \frac{\phi(x,t_{n+1}^-)}{||\phi(x,t_{n+1}^-)||}, \qquad n \ge 0, \tag{4.2}$$

$$\phi(x,0) = \phi_0(x), \quad \text{with} \quad ||\phi_0||^2 = \int_a^b \phi_0^2(x)dx = 1, \tag{4.3}$$

$$\phi(a,t) = \phi(b,t) = 0, \tag{4.4}$$

where $V_1(x)$ is the external potential given as

1. Box potential in 1D:

$$V_{\text{box}}(x) = \begin{cases} 0, & 0 < x < 1, \\ \infty, & \text{otherwise}, \end{cases} \tag{4.5}$$

2. or harmonic oscillator potential in 1D:

$$V_{\text{ho}}(x) = \frac{x^2}{2}. \tag{4.6}$$

4.2 Discretization with uniform mesh in 1D

In order to discretize the gradient flow equation (4.1), we divide the spatial interval $\Omega = [a,b]$ into N sub-intervals. Then, the mesh size h, time step k, spatial grid points x_j and time grid points t_n are given by

$$h = \Delta x = \frac{b-a}{N}, \qquad k = \Delta t > 0, \tag{4.7}$$

$$x_j = a + jh, \qquad j = 0,1,2,\ldots,N, \tag{4.8}$$

$$t_n = nk, \qquad n = 0,1,2,\ldots \tag{4.9}$$

Let $\phi_j^n \approx \phi(x_j, t_n)$, $\phi_j^* \approx \phi(x_j, t^* = t_{n+1}^-)$ and $V_j = V_1(x_j)$. In order to discretize the time derivative, we use the backward Euler scheme. For the spatial derivative, the second order central finite difference scheme is used. From time $t = t_n$ to $t = t^*$, the equation (4.1) is discretized as

$$\frac{\phi_j^* - \phi_j^n}{k} = \frac{\varepsilon^2}{2}\frac{\phi_{j-1}^* - 2\phi_j^* + \phi_{j+1}^*}{h^2} - V_j\phi_j^* - |\phi_j^n|^2\phi_j^*, \qquad (4.10)$$
$$j = 1, 2, \ldots, N-1,$$

with boundary conditions

$$\phi_0^* = \phi_N^* = 0.$$

At every time step, normalization step (4.2) is discretized as

$$\phi_j^{n+1} = \frac{\phi_j^*}{||\Phi^*||}, \qquad j = 1, 2, \ldots, N-1,$$
$$||\Phi^*|| = \sqrt{h\sum_{j=1}^{N-1}(\phi_j^*)^2},$$

with the initial condition (4.3) discretized as

$$\phi_j^0 = \phi_0(x_j), \qquad j = 0, 1, 2, \ldots, N.$$

The above is known as the backward Euler finite difference scheme (BEFD) and it preserves the energy diminishing property of the normalized gradient flow [4]. The method is implicit and the solution can be obtained by solving the following linear system using Thomas algorithm at every time step,

$$A\Phi^* = \Phi^n, \qquad (4.11)$$

where $\Phi^n \in \mathbb{R}^{N-1}$, $\Phi^* \in \mathbb{R}^{N-1}$ and A is a $(N-1)\times(N-1)$ symmetric tridiagonal matrix, i.e.

$$\Phi^* = \begin{pmatrix} \phi_1^* \\ \phi_2^* \\ \vdots \\ \phi_{N-2}^* \\ \phi_{N-1}^* \end{pmatrix}, \qquad \Phi^n = \begin{pmatrix} \phi_1^n \\ \phi_2^n \\ \vdots \\ \phi_{N-2}^n \\ \phi_{N-1}^n \end{pmatrix}, \tag{4.12}$$

$$A = \begin{pmatrix} d_1 & -\frac{\varepsilon^2 k}{2h^2} & 0 & \cdots & 0 & 0 & 0 \\ -\frac{\varepsilon^2 k}{2h^2} & d_2 & -\frac{\varepsilon^2 k}{2h^2} & \cdots & 0 & 0 & 0 \\ 0 & -\frac{\varepsilon^2 k}{2h^2} & d_3 & \cdots & 0 & 0 & 0 \\ \vdots & \vdots & \vdots & \ddots & \vdots & \vdots & \vdots \\ 0 & 0 & 0 & \cdots & d_{N-3} & -\frac{\varepsilon^2 k}{2h^2} & 0 \\ 0 & 0 & 0 & \cdots & -\frac{\varepsilon^2 k}{2h^2} & d_{N-2} & -\frac{\varepsilon^2 k}{2h^2} \\ 0 & 0 & 0 & \cdots & 0 & -\frac{\varepsilon^2 k}{2h^2} & d_{N-1} \end{pmatrix},$$

with the diagonal entries of A as

$$d_j = 1 + k\left(\frac{\varepsilon^2}{h^2} + V_j + |\phi_j^n|^2\right), \qquad j = 1, 2, \cdots, N-1. \tag{4.13}$$

After solving the linear system for Φ^* followed by normalization to obtain Φ^{n+1} for time t_{n+1}, we can repeat the same procedure to calculate the solution for the next time step. The energy functional is discretized as

$$\begin{aligned} E_\varepsilon(\phi) &= \int_a^b \left(\frac{\varepsilon^2}{2}|\phi_x(x)|^2 + V_1(x)|\phi(x)|^2 + \frac{1}{2}|\phi(x)|^4\right) dx \\ &= \sum_{j=1}^{N-1} \int_{x_j}^{x_{j+1}} \frac{\varepsilon^2}{2}|\phi_x(x)|^2 dx + \sum_{j=1}^{N-1} \int_{x_j}^{x_{j+1}} \left[V_1(x)|\phi(x)|^2 + \frac{1}{2}|\phi(x)|^4\right] dx \\ &\approx h\left[\sum_{j=1}^{N-1} \frac{\varepsilon^2}{2}\left(\frac{\phi_{j+1}-\phi_j}{h}\right)^2 + \sum_{j=1}^{N-1}\left(V_j|\phi_j|^2 + \frac{1}{2}|\phi_j|^4\right)\right]. \end{aligned} \tag{4.14}$$

Here, we used the composite midpoint rule for the first term and the composite trapezoidal quadrature rule for the second term. Both quadrature rules are second order accuracy. Similarly to energy, the chemical potential is discretized as

$$\begin{aligned}\mu_\varepsilon(\phi) &= \int_a^b \left(\frac{\varepsilon^2}{2}|\phi_x(x)|^2 + V_1(x)|\phi(x)|^2 + |\phi(x)|^4\right) dx \\ &= \sum_{j=1}^{N-1}\int_{x_j}^{x_{j+1}} \frac{\varepsilon^2}{2}|\phi_x(x)|^2 dx + \sum_{j=1}^{N-1}\int_{x_j}^{x_{j+1}} \left[V_1(x)|\phi(x)|^2 + |\phi(x)|^4\right] dx \\ &\approx h\left[\sum_{j=1}^{N-1}\frac{\varepsilon^2}{2}\left(\frac{\phi_{j+1}-\phi_j}{h}\right)^2 + \sum_{j=1}^{N-1}\left(V_j|\phi_j|^2 + |\phi_j|^4\right)\right]. \end{aligned} \tag{4.15}$$

4.3 Discretization with piecewise uniform mesh in 1D

In this section, we discretize the gradient flow equation (4.1) by adapting the piecewise uniform mesh proposed by Shishkin [42] for the singular perturbed two-point boundary value problem. We divide the spatial interval $\Omega = [a, b]$ into N subintervals, i.e., $a = x_0^* < x_1^* < ... < x_N^* = b$ is a partition of the interval $[a, b]$. Let $\triangle x_j = x_{j+1}^* - x_j^*$ for $j = 0, 1, ..., N-1$. The piecewise uniform mesh $\{x_j^*\}_{j=0}^N$ for the interval [a,b] will be adapted to the features of the solution, i.e., there will be more mesh points in regions where there are boundary or interior layers.

4.3.1 The full discretization with piecewise uniform mesh

Based on the new mesh, assuming that $\phi_j^* \approx \phi(x_j^*, t^* = t_{n+1}^-)$ and $\phi_j^n \approx \phi(x_j^*, t_n)$, the numerical scheme to discretize the gradient flow equation (4.1) at time $t^* = t_{n+1}^-$ is given by

$$\begin{aligned}\frac{\phi_j^* - \phi_j^n}{k} &= \frac{\varepsilon^2}{2}\left(\frac{2\phi_{j-1}^*}{\Delta x_{j-1}(\Delta x_{j-1} + \Delta x_j)} - \frac{2\phi_j^*}{\Delta x_{j-1}\Delta x_j} + \frac{2\phi_{j+1}^*}{\Delta x_j(\Delta x_{j-1} + \Delta x_j)}\right) \\ &- V_j\phi_j^* - |\phi_j^n|^2\phi_j^*, \qquad j = 1, 2, \ldots, N-1, \end{aligned} \tag{4.16}$$

with boundary conditions

$$\phi_0^* = \phi_N^* = 0. \tag{4.17}$$

V_j and Δx_j are defined as

$$V_j = V_1(x_j^*), \quad \Delta x_j = x_{j+1}^* - x_j^*, \quad j = 0, 1, 2, \ldots, N. \tag{4.18}$$

At every time step, normalization of the solution is done by letting

$$\phi_j^{n+1} = \frac{\phi_j^*}{||\Phi^*||}, \quad j = 0, 1, 2, \ldots, N. \tag{4.19}$$

$$\begin{aligned} \|\Phi^*\|^2 &= \int_a^b (\phi^*(x))^2 dx = \sum_{j=0}^{N-1} \int_{x_j}^{x_{j+1}} (\phi^*(x))^2 dx \approx \sum_{j=0}^{N-1} \left[(\phi_j^*)^2 + (\phi_{j+1}^*)^2\right] \frac{\Delta x_j}{2} \\ &= \sum_{j=1}^{N-1} \left[\frac{\Delta x_j + \Delta x_{j-1}}{2} (\phi_j^*)^2\right]. \end{aligned} \tag{4.20}$$

Similarly, here we can solve the linear system by using the Thomas algorithm,

$$A\Phi^* = \Phi^n, \tag{4.21}$$

where $\Phi^n \in \mathbb{R}^{N-1}$ and $\Phi^* \in \mathbb{R}^{N-1}$ and A is a $(N-1)\times(N-1)$ symmetric tridiagonal matrix

$$\Phi^* = \begin{pmatrix} \phi_1^* \\ \phi_2^* \\ \vdots \\ \phi_{N-2}^* \\ \phi_{N-1}^* \end{pmatrix}, \qquad \Phi^n = \begin{pmatrix} \phi_1^n \\ \phi_2^n \\ \vdots \\ \phi_{N-2}^n \\ \phi_{N-1}^n \end{pmatrix},$$

$$A = \begin{pmatrix} d_1 & e_1 & 0 & \cdots & 0 & 0 & 0 \\ c_2 & d_2 & e_2 & \cdots & 0 & 0 & 0 \\ 0 & c_3 & d_3 & \cdots & 0 & 0 & 0 \\ \vdots & \vdots & \vdots & \ddots & \vdots & \vdots & \vdots \\ 0 & 0 & 0 & \cdots & d_{N-3} & e_{N-3} & 0 \\ 0 & 0 & 0 & \cdots & c_{N-2} & d_{N-2} & e_{N-2} \\ 0 & 0 & 0 & \cdots & 0 & c_{N-1} & d_{N-1} \end{pmatrix},$$

with the matrix entries of A as

$$\begin{aligned} c_j &= \frac{-\varepsilon^2 k}{\Delta x_{j-1}(\Delta x_{j-1} + \Delta x_j)}, \quad j = 2, 3, \cdots, N-1, \\ d_j &= 1 + k\left(\frac{\varepsilon^2}{\Delta x_{j-1}\Delta x_j} + V_j + |\phi_j^n|^2\right), \quad j = 1, 2, \cdots, N-1, \\ e_j &= \frac{-\varepsilon^2 k}{\Delta x_j(\Delta x_{j-1} + \Delta x_j)}, \quad j = 1, 2, \cdots, N-2. \end{aligned}$$

Similarly, we can calculate the discretized energy as follows

$$\begin{aligned} E_\varepsilon(\phi) &= \int_a^b \frac{\varepsilon^2}{2}|\phi_x(x)|^2 dx + \int_a^b \left[V_1(x)|\phi(x)|^2 + \frac{1}{2}|\phi(x)|^4\right] dx \\ &\approx \sum_{j=1}^{N-1} \frac{\varepsilon^2 \Delta x_j}{2}\left(\frac{\phi_{j+1} - \phi_j}{\Delta x_j}\right)^2 + \sum_{j=1}^{N-1} \frac{\Delta x_j + \Delta x_{j-1}}{2}\left(V_j^*|\phi_j|^2 + \frac{1}{2}|\phi_j|^4\right). \end{aligned} \tag{4.22}$$

Again, here we used the composite midpoint rule for the first term and the composite trapezoidal quadrature rule for the second term. Both quadrature rules are second order accuracy. Similarly, the chemical potential is discretized as

$$\begin{aligned} \mu_\varepsilon(\phi) &= \int_a^b \frac{\varepsilon^2}{2}|\phi_x|^2 dx + \int_a^b V_1|\phi|^2 + |\phi|^4 \, dx \\ &\approx \sum_{j=1}^{N-1} \frac{\varepsilon^2 \Delta x_j}{2}\left(\frac{\phi_{j+1} - \phi_j}{\Delta x_j}\right)^2 + \sum_{j=1}^{N-1} \frac{\Delta x_j + \Delta x_{j-1}}{2}\left(V_j^*|\phi_j|^2 + |\phi_j|^4\right). \end{aligned} \tag{4.23}$$

4.3.2 Piecewise uniform mesh for ground state with box potential

Recall from the subsection 3.2.2, we know that for BEC in ground state of box potential, there are boundary layers in the region near $x = 0$ and $x = 1$ and that the width of these boundary layers are of $\mathrm{O}(\varepsilon)$. Taking $[a, b] = [0, 1]$ for computation, we choose the mesh as

$$\begin{cases} x_j^* = x_{j-1}^* + h_1, & 0 < j \leq N/4, \\ x_j^* = x_{j-1}^* + h_2, & N/4 < j \leq 3N/4, \\ x_j^* = x_{j-1}^* + h_1, & 3N/4 < j \leq N, \end{cases} \tag{4.24}$$

where

$$\begin{aligned} & x_{N/4}^* = \min\left\{\frac{1}{4}, \varepsilon \ln N\right\}, \\ & x_{3N/4}^* = 1 - x_{N/4}^*, \\ & h_1 = \frac{4x_{N/4}^*}{N}, \quad h_2 = \frac{2(x_{3N/4}^* - x_{N/4}^*)}{N}. \end{aligned} \tag{4.25}$$

In fact, we have used $\frac{N}{4}$ points for the boundary layer near $x = 0$, $\frac{N}{4}$ points for the boundary layer near $x = 1$, and $\frac{N}{2}$ points for the remaining middle portion of the interval [0,1].

4.3.3 Piecewise uniform mesh for first excited state with box potential

Recall from the subsection 3.2.3, we know that for BEC in the first excited state of box potential, there are boundary layers in the region near $x = 0$ and $x = 1$ and one interior layer in the region at $x = 0.5$. By taking $[a, b] = [0, 1]$ for computation,

we choose the mesh as

$$\begin{cases} x_j^* = x_{j-1}^* + h_1, & 0 < j \leq N/8. \\ x_j^* = x_{j-1}^* + h_2, & N/8 < j \leq 3N/8. \\ x_j^* = x_{j-1}^* + h_1, & 3N/8 < j \leq 5/8. \\ x_j^* = x_{j-1}^* + h_2, & 5N/8 < j \leq 7N/8. \\ x_j^* = x_{j-1}^* + h_1, & 7N/8 < j \leq N, \end{cases} \tag{4.26}$$

where

$$\begin{aligned} x_{N/8}^* &= \min\left\{\frac{1}{8}, \varepsilon \ln N\right\}, \\ x_{3N/8}^* &= \frac{1}{2} - x_{N/8}^*, \\ x_{5N/8}^* &= \frac{1}{2} + x_{N/8}^*, \\ x_{7N/8}^* &= 1 - x_{N/8}^*. \\ h_1 &= \frac{8x_{N/8}^*}{N}, \quad h_2 = \frac{4(x_{3N/8}^* - x_{N/8}^*)}{N}. \end{aligned} \tag{4.27}$$

In fact, we have used $\frac{N}{8}$ points for the boundary layer near $x = 0$, $\frac{N}{8}$ points for the boundary layer near $x = 1$, $\frac{N}{4}$ points for the interior layer near $x = 0.5$ and the remaining $\frac{N}{2}$ points for the remaining portion of the interval [0,1] which do not contain any boundary or interior layers. By extending the above idea, we can obtain the piecewise uniform mesh for the other excited states in box potential.

4.3.4 Piecewise uniform mesh for first excited state with harmonic potential

Recall from the subsection 3.3.3, we know that for the first excited state of BEC with harmonic potential, there is an interior layer in the region of $x = 0$ when $0 < \varepsilon \ll 1$.

Taking $[a,b]=[-c,c]$ for computation, we choose the mesh as

$$\begin{cases} x_j^* = x_{j-1}^* + h_2, & 0 < j \le N/4, \\ x_j^* = x_{j-1}^* + h_1, & N/4 < j \le 3N/4, \\ x_j^* = x_{j-1}^* + h_2, & 3N/4 < j \le N, \end{cases} \tag{4.28}$$

where

$$\begin{aligned} & x_0^* = -c < 0, \qquad x_N^* = c > 0, \\ & x_{N/4}^* = -\min\left\{\frac{c}{2}, \varepsilon \ln N\right\}, \\ & x_{3N/4}^* = 0 - x_{N/4}^*, \\ & h_1 = \frac{|x_{N/4}^*|}{N}, \quad h_2 = \frac{2(c + x_{N/4}^*)}{N}. \end{aligned} \tag{4.29}$$

In fact, we have used $\frac{N}{2}$ points for the interior layer near $x=0$ and the remaining $\frac{N}{2}$ points for the remaining portion of the interval [-c,c] which do not contain any boundary or interior layers.

4.4 Choice of initial data

In this section, we apply the proposed adaptive numerical scheme to solve the singularly perturbed nonlinear eigenvalue problems (3.8) under the constraint (3.9) in 1D. We consider the following cases:

1. Ground state of BEC in 1D box potential;

2. First, third and ninth excited states of BEC in 1D box potential;

3. First excited state of BEC in 1D harmonic potential.

The initial data are carefully chosen for different potentials. For the box potential, the problem is solved on $\Omega=[0,1]$. The initial condition in (4.3) for finding

the ground state is taken as

$$\phi_0(x) = \sqrt{2}\sin(\pi x), \qquad x \in [0,1], \tag{4.30}$$

and the boundary conditions are

$$\phi(0,t) = \phi(1,t) = 0. \tag{4.31}$$

In order to obtain the kth excited state, we choose the initial conditions in (4.3) as

$$\phi_0(x) = \sqrt{2}\sin((k+1)\pi x), \qquad x \in [0,1], \tag{4.32}$$

and the boundary conditions is the same as (4.31).

For the harmonic potential, the problem is solved on $\Omega = [-c, c]$ (where c is some large enough positive constant). The initial condition for finding the first excited state in (4.3) is taken as

$$\phi_0(x) = x\frac{e^{-x^2/2}}{\pi^{1/4}}, \tag{4.33}$$

and the boundary conditions are $\phi(-c,t) = \phi(c,t) = 0$.

In our numerical calculations presented in the next three sections, an "exact" solution $\phi(x)$ is defined as a solution generated using our adaptive schemes with $2^{14}+1$ mesh points. This solution $\phi(x)$ is used as the basis to validate the numerical accuracy of the solutions obtained by using the piecewise uniform mesh or uniform mesh methods.

Let $\phi_{\varepsilon,N}(x)$ be the numerical solution with parameters ε and $N+1$ mesh points. In the next three sections, error plots refer to the plot of $|\phi(x)-\phi_{\varepsilon,N}(x)|$ for different ε and N values using the two different meshes presented in this chapter.

4.5 Error analysis of uniform mesh

In this section, by means of the scheme based on uniform mesh, we calculate and compare the ground state of BEC with box potential, first excited state of BEC with box potential and first excited state of BEC with harmonic potential.

For the results related to ground state of BEC with box potential based on the uniform mesh scheme, we refer to Figure 4.1 and Figure 4.2. We observe that most of the errors are concentrated near the boundary i.e., near $x = 0$ and $x = 1$. This is expected as there are boundary layers at $x = 0$ and $x = 1$. When ε becomes smaller, the pointwise errors increase. When more mesh points are used, the pointwise errors in general are reduced. However, this reduction is very insignificant for smaller values of ε.

For the results related to first excited state of BEC with box potential based on the uniform mesh scheme, we refer to Figure 4.3 and Figure 4.4. The results are similar to results of the ground state of BEC with box potential. We observe that most of the errors are concentrated near the boundary, i.e., near $x = 0$ and $x = 1$ and near $x = 0.5$. This is expected as there are boundary layers at $x = 0$ and $x = 1$ and an interior layer exist at $x = 0.5$. When ε becomes smaller, the pointwise errors increase. When more mesh points are used, the pointwise errors in general are reduced. However, this reduction is very insignificant for smaller values of ε.

For the results related to first excited state of BEC with harmonic potential based on the uniform mesh scheme, we refer to Figure 4.5 and Figure 4.6. We observe that the largest errors are concentrated near $x = 0$ and the rest of the errors are concentrated at $x = -1.2$ and $x = 1.2$. This is expected as an interior layer exists at $x = 0$. The second largest errors are mainly at $x = -1.2$ and $x = 1.2$ because the gradient of $\phi(x)$ at those points are steep. When ε becomes smaller, the change in errors is not noticeable. When more mesh points are used, the pointwise errors in

general are reduced. However, this reduction is very insignificant for smaller values of ε, especially near $x = 0$ where there is an interior layer.

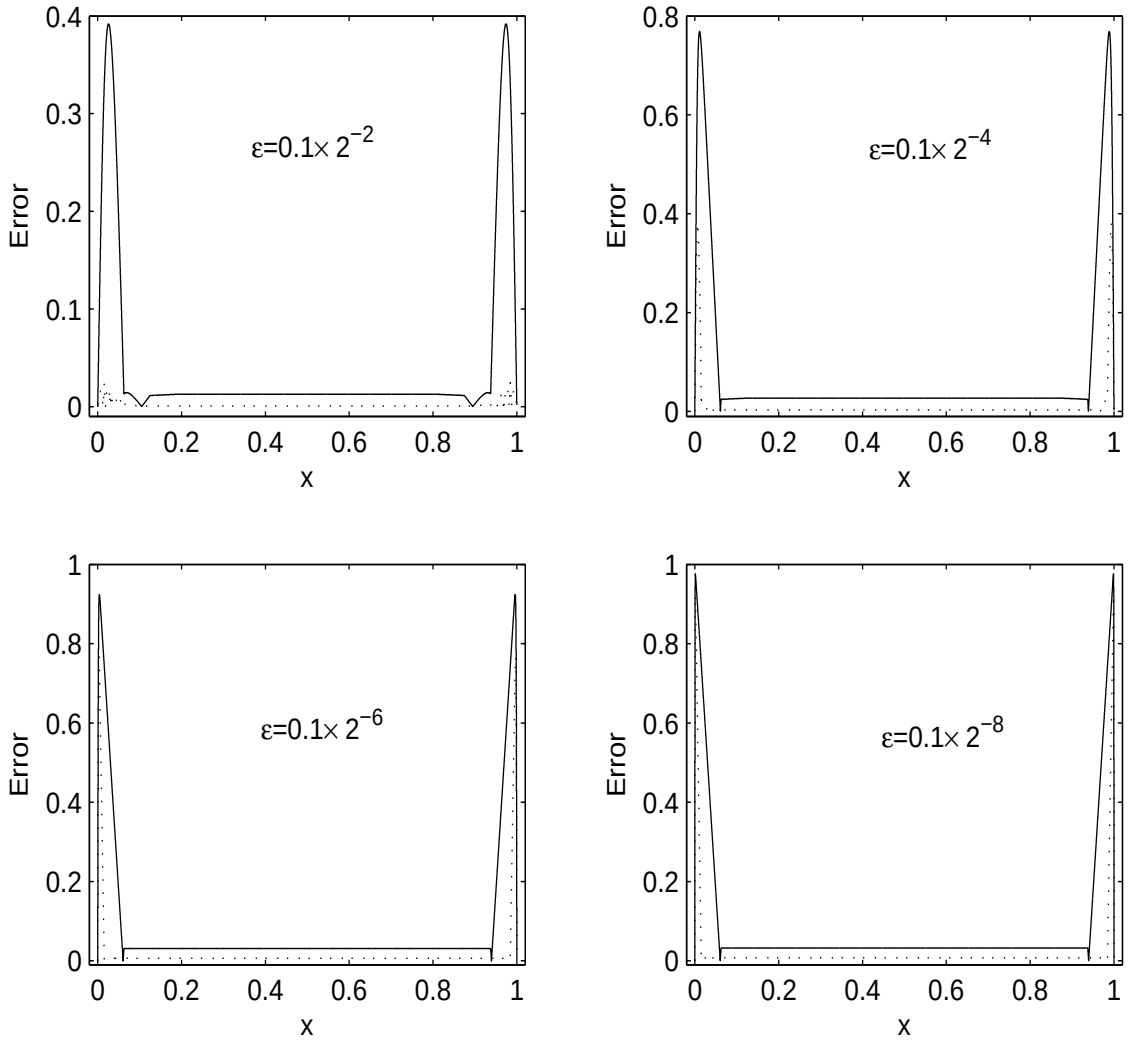

Figure 4.1: Error plot for ground state of BEC in box potential with fixed mesh points using uniform mesh scheme. N, the total number of mesh points used is $N = 2^4 + 1$ (full line) and $N = 2^6 + 1$ (dotted line). A comparison is made for increasing values of ε from $\varepsilon = 0.1 \times 2^{-8}$ to $\varepsilon = 0.1 \times 2^{-2}$.

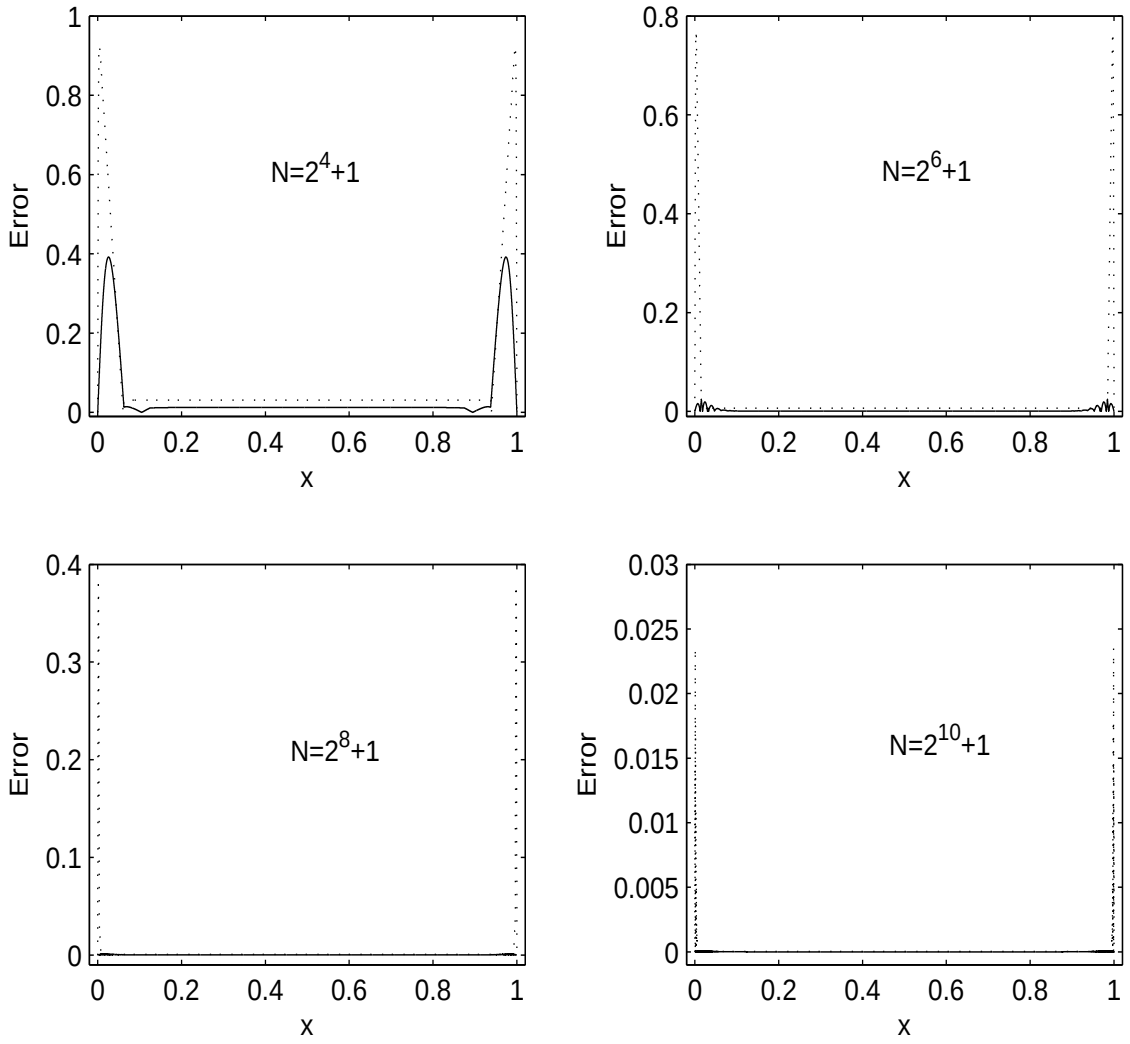

Figure 4.2: Error plot for ground state of BEC in box potential with fixed ε values using uniform mesh scheme. The ε values used are $\varepsilon = 0.1 \times 2^{-2}$ (full line) and $\varepsilon = 0.1 \times 2^{-6}$ (dotted line). A comparison is made for increasing values of N, the total number of mesh points used from $N = 2^4 + 1$ to $N = 2^{10} + 1$.

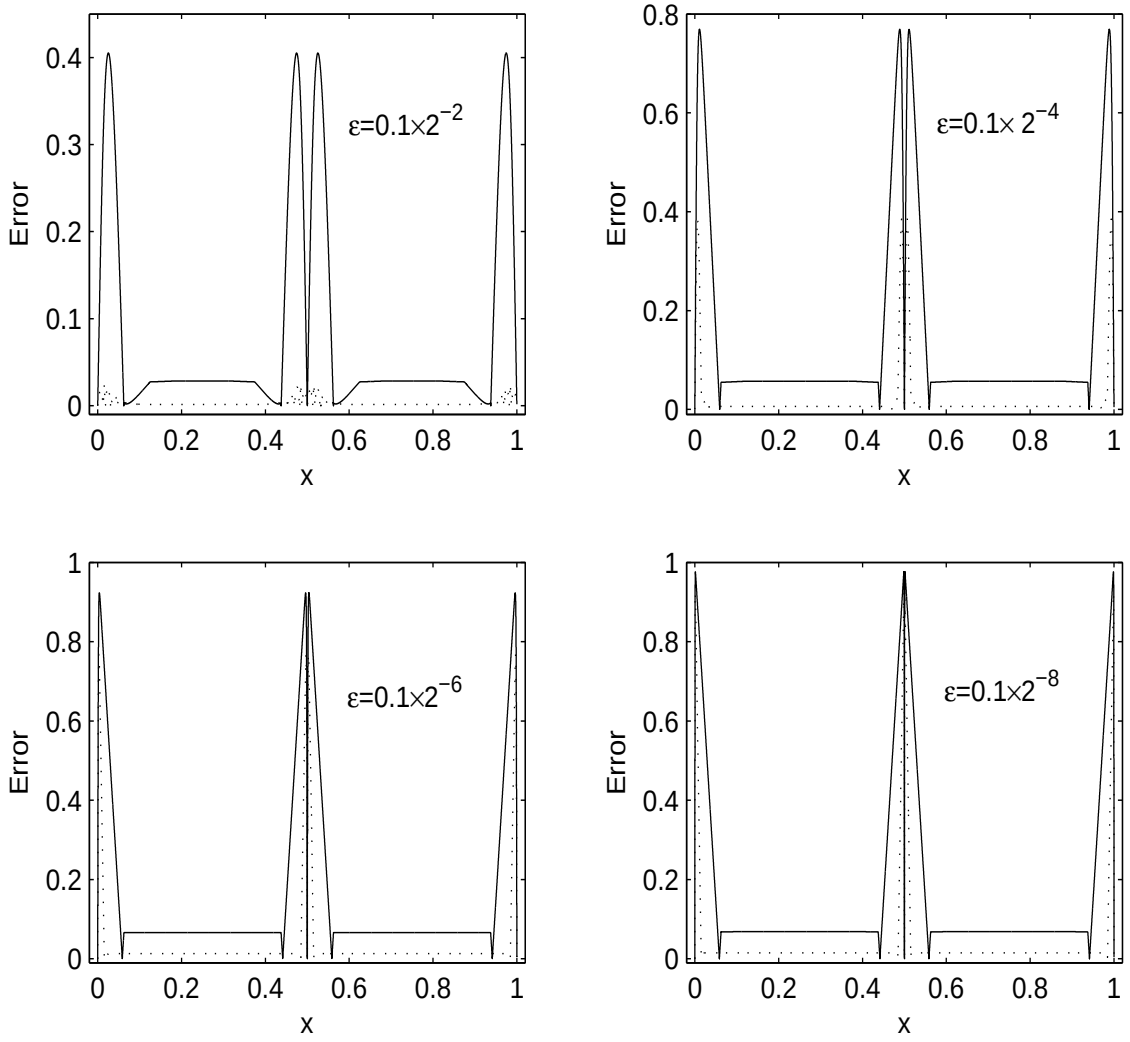

Figure 4.3: Error plot for first excited state of BEC in box potential with fixed mesh points using uniform mesh scheme. N, the total number of mesh points used is $N = 2^4 + 1$ (full line) and $N = 2^6 + 1$ (dotted line). A comparison is made for increasing values of ε from $\varepsilon = 0.1 \times 2^{-8}$ to $\varepsilon = 0.1 \times 2^{-2}$.

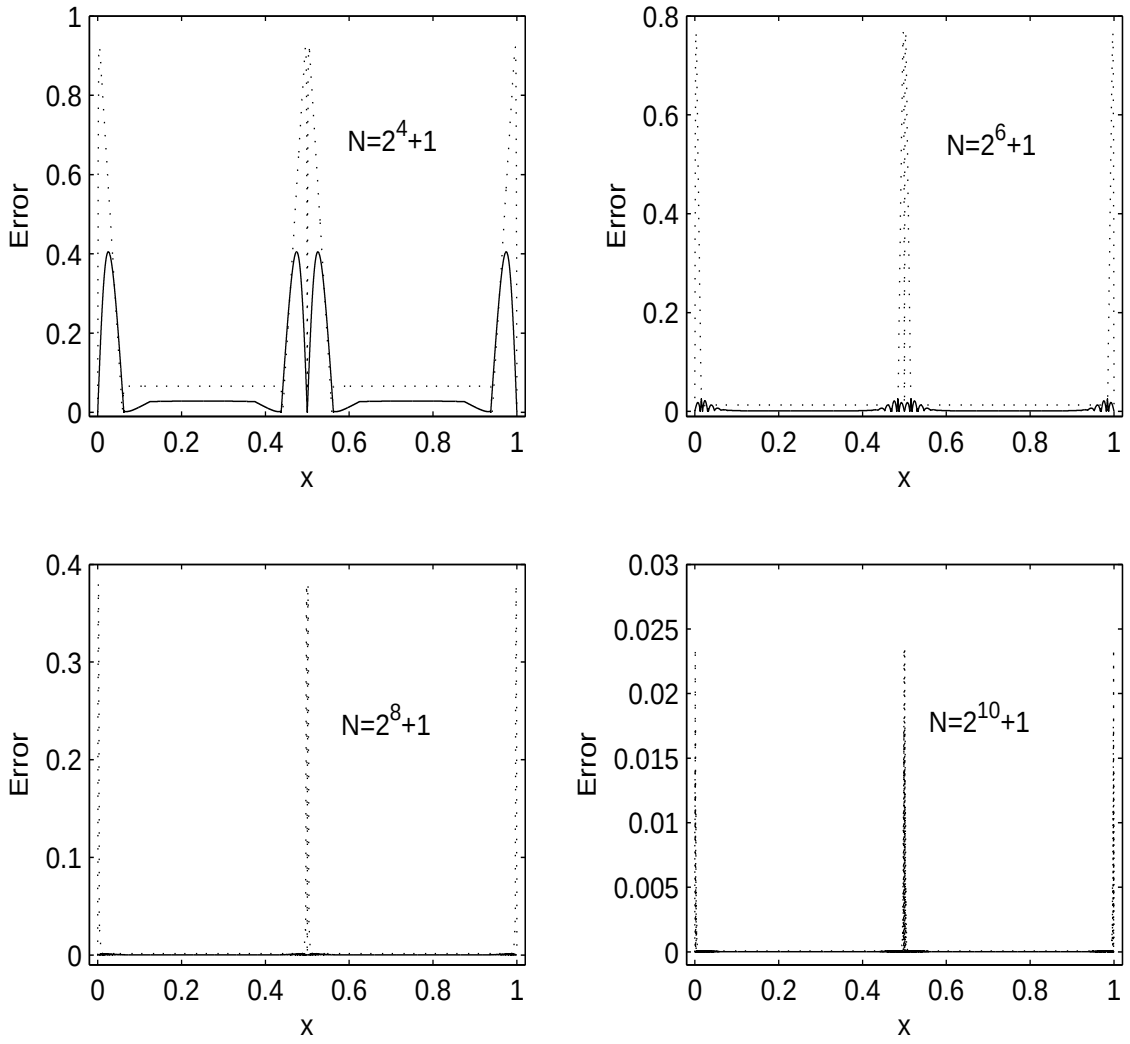

Figure 4.4: Error plot for first excited state of BEC in box potential with fixed ε values using uniform mesh scheme. The ε values used are $\varepsilon = 0.1 \times 2^{-2}$ (full line) and $\varepsilon = 0.1 \times 2^{-6}$ (dotted line). A comparison is made for increasing values of N, the total number of mesh points used from $N = 2^4 + 1$ to $N = 2^{10} + 1$.

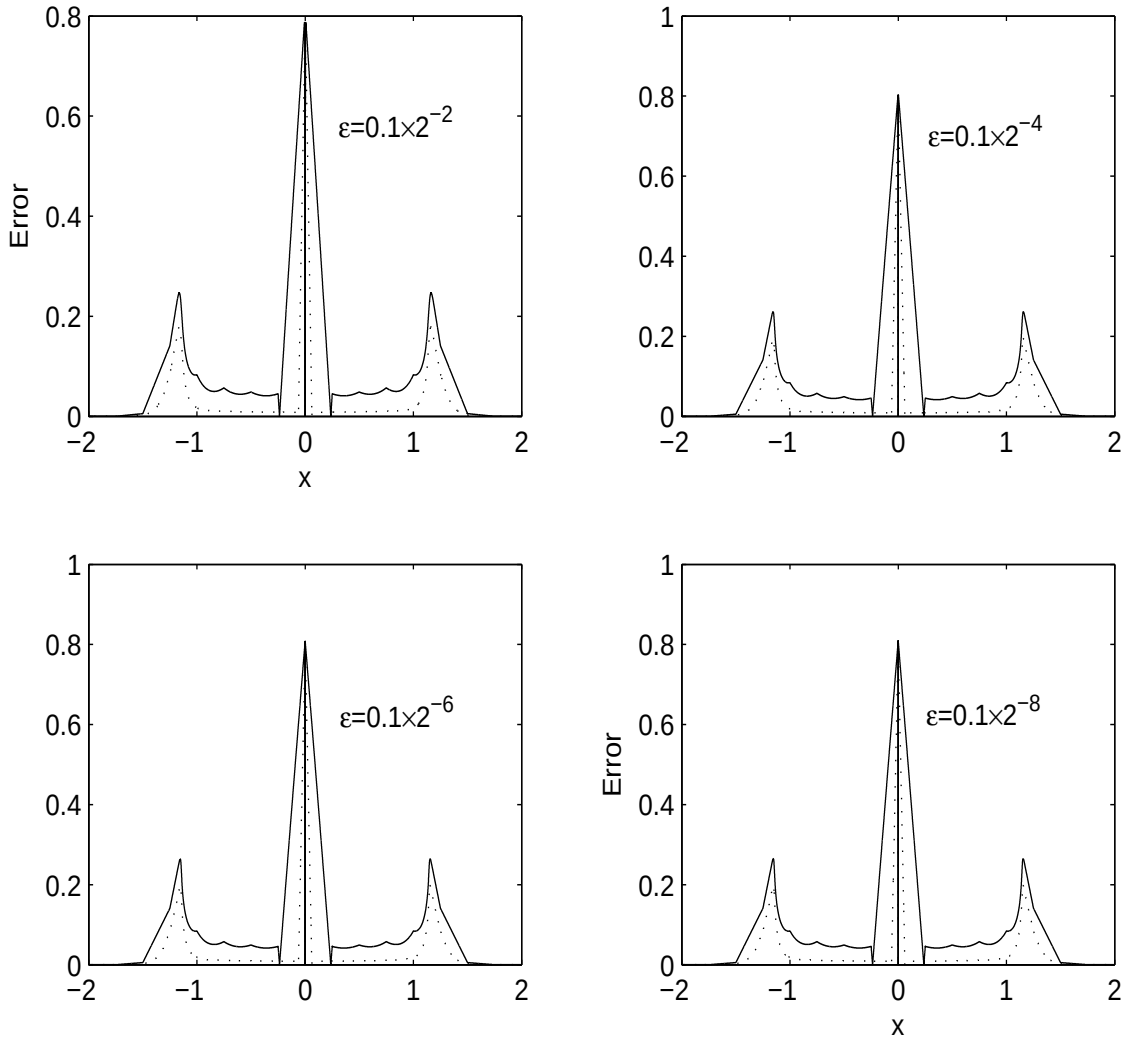

Figure 4.5: Error plot for first excited state of BEC in harmonic potential with fixed mesh points using uniform mesh scheme. N, the total number of mesh points used is $N = 2^4 + 1$ (full line) and $N = 2^6 + 1$ (dotted line). A comparison is made for increasing values of ε from $\varepsilon = 0.1 \times 2^{-8}$ to $\varepsilon = 0.1 \times 2^{-2}$.

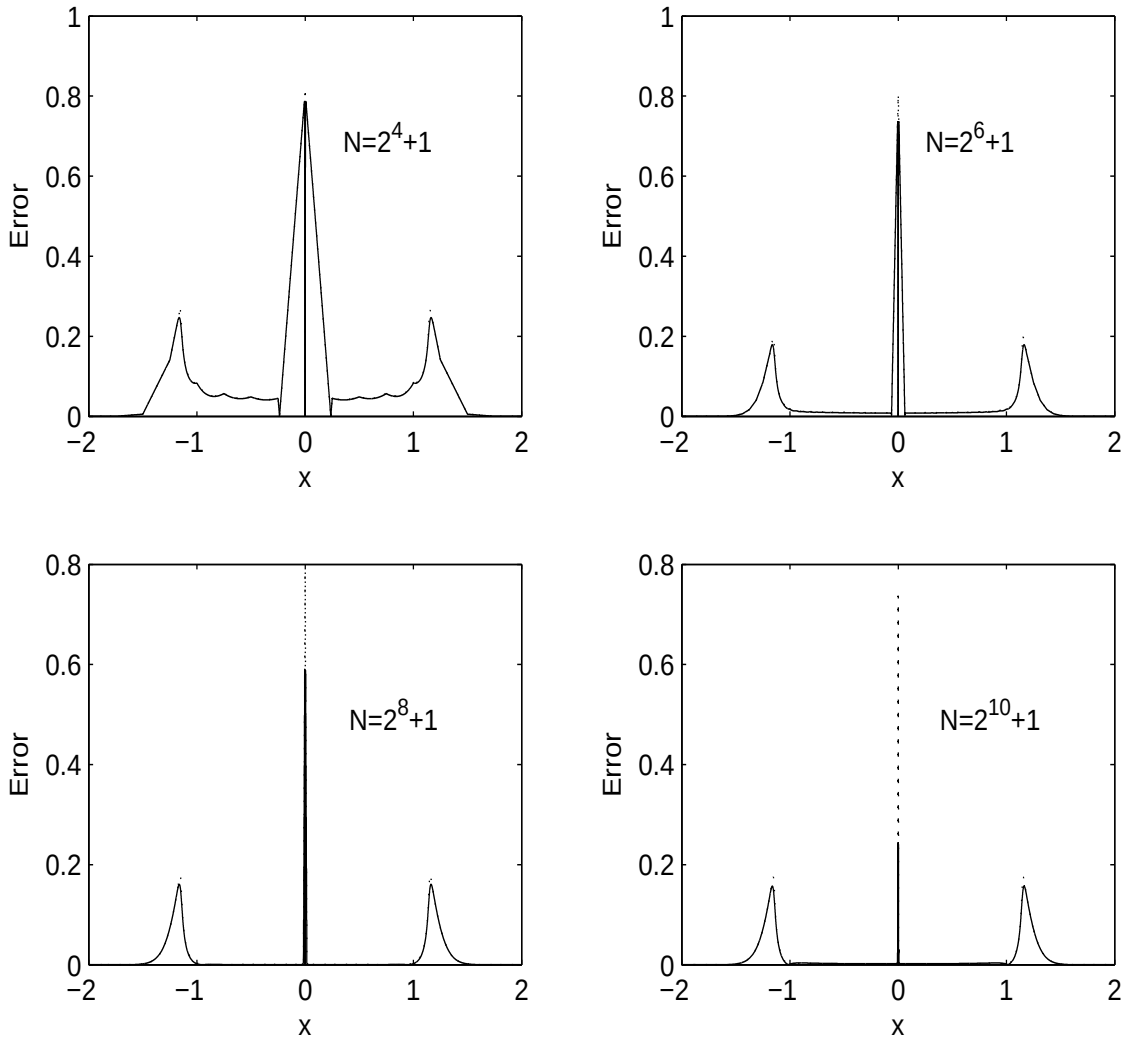

Figure 4.6: Error plot for first excited state of BEC in harmonic potential with fixed ε using uniform mesh scheme. The ε values used are $\varepsilon = 0.1 \times 2^{-2}$ (full line) and $\varepsilon = 0.1 \times 2^{-6}$ (dotted line). A comparison is made for increasing values of N, the total number of mesh points used from $N = 2^4 + 1$ to $N = 2^{10} + 1$.

4.6 Error analysis of piecewise uniform mesh

In this section, by means of the scheme based on piecewise uniform mesh, we calculate and compute the ground state of BEC with box potential, first excited state of BEC with box potential and first excited state of BEC with harmonic potential.

For the results related to ground state of BEC with box potential based on the piecewise uniform mesh scheme, we refer to Figure 4.7 and Figure 4.8. We observe that most of the errors are concentrated near the boundary i.e., near $x = 0$ and $x = 1$. This is expected as there are boundary layers at $x = 0$ and $x = 1$. When ε becomes smaller, the maximum error remained unchanged near 0.028. When more mesh points are used, the maximum errors at the boundary layers are significantly reduced.

For the results related to first excited state of BEC with box potential based on the piecewise uniform mesh scheme, we refer to Figure 4.9 and Figure 4.10. We observe that most of the errors are concentrated near $x = 0$, $x = 0.5$ and $x = 1$. This is expected as there are boundary layers at $x = 0$ and $x = 1$ and an interior layer at $x = 0.5$. When ε becomes smaller, the maximum error remained unchanged near 0.17. When more mesh points are used, the maximum errors at the boundary and interior layers are significantly reduced.

For the results related to first excited state of BEC with harmonic potential based on the piecewise uniform mesh scheme, we refer to Figure 4.11 and Figure 4.12. We observe that the largest errors are concentrated near $x = -1.2$ and $x = 1.2$. Using the piecewise uniform has significantly reduced the errors at the interior layer. When ε becomes smaller, the maximum error remained unchanged near 0.27. When more mesh points are used, the maximum errors at the boundary and interior layers are significantly reduced.

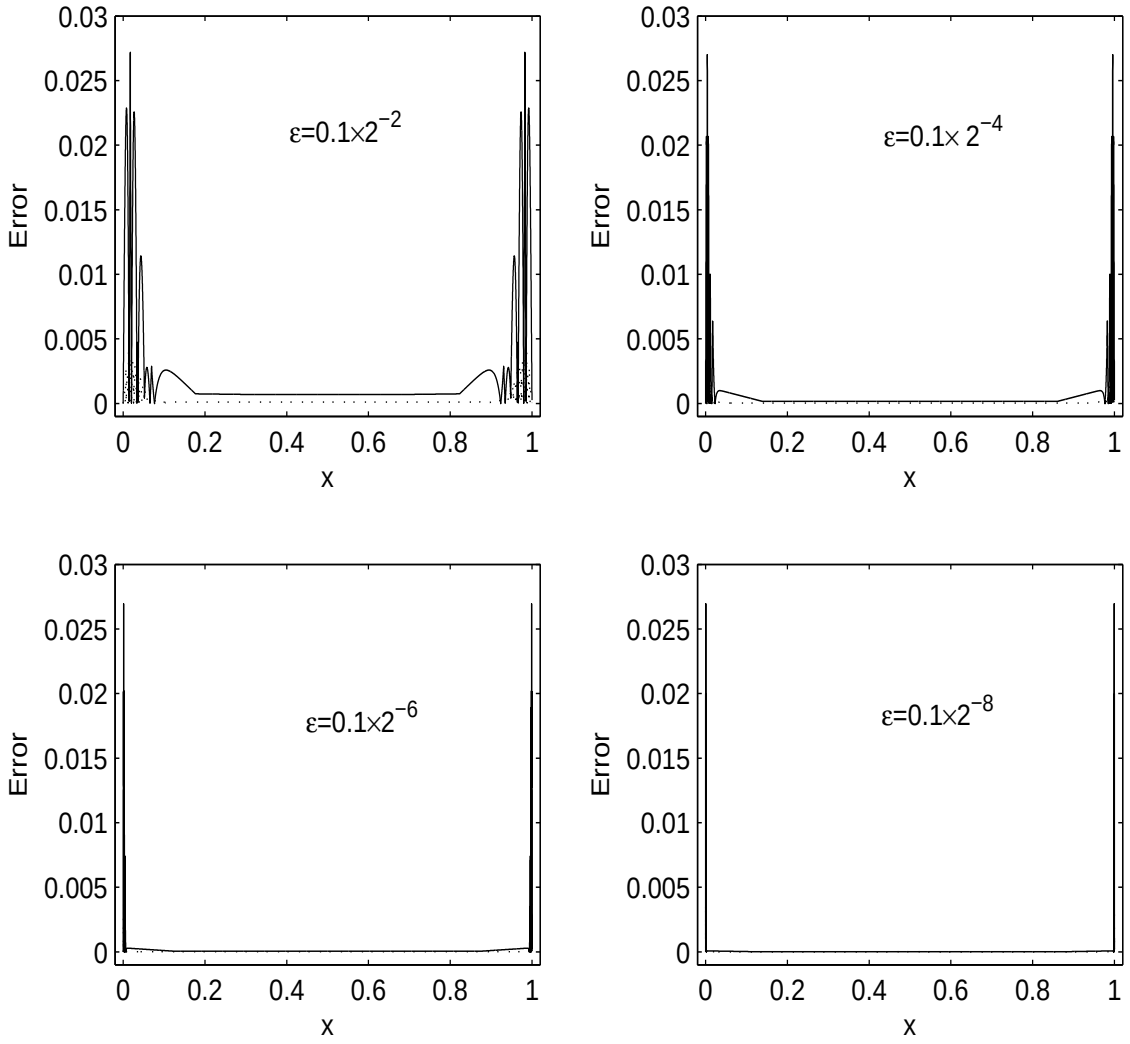

Figure 4.7: Error plot for first excited state of BEC in box potential with fixed mesh points using piecewise uniform mesh scheme. N, the total number of mesh points used is $N = 2^4 + 1$ (full line) and $N = 2^6 + 1$ (dotted line). A comparison is made for increasing values of ε from $\varepsilon = 0.1 \times 2^{-8}$ to $\varepsilon = 0.1 \times 2^{-2}$.

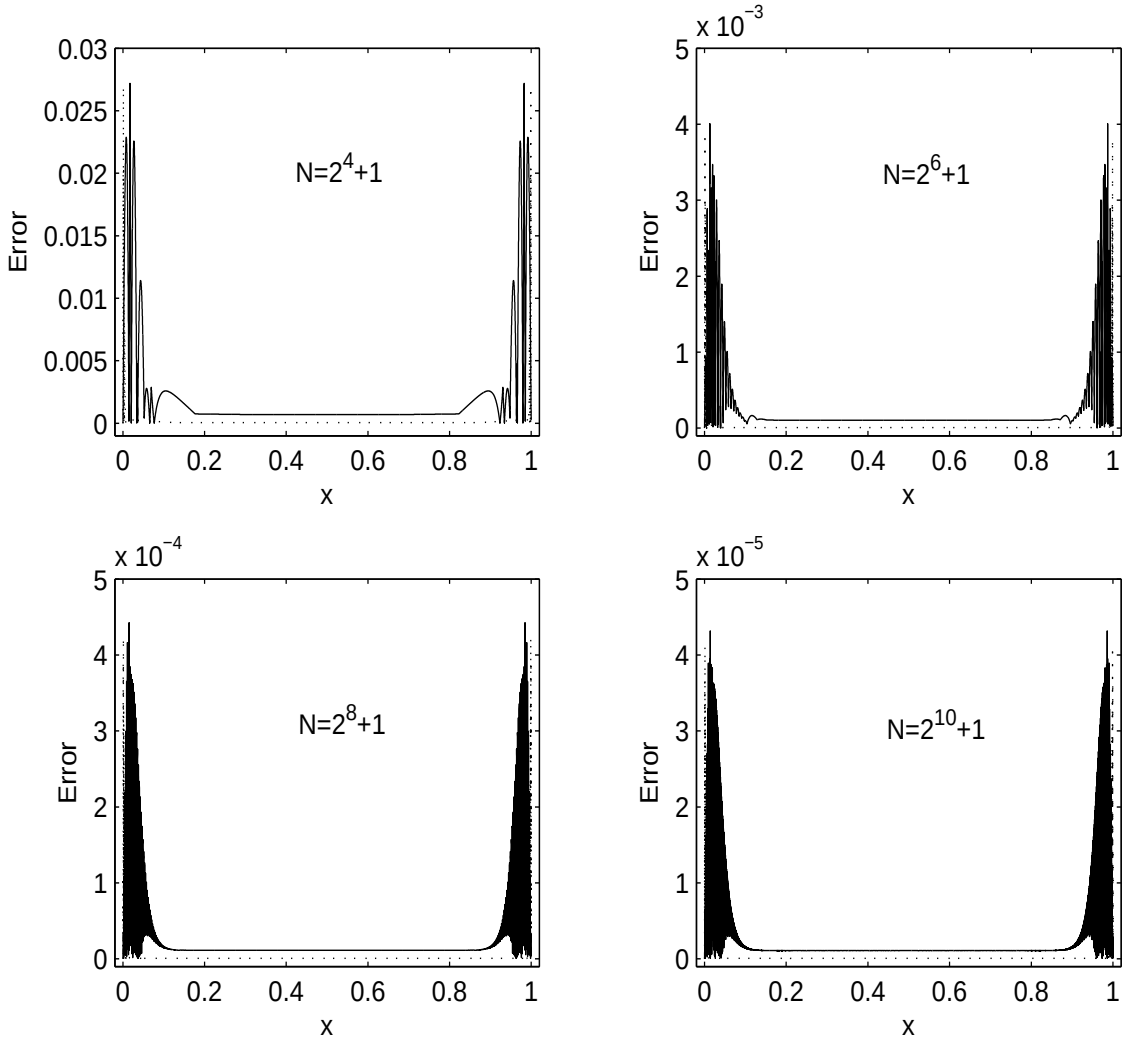

Figure 4.8: Error plot for ground state of BEC in box potential with fixed ε values using piecewise uniform mesh scheme. The ε values used are $\varepsilon = 0.1 \times 2^{-2}$ (full line) and $\varepsilon = 0.1 \times 2^{-6}$ (dotted line). A comparison is made for increasing values of N, the total number of mesh points used from $N = 2^4 + 1$ to $N = 2^{10} + 1$.

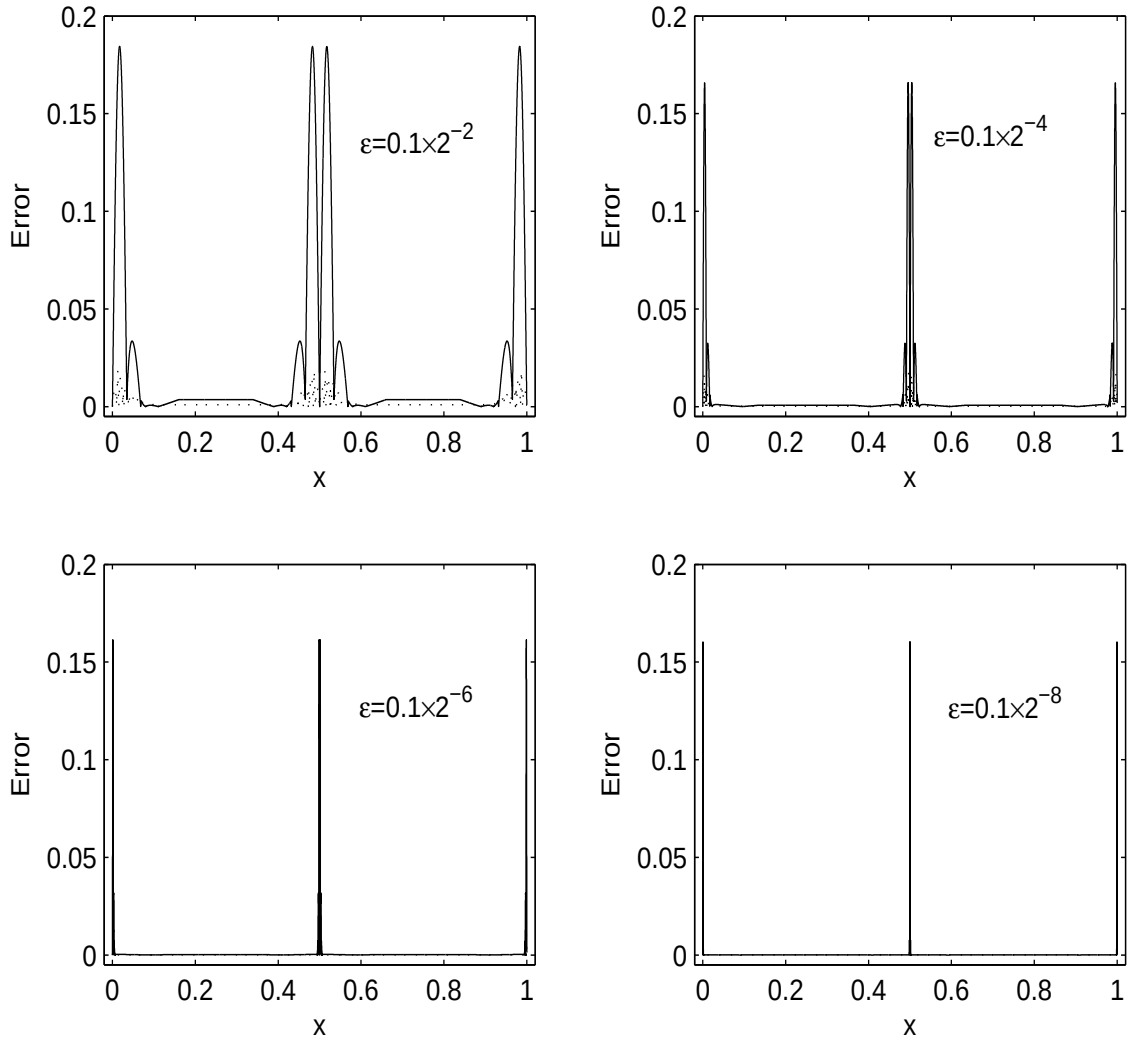

Figure 4.9: Error plot for first excited state of BEC in box potential with fixed mesh points using piecewise uniform mesh scheme. N, the total number of mesh points used is $N = 2^4 + 1$ (full line) and $N = 2^6 + 1$ (dotted line). A comparison is made for increasing values of ε from $\varepsilon = 0.1 \times 2^{-8}$ to $\varepsilon = 0.1 \times 2^{-2}$.

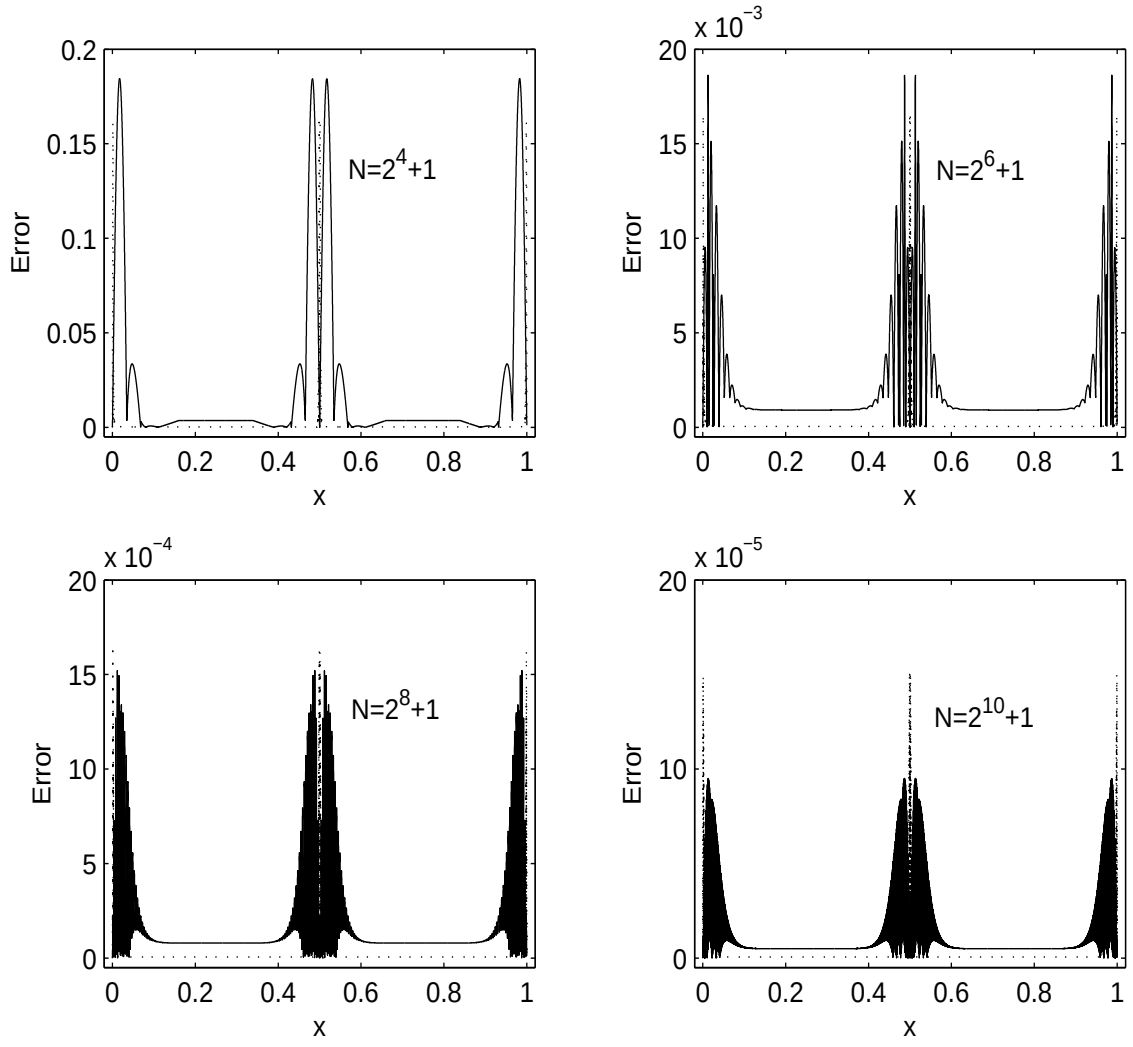

Figure 4.10: Error plot for first excited state of BEC in box potential with fixed ε values using piecewise uniform mesh scheme. The ε values used are $\varepsilon = 0.1 \times 2^{-2}$ (full line) and $\varepsilon = 0.1 \times 2^{-6}$ (dotted line). A comparison is made for increasing values of N, the total number of mesh points used from $N = 2^4 + 1$ to $N = 2^{10} + 1$.

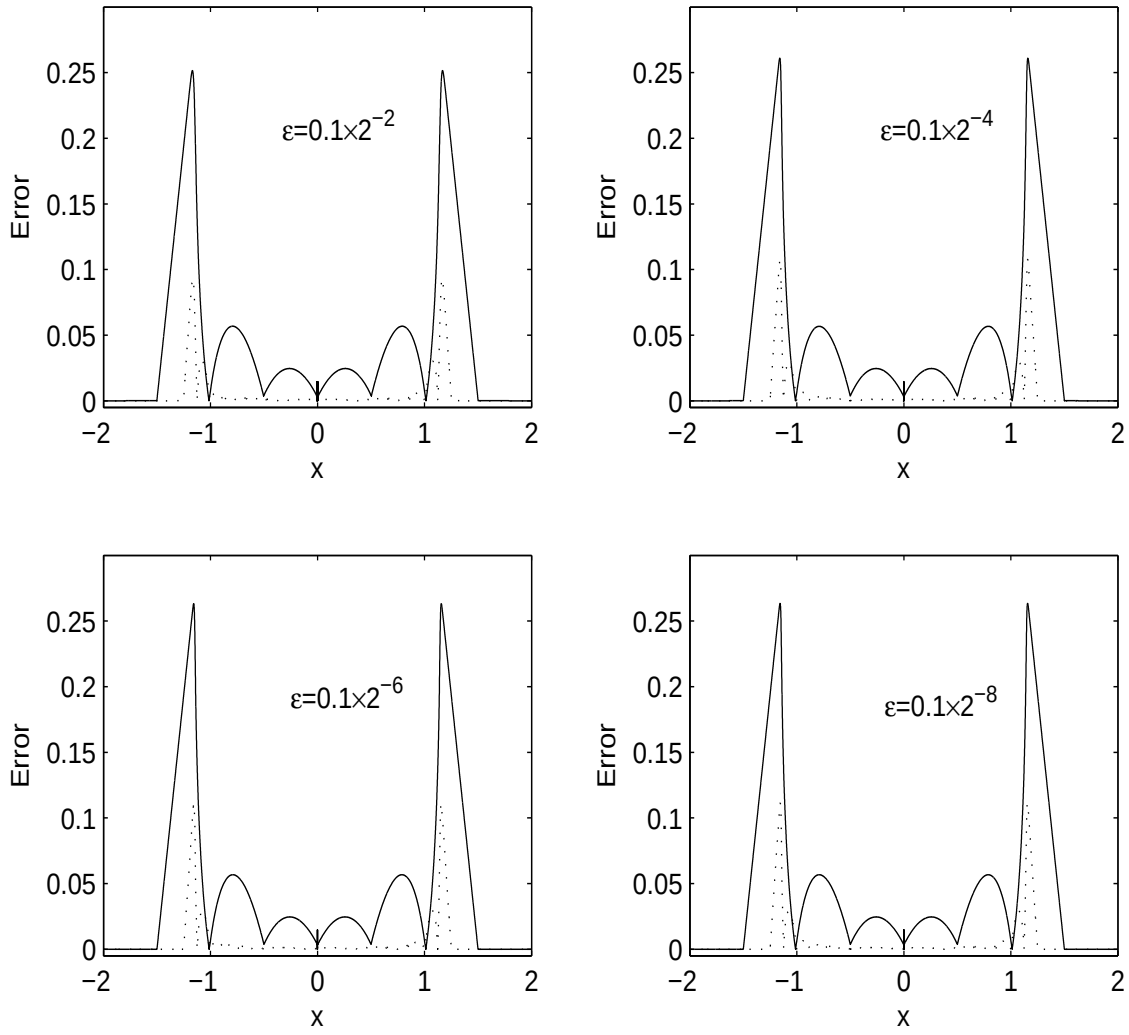

Figure 4.11: Error plot for first excited state of BEC in harmonic potential with fixed mesh points using piecewise uniform mesh scheme. N, the total number of mesh points used is $N = 2^4+1$ (full line) and $N = 2^6+1$ (dotted line). A comparison is made for increasing values of ε from $\varepsilon = 0.1 \times 2^{-8}$ to $\varepsilon = 0.1 \times 2^{-2}$.

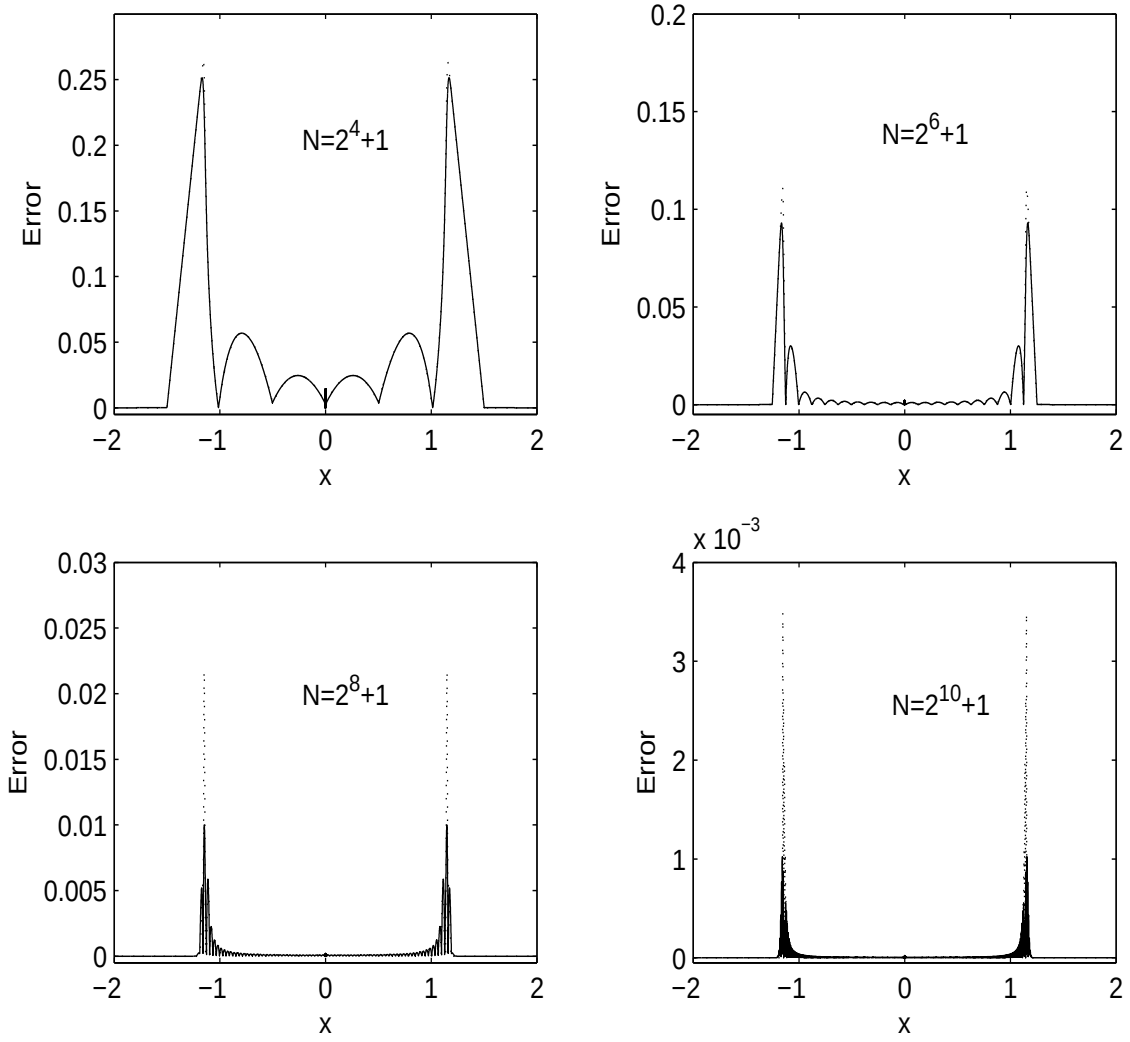

Figure 4.12: Error plot for first excited state of BEC in harmonic potential with fixed ε using piecewise uniform mesh scheme. The ε values used are $\varepsilon = 0.1 \times 2^{-2}$ (full line) and $\varepsilon = 0.1 \times 2^{-6}$ (dotted line). A comparison is made for increasing values of N, the total number of mesh points used from $N = 2^4 + 1$ to $N = 2^{10} + 1$.

4.7 Numerical comparisons

In order to compare the new numerical scheme based on piecewise uniform mesh against the classical uniform mesh scheme, we used a fixed number of mesh points (i.e. 2^4+1 mesh points) with decreasing ε values. (i.e. $\varepsilon = 0.1\times 2^{-2}, 0.1\times 2^{-4}, 0.1\times 2^{-6}$ or 0.1×2^{-8}.)

From Figure 4.13, Figure 4.14 and Figure 4.15, we observe that the largest errors mainly occurs at the boundary layers or the interior layers when using the uniform mesh method. These errors found at the boundary or interior layers are significantly reduced when the piecewise uniform mesh method is being applied. Furthermore, all errors at other regions using piecewise uniform mesh scheme is also smaller than the those using uniform mesh scheme.

Based on the numerical results for the 3 types of potentials, we noted the maximum errors, i.e. $\max_{a\le x\le b}|\phi(x)-\phi_{\varepsilon,N}(x)|$, for different values of ε and the different numbers of mesh points used for both piecewise uniform mesh and uniform mesh methods. A summary of these results are given in Tables 4.1 to 4.6.

From these Tables, we observe that as ε decreases, the maximum error increases. This is expected because the gradient change in the boundary layer or interior layer is larger for smaller values of ε.

Comparing the results from these Tables, we also observe that the advantage of using piecewise uniform mesh scheme over uniform mesh scheme is more significant when comparing solutions with smaller values of ε. When ε is very small, adding more mesh points with the uniform mesh method does not reduce the maximum error significantly. However, when we use more mesh points with the piecewise uniform mesh scheme, the reduction in maximum errors is much more significant.

From Tables 4.7 to 4.9, we observe that the numerical scheme based on piecewise uniform mesh is uniformly convergent. From Tables 4.10 to 4.12, we observe that

the numerical scheme based on uniform mesh is not convergent.

In the next chapter, we will apply the piecewise uniform mesh scheme to find the ground state and excited states of BEC with box potential and first excited state of BEC with harmonic potential in 1D. We will also extend the method to solve the singularly perturbed problems (3.8) under the constraint (3.9) in 2D, in order to find the ground state or excited states of BEC with box potential or harmonic potential or harmonic plus optical potential in 2D.

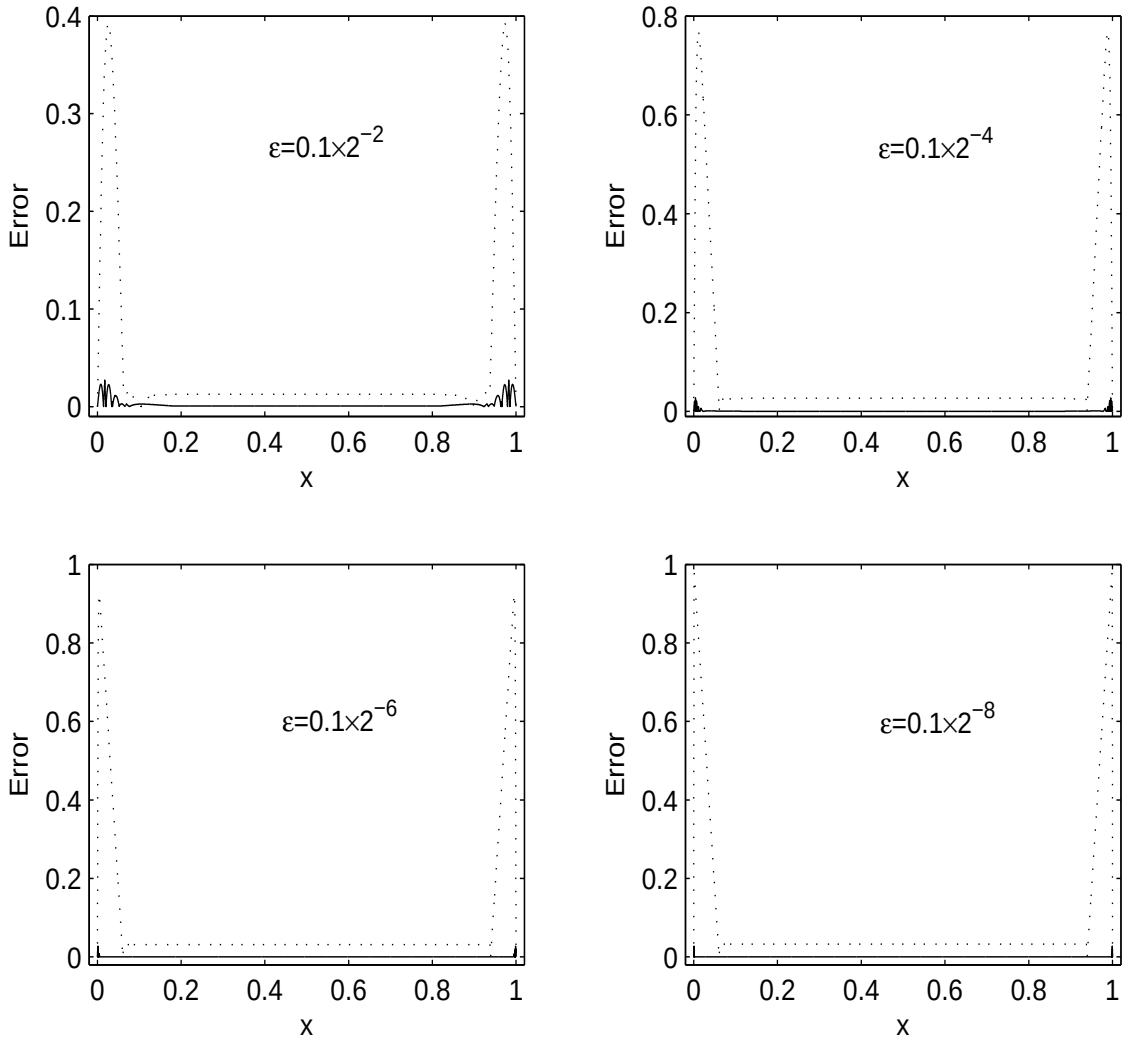

Figure 4.13: Error comparison between piecewise uniform mesh and uniform mesh obtained from ground state of BEC with box potential. Piecewise uniform mesh (full line), uniform mesh (dotted line).

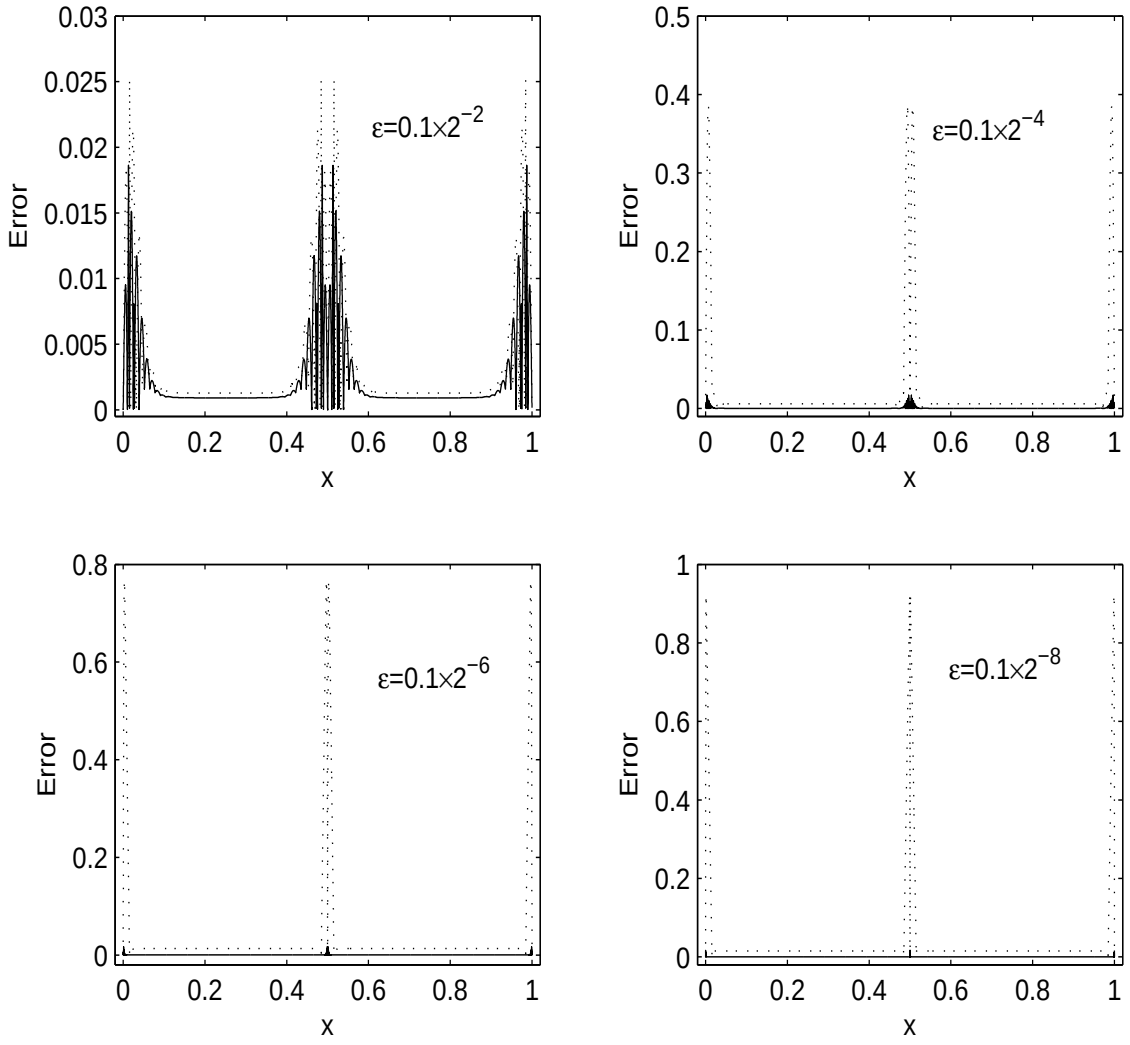

Figure 4.14: Error comparison between piecewise uniform mesh and uniform mesh obtained from first excited state of BEC with box potential. Piecewise uniform mesh (full line), uniform mesh (dotted line).

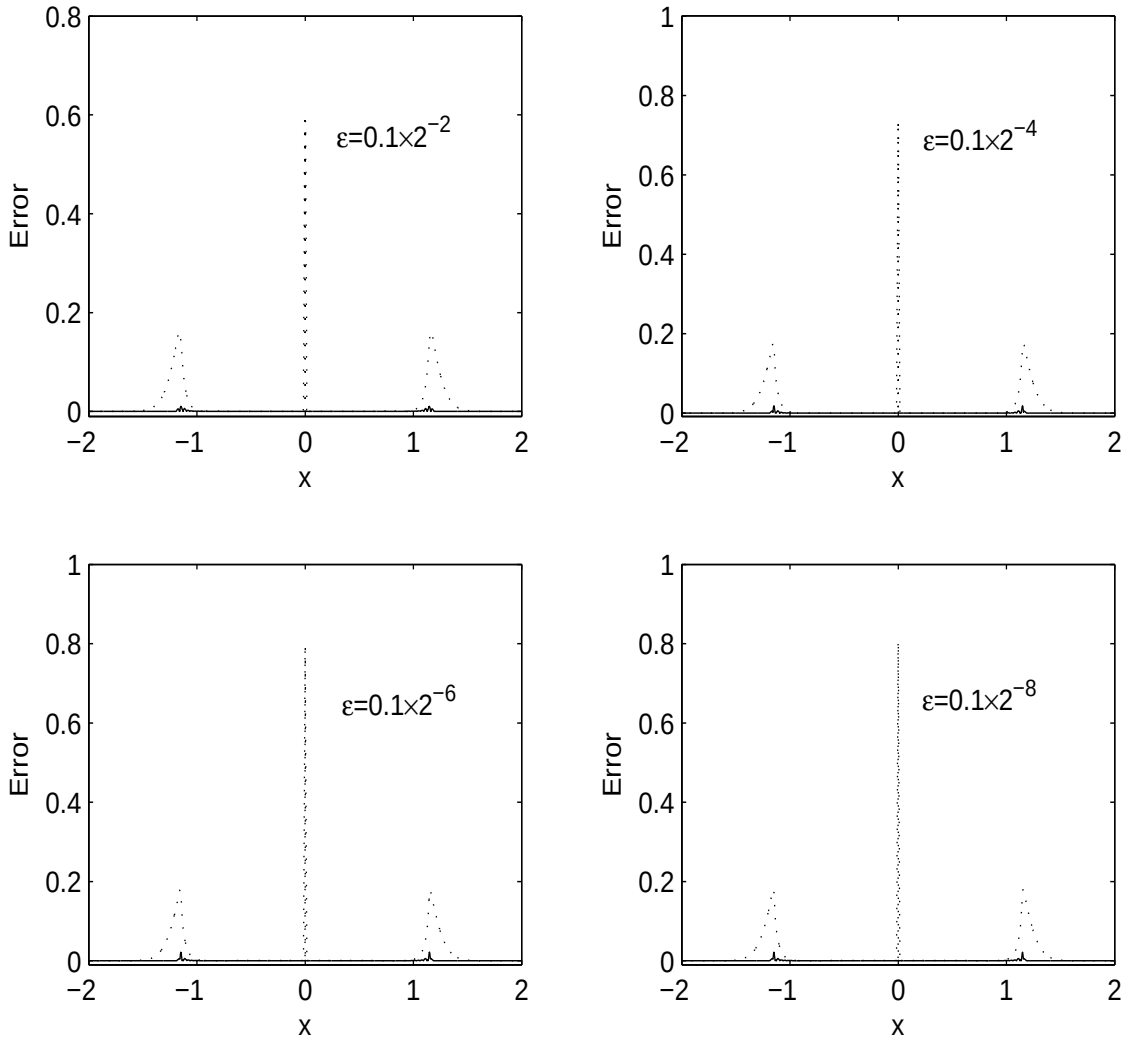

Figure 4.15: Error comparison between piecewise uniform mesh and uniform mesh obtained from first excited state of BEC with harmonic potential.Piecewise uniform mesh (full line), uniform mesh (dotted line).

ε	Number of mesh points used				
	$2^{12}+1$	$2^{10}+1$	$2^{8}+1$	$2^{6}+1$	$2^{4}+1$
0.1×2^{0}	4.57e-07	6.58e-06	1.06e-04	1.70e-03	2.64e-02
0.1×2^{-2}	3.62e-06	4.32e-05	4.42e-04	4.01e-03	2.72e-02
0.1×2^{-4}	3.68e-06	4.16e-05	4.27e-04	3.84e-03	2.70e-02
0.1×2^{-6}	5.76e-06	4.12e-05	4.23e-04	3.81e-03	2.70e-02
0.1×2^{-8}	2.06e-05	4.27e-05	4.22e-04	3.78e-03	2.69e-02
0.1×2^{-10}	7.71e-05	9.26e-05	4.22e-04	3.78e-03	2.69e-02
0.1×2^{-12}	3.38e-04	3.72e-04	5.46e-04	3.96e-03	2.70e-02
0.1×2^{-14}	1.47e-03	1.39e-03	1.43e-03	4.67e-03	2.72e-02

Table 4.1: Maximum errors for ground state of BEC with box potential using piecewise uniform mesh.

ε	Number of mesh points used				
	$2^{12}+1$	$2^{10}+1$	$2^{8}+1$	$2^{6}+1$	$2^{4}+1$
0.1×2^{0}	4.57e-07	6.58e-06	1.06e-04	1.70e-03	2.64e-02
0.1×2^{-2}	5.08e-06	8.38e-05	1.41e-03	2.43e-02	3.92e-01
0.1×2^{-4}	8.10e-05	1.36e-03	2.37e-02	3.82e-01	7.68e-01
0.1×2^{-6}	1.35e-03	2.35e-02	3.79e-01	7.68e-01	9.24e-01
0.1×2^{-8}	2.35e-02	3.79e-01	7.67e-01	9.24e-01	9.76e-01
0.1×2^{-10}	3.78e-01	7.67e-01	9.24e-01	9.77e-01	9.93e-01
0.1×2^{-12}	7.67e-01	9.24e-01	9.77e-01	9.93e-01	9.98e-01
0.1×2^{-14}	9.24e-01	9.77e-01	9.93e-01	9.98e-01	9.99e-01

Table 4.2: Maximum errors for ground state of BEC with box potential using uniform mesh.

ε	Number of mesh points used				
	$2^{12}+1$	$2^{10}+1$	$2^{8}+1$	$2^{6}+1$	$2^{4}+1$
0.1×2^{0}	6.75e-07	9.87e-06	1.57e-04	2.51e-03	3.84e-02
0.1×2^{-2}	5.61e-06	9.50e-05	1.52e-03	1.86e-02	1.84e-01
0.1×2^{-4}	1.40e-05	1.52e-04	1.66e-03	1.69e-02	1.66e-01
0.1×2^{-6}	1.46e-05	1.50e-04	1.62e-03	1.66e-02	1.61e-01
0.1×2^{-8}	2.30e-05	1.50e-04	1.62e-03	1.65e-02	1.60e-01
0.1×2^{-10}	8.62e-05	1.79e-04	1.60e-03	1.65e-02	1.60e-01
0.1×2^{-12}	2.86e-04	3.36e-04	1.63e-03	1.64e-02	1.60e-01
0.1×2^{-14}	1.47e-03	1.21e-03	1.84e-03	1.66e-02	1.60e-01

Table 4.3: Maximum errors for 1st excited state of BEC with box potential using piecewise uniform mesh.

ε	Number of mesh points used				
	$2^{12}+1$	$2^{10}+1$	$2^{8}+1$	$2^{6}+1$	$2^{4}+1$
0.1×2^{0}	6.75e-07	9.87e-06	1.57e-04	2.51e-03	3.84e-02
0.1×2^{-2}	5.61e-06	9.50e-05	1.52e-03	2.52e-02	4.05e-01
0.1×2^{-4}	7.96e-05	1.38e-03	2.39e-02	3.85e-01	7.69e-01
0.1×2^{-6}	1.35e-03	2.36e-02	3.80e-01	7.68e-01	9.23e-01
0.1×2^{-8}	2.35e-02	3.79e-01	7.67e-01	9.24e-01	9.76e-01
0.1×2^{-10}	3.78e-01	7.67e-01	9.24e-01	9.77e-01	9.93e-01
0.1×2^{-12}	7.67e-01	9.24e-01	9.77e-01	9.93e-01	9.98e-01
0.1×2^{-14}	9.24e-01	9.77e-01	9.93e-01	9.98e-01	9.99e-01

Table 4.4: Maximum errors for 1st excited state of BEC with box potential using uniform mesh.

ε	Number of mesh points used				
	$2^{12}+1$	$2^{10}+1$	$2^{8}+1$	$2^{6}+1$	$2^{4}+1$
0.1×2^{0}	1.76e-05	2.67e-04	3.97e-03	5.73e-02	2.26e-01
0.1×2^{-2}	6.37e-05	1.02e-03	1.00e-02	9.30e-02	2.51e-01
0.1×2^{-4}	2.57e-04	2.49e-03	1.84e-02	1.08e-01	2.61e-01
0.1×2^{-6}	3.80e-04	3.49e-03	2.17e-02	1.11e-01	2.63e-01
0.1×2^{-8}	3.59e-04	3.67e-03	2.19e-02	1.11e-01	2.63e-01
0.1×2^{-10}	3.44e-04	3.69e-03	2.18e-02	1.12e-01	2.63e-01
0.1×2^{-12}	3.40e-04	3.69e-03	2.18e-02	1.12e-01	2.63e-01
0.1×2^{-14}	3.39e-04	3.69e-03	2.18e-02	1.12e-01	2.63e-01

Table 4.5: Maximum errors for first excited state of of BEC with harmonic potential using piecewise uniform mesh.

ε	Number of mesh points used				
	$2^{12}+1$	$2^{10}+1$	$2^{8}+1$	$2^{6}+1$	$2^{4}+1$
0.1×2^{0}	1.24e-01	1.24e-01	2.44e-01	5.89e-01	7.37e-01
0.1×2^{-2}	1.57e-01	2.44e-01	5.88e-01	7.36e-01	7.87e-01
0.1×2^{-4}	2.46e-01	5.89e-01	7.36e-01	7.87e-01	8.03e-01
0.1×2^{-6}	5.90e-01	7.36e-01	7.87e-01	8.03e-01	8.07e-01
0.1×2^{-8}	7.37e-01	7.87e-01	8.03e-01	8.07e-01	8.09e-01
0.1×2^{-10}	7.87e-01	8.03e-01	8.07e-01	8.09e-01	8.09e-01
0.1×2^{-12}	8.03e-01	8.07e-01	8.09e-01	8.09e-01	8.09e-01
0.1×2^{-14}	8.07e-01	8.09e-01	8.09e-01	8.09e-01	8.09e-01

Table 4.6: Maximum errors for 1st excited state of BEC with harmonic potential using uniform mesh.

N	2^4+1	2^6+1	2^8+1	$2^{10}+1$	$2^{12}+1$
ε	0.1×2^0	0.1×2^{-2}	0.1×2^{-4}	0.1×2^{-6}	0.1×2^{-8}
Error	2.64e-02	4.01e-03	4.27e-04	4.12e-05	2.06e-05

Table 4.7: Maximum errors for ground state of BEC with box potential using piecewise uniform mesh.

N	2^4+1	2^6+1	2^8+1	$2^{10}+1$	$2^{12}+1$
ε	0.1×2^0	0.1×2^{-2}	0.1×2^{-4}	0.1×2^{-6}	0.1×2^{-8}
Error	3.84e-02	1.86e-02	1.66e-03	1.50e-04	2.30e-04

Table 4.8: Maximum errors for first excited state of BEC with box potential using piecewise uniform mesh.

N	2^4+1	2^6+1	2^8+1	$2^{10}+1$	$2^{12}+1$
ε	0.1×2^0	0.1×2^{-2}	0.1×2^{-4}	0.1×2^{-6}	0.1×2^{-8}
Error	2.26e-01	9.30e-02	1.84e-02	3.49e-03	3.59e-04

Table 4.9: Maximum errors for first excited state of BEC with harmonic potential using piecewise uniform mesh.

N	2^4+1	2^6+1	2^8+1	$2^{10}+1$	$2^{12}+1$
ε	0.1×2^0	0.1×2^{-2}	0.1×2^{-4}	0.1×2^{-6}	0.1×2^{-8}
Error	2.64e-02	2.43e-02	2.37e-02	2.35e-02	2.35e-02

Table 4.10: Maximum errors for ground state of BEC with box potential using uniform mesh.

N	2^4+1	2^6+1	2^8+1	$2^{10}+1$	$2^{12}+1$
ε	0.1×2^0	0.1×2^{-2}	0.1×2^{-4}	0.1×2^{-6}	0.1×2^{-8}
Error	3.84e-02	2.52e-02	2.39e-02	2.36e-02	2.35e-02

Table 4.11: Maximum errors for first excited state of BEC with box potential using uniform mesh.

N	2^4+1	2^6+1	2^8+1	$2^{10}+1$	$2^{12}+1$
ε	0.1×2^0	0.1×2^{-2}	0.1×2^{-4}	0.1×2^{-6}	0.1×2^{-8}
Error	7.37e-01	7.36e-01	7.36e-01	7.36e-01	7.37e-01

Table 4.12: Maximum errors for first excited state of BEC with harmonic potential using uniform mesh.

Chapter 5

Numerical Applications

In this chapter, we first apply the newly proposed numerical scheme based on piecewise uniform mesh to find the ground state and excited states of BEC with box potential in 1D or with harmonic potential in 1D.

We next extend the gradient flow with discrete normalization based on adaptive mesh method shown in Chapter 4 to solve the singularly perturbed nonlinear eigenvalue problems (3.8) under the constraint (3.9) in two dimensions (2D). We are particularly interested in the ground state and various excited states for BEC with box potential in 2D, or harmonic potential in 2D, or harmonic plus optical lattice potential in 2D. These stationary states are particularly interesting because the particle number of the BEC at equilibrium is usually very large or the BEC is in a semiclassical regime (this corresponds to that ε goes to zero). This is also to illustrate the capability of the piecewise uniform mesh method in solving singularly perturbed problems and find boundary layers or interior layers in higher dimensions. The problem now is solved in two dimensions and there are different excited states in both the x- and y-direction. For given positive integers j and k, a (j,k)-th excited state is where the BEC is in the j-th excited state in the x-direction and k-th excited state in the y-direction. The (0,0)-th state is the ground state.

5.1 Numerical results in 1D

5.1.1 Ground state and excited states with box potential

Figure 5.1 shows the numerical result for the ground state using our adaptive mesh numerical scheme based on piecewise uniform mesh with $2^4 + 1$ mesh points. There are boundary layers near $x = 0$ and $x = 1$ respectively when ε goes near 0. These agree well with the asymptotic approximation presented in the subsection 3.2.2.

Figure 5.2 shows the numerical result for the first excited state using our adaptive mesh numerical scheme based on piecewise uniform mesh with $2^4 + 1$ mesh points. There are boundary layers near $x = 0$ and $x = 1$ respectively when ε goes near 0. Moreover, there is an interior layer near $x = \frac{1}{2}$.

Figure 5.3 shows the numerical result for the third excited state using our adaptive mesh numerical scheme based on piecewise uniform mesh with $2^6 + 1$ mesh points. There are boundary layers near $x = 0$ and $x = 1$ respectively when ε goes near 0. There are interior layers near $x = \frac{1}{4}, \frac{1}{2}, \frac{3}{4}$ respectively.

Figure 5.4 shows the numerical result for the ninth excited state using our adaptive mesh numerical scheme based on piecewise uniform mesh with 1281 mesh points. There are boundary layers near $x = 0$ and $x = 1$ respectively when ε goes near 0. There are interior layers near $x = \frac{1}{10}, \frac{1}{5}, \cdots, \frac{9}{10}$ respectively.

Table 5.1 shows the energy and chemical potential values for different values of ε in the different states of the BEC in box potentials. We observe that for larger values of ε, the corresponding energy and chemical potentials are also higher. Also, box potentials in higher excited states have higher energy and chemical potentials levels compared to box potentials in lower excited states.

All these numerical results agree well with the asymptotic approximation presented in the subsection 3.2.3.

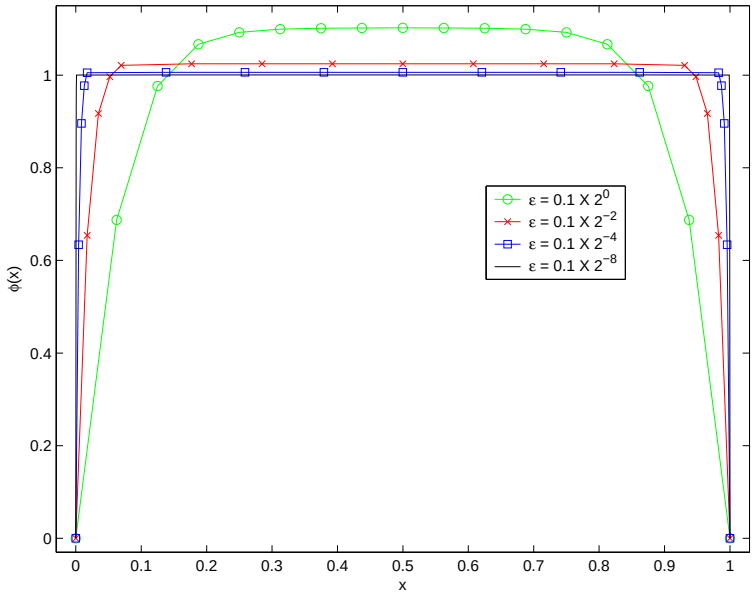

Figure 5.1: Solution for ground state with box potential in 1D, $2^4 + 1$ mesh points.

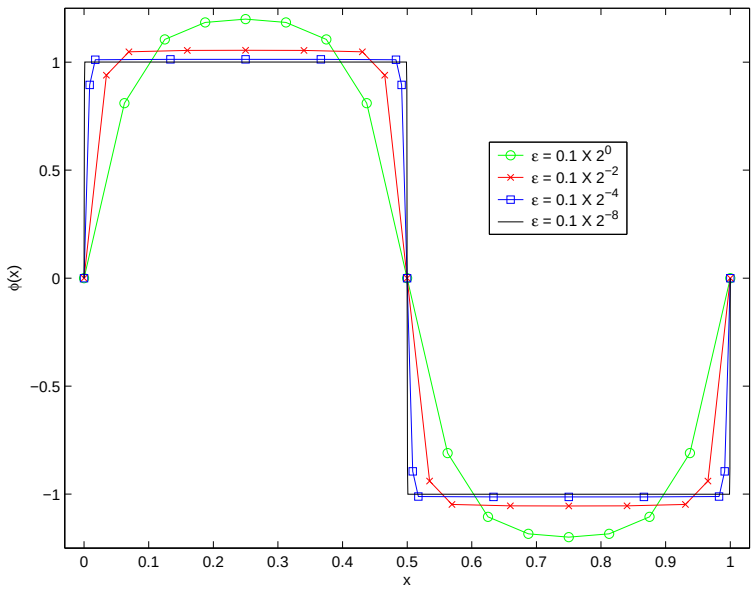

Figure 5.2: Solution for first excited state of BEC with box potential in 1D, $2^4 + 1$ mesh points.

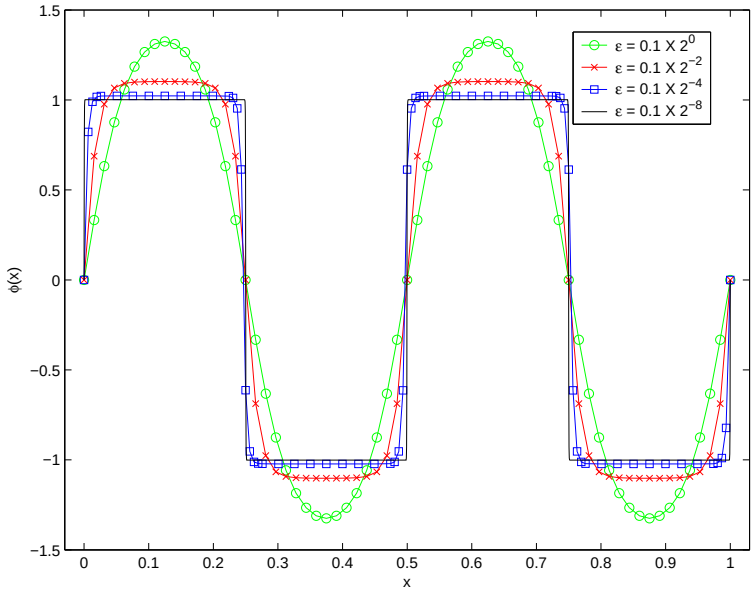

Figure 5.3: Solution for third excited state of BEC with box potential in 1D, $2^6 + 1$ mesh points.

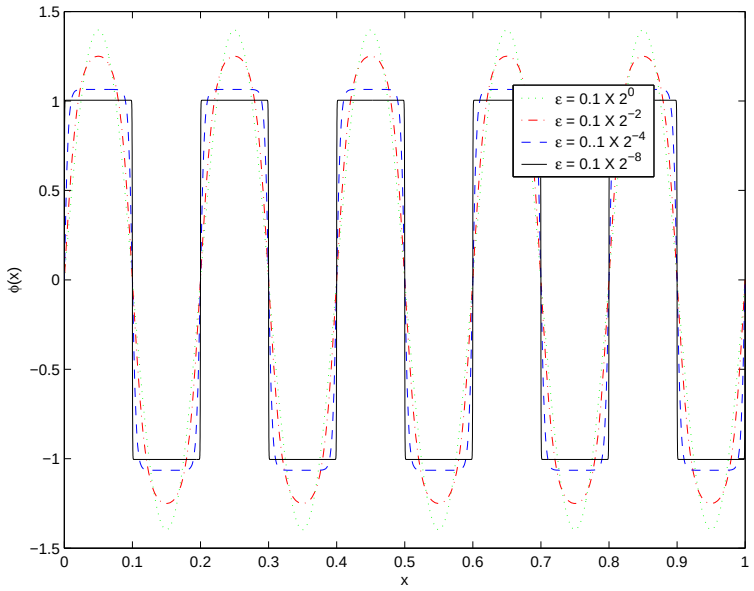

Figure 5.4: Solution for ninth excited state of BEC with box potential in 1D , 1281 mesh points.

ε	0.1×2^{-2}	0.1×2^{-4}	0.1×2^{-6}	0.1×2^{-8}
E_g	0.5345	0.5084	0.5021	0.5005
μ_g	1.0512	1.0126	1.0031	1.0008
E_1	0.5718	0.5169	0.5042	0.5010
μ_1	1.1051	1.0253	1.0063	1.0016
E_3	0.6553	0.5345	0.5084	0.5021
μ_3	1.2208	1.0511	1.0126	1.0031
E_9	0.9938	0.5909	0.5210	0.5052
μ_9	1.6400	1.1322	1.0314	1.0078

Table 5.1: Energy and chemical potential of different states of BEC with box potential in 1D for different ε.

ε	0.2	0.1	0.05	0.025	0.0125
E_g	0.4164	0.4002	0.3952	0.3937	0.3933
μ_g	0.6676	0.6587	0.6561	0.6554	0.6552
E_1	0.5787	0.4764	0.4320	0.4117	0.4022
μ_1	0.8180	0.7314	0.6920	0.6732	0.6641

Table 5.2: Energy and chemical potential of different states of BEC with harmonic potential in 1D for different ε.

5.1.2 Ground state and excited states with harmonic potential in 1D

In this subsection, we calculate the ground state and first excited state with harmonic potential in 1D.

Figure 5.5 shows the numerical result for ground state by using our uniform mesh numerical scheme with $2^5 + 1$ mesh points. The uniform mesh is used because there are neither boundary layers nor interior layers inside the computed domain $[-2, 2]$.

Figure 5.6 shows the numerical result for the first excited state by using our adaptive numerical scheme based on piecewise uniform mesh with 2^5+1 mesh points. There is an interior layer near $x = 0$.

Table 5.2 shows the energy and chemical potential values for different values of ε in the different states of the BEC in harmonic potentials. We observe that for larger values of ε, the corresponding energy and chemical potentials are also higher. Also, the energy and chemical potential levels in the first excited excited states are higher than the energy and chemical potential levels in the ground state.

All these numerical results agree well with the asymptotic approximation presented in the subsection 3.3.3.

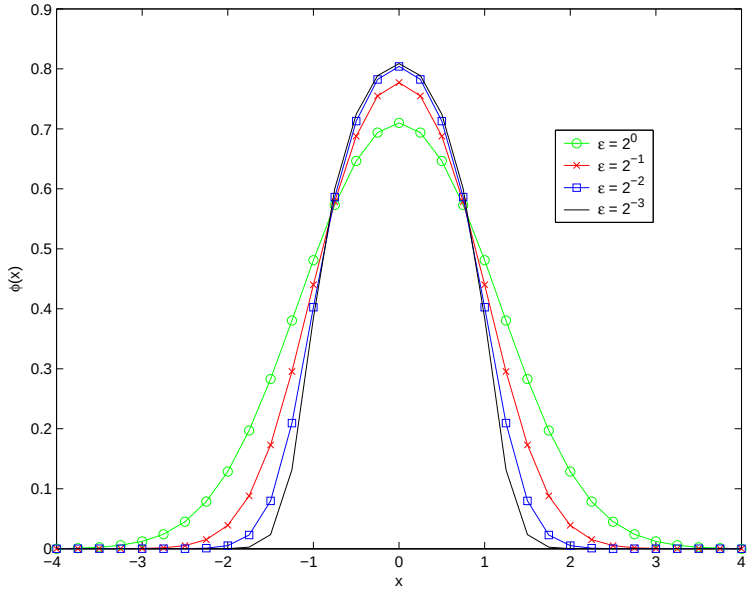

Figure 5.5: Solution for ground state of BEC with harmonic potential in 1D, $2^5 + 1$ mesh points.

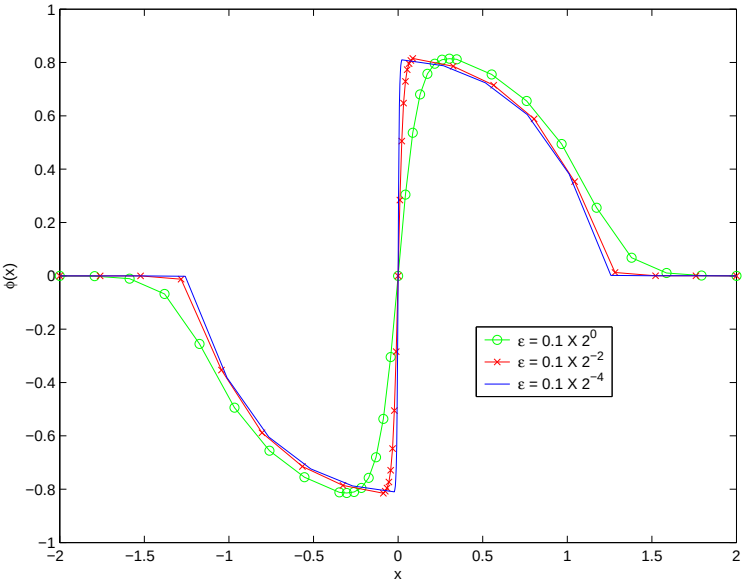

Figure 5.6: Solution for first excited state of BEC with harmonic potential in 1D, $2^5 + 1$ mesh points.

5.2 Numerical results in 2D for box potential

In this section, we calculate the ground state and excited states solutions for the BEC confined in box potential. The box potential in 2D is given as:

$$V(x,y) = \begin{cases} 0, & 0 < x, y < 1, \\ \infty, & \text{otherwise.} \end{cases} \tag{5.1}$$

The problem is solved on the domain $\Omega = [0,1] \times [0,1]$ and the mesh size is 257×257.

5.2.1 Choice of mesh

The mesh used is based on the idea mentioned previously in section 4.3. Using the same idea, we extend the mesh in both x and y directions. Hence, for a 2D BEC under box potential in the (0,1)th excited state, we will choose the mesh in the x-direction as

$$\begin{cases} x_j^* = x_{j-1}^* + h_{x1}, & 0 < j \leq 64, \\ x_j^* = x_{j-1}^* + h_{x2}, & 64 < j \leq 192, \\ x_j^* = x_{j-1}^* + h_{x1}, & 192 < j \leq 256, \end{cases} \tag{5.2}$$

where

$$\begin{aligned} x_{64}^* &= \min\left\{\frac{1}{4}, \varepsilon \ln(256)\right\}, \\ x_{192}^* &= 1 - x_{64}^*, \\ h_{x1} &= \frac{x_{64}^*}{64}, \quad h_{x2} = \frac{x_{192}^* - x_{64}^*}{128}. \end{aligned} \tag{5.3}$$

Similarly, we choose the mesh in the y-direction as

$$\begin{cases} y_k^* = y_{k-1}^* + h_{y1}, & 0 < k \leq 32, \\ y_k^* = y_{k-1}^* + h_{y2}, & 32 < k \leq 96, \\ y_k^* = y_{k-1}^* + h_{y1}, & 96 < k \leq 160, \\ y_k^* = y_{k-1}^* + h_{y2}, & 160 < k \leq 224, \\ y_k^* = y_{k-1}^* + h_{y1}, & 224 < k \leq 256, \end{cases} \tag{5.4}$$

where

$$\begin{aligned} y^*_{32} &= \min\left\{\frac{1}{8}, \varepsilon \ln(256)\right\}, \\ y^*_{96} &= \frac{1}{2} - y^*_{32}, \\ y^*_{160} &= \frac{1}{2} + y^*_{32}, \\ y^*_{224} &= 1 - y^*_{32}, \\ h_{y1} &= \frac{y^*_{N/8}}{32}, \quad h_{y2} = \frac{y^*_{96} - y^*_{32}}{64}. \end{aligned} \tag{5.5}$$

By extending the idea accordingly, we can obtain the piecewise uniform mesh for the other states in 2D box potential.

5.2.2 Choice of initial data

The initial data used is based on the idea mentioned previously in section 4.4. By extension of the same idea, the initial data used for finding the (j,k)th excited state of a 2D BEC under box potential is given as

$$\phi_0(x,y) = 2\sin((j+1)\pi x)\sin((k+1)\pi y), \qquad x,y \in [0,1], \tag{5.6}$$

5.2.3 Results

For the ground state in the 2D box potential, Figures 5.7 and 5.8 show the surface plot and image plot of (0,0)th state with box potential in 2D with $\varepsilon = 10^{-3}$, respectively. It is clearly seen that ground state with box potential in 2D has boundary layers near the boundary of the domain Ω.

For the various excited states in the 2D box potential, Figures 5.9 and 5.10 show the surface plot and image plot of (1,1)-th state with box potential in 2D with $\varepsilon = 10^{-3}$, respectively. Figures 5.11 and 5.12 show the surface plot and image plot

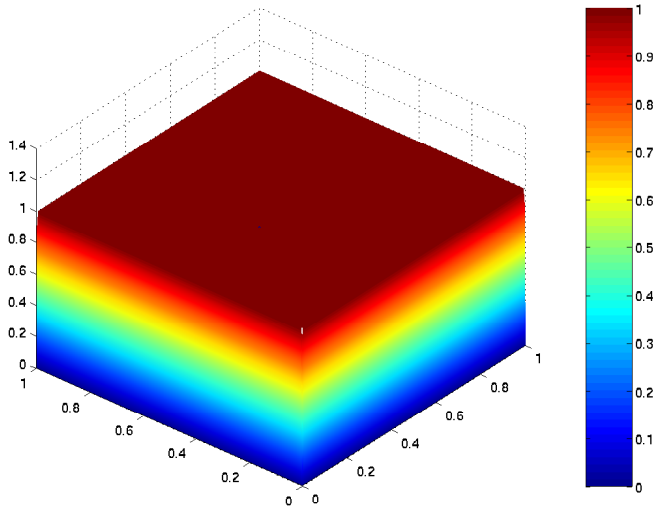

Figure 5.7: Surface plot of ground state with box potential in 2D, $\varepsilon = 10^{-3}$.

of (1,3)-th state with box potential in 2D with $\varepsilon = 10^{-3}$, respectively. Figures 5.13 and 5.14 show the surface plot and image plot of (9,9)-th state with box potential in 2D with $\varepsilon = 10^{-3}$, respectively. Figures 5.15 and 5.16 show the surface plot and image plot of (19,19)-th state with box potential in 2D with $\varepsilon = 10^{-3}$, respectively. It is clearly seen that excited states in the 2D box potential not only have boundary layers near the boundary of the domain Ω but also have interior layer inside the domain Ω.

Table 5.3 shows the energy and chemical potential values for different values of ε in the different states of the BEC in 2D box potentials. The trends are similar to those observed in Table 5.1. We observe that for larger values of ε, the corresponding energy and chemical potentials are also higher. Also, box potentials in higher excited states have higher energy and chemical potential levels compared to box potentials in lower excited states.

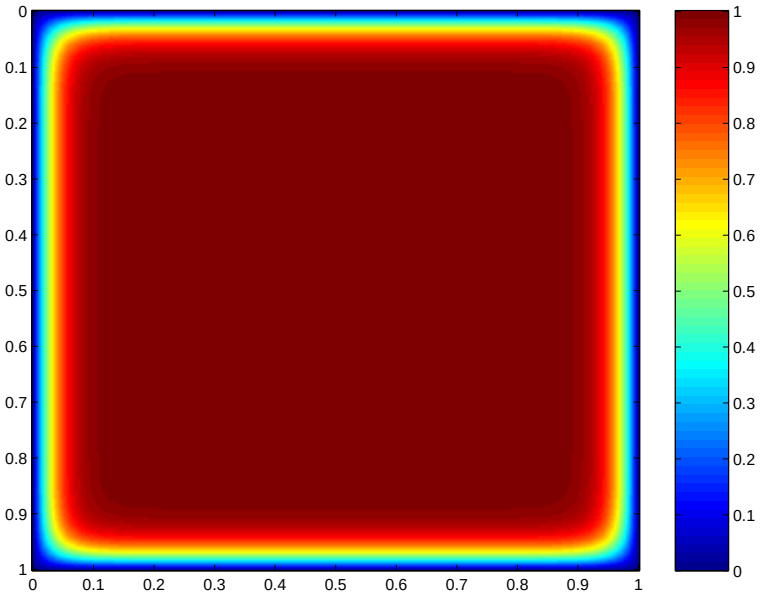

Figure 5.8: Image plot of ground state with box potential in 2D, $\varepsilon = 10^{-3}$.

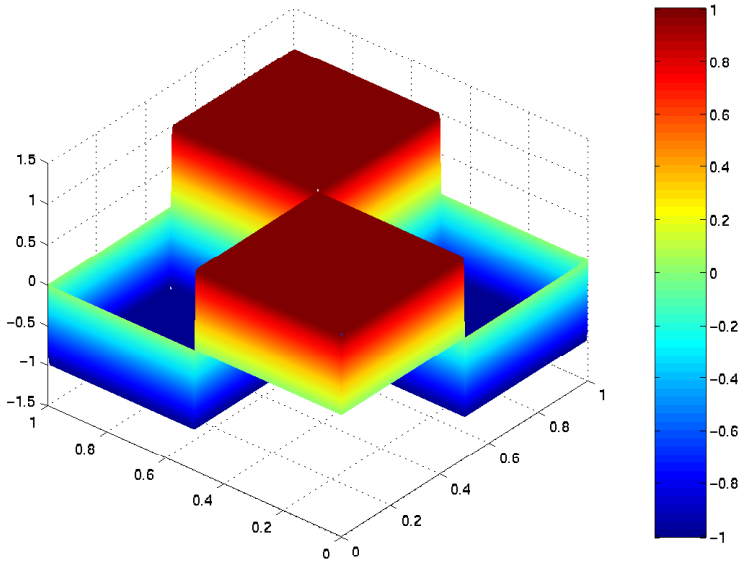

Figure 5.9: Surface plot of (1,1)-th excited state with box potential in 2D, $\varepsilon = 10^{-3}$.

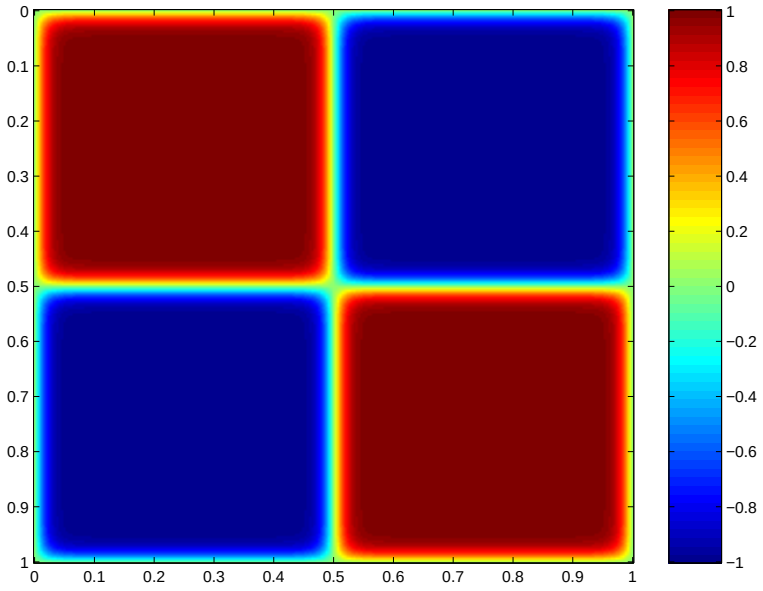

Figure 5.10: Image plot of (1,1)-th excited state with box potential in 2D, $\varepsilon = 10^{-3}$.

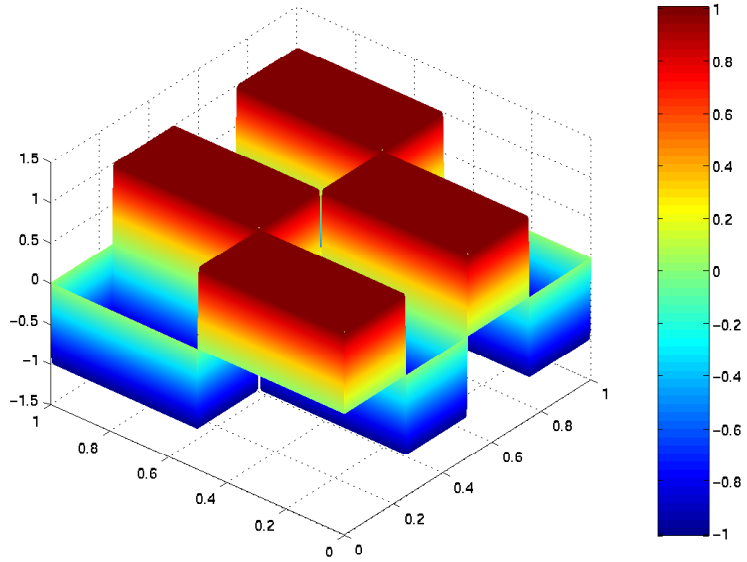

Figure 5.11: Surface plot of (1,3)-th excited state with box potential in 2D, $\varepsilon = 10^{-3}$.

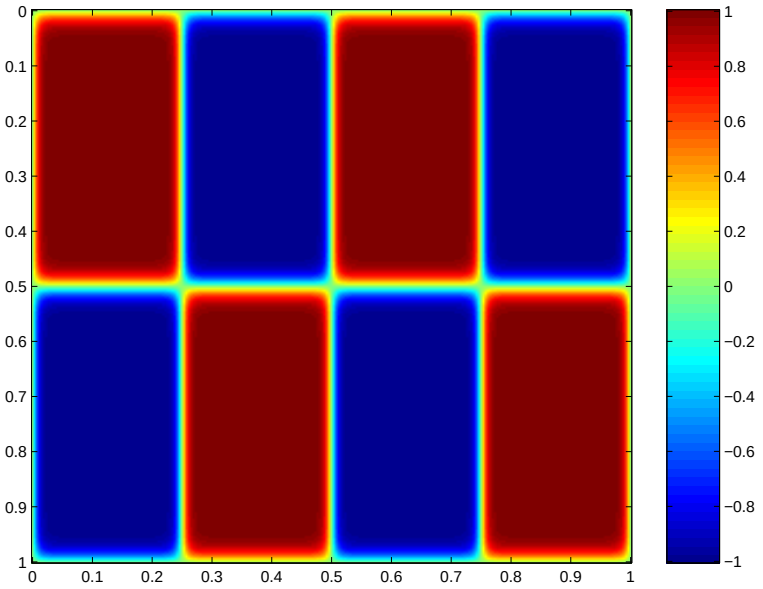

Figure 5.12: Image plot of (1,3)-th state with box potential in 2D, $\varepsilon = 10^{-3}$.

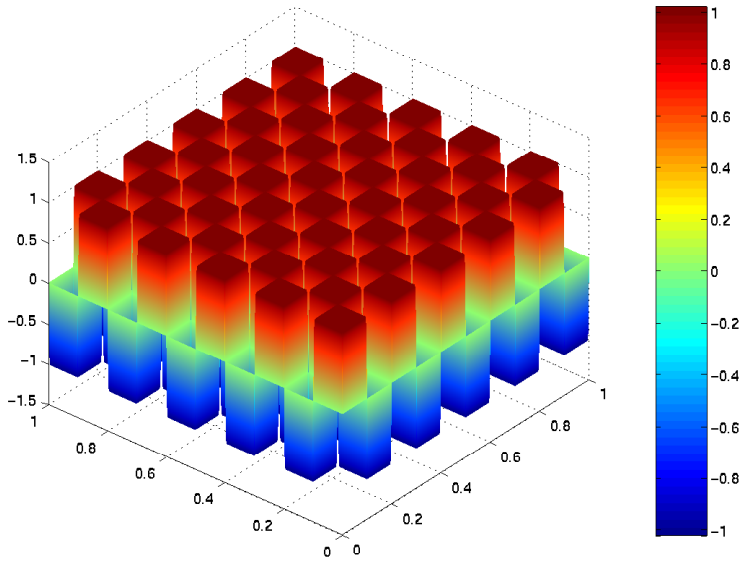

Figure 5.13: Surface plot of (9,9)-th state with box potential in 2D, $\varepsilon = 10^{-3}$.

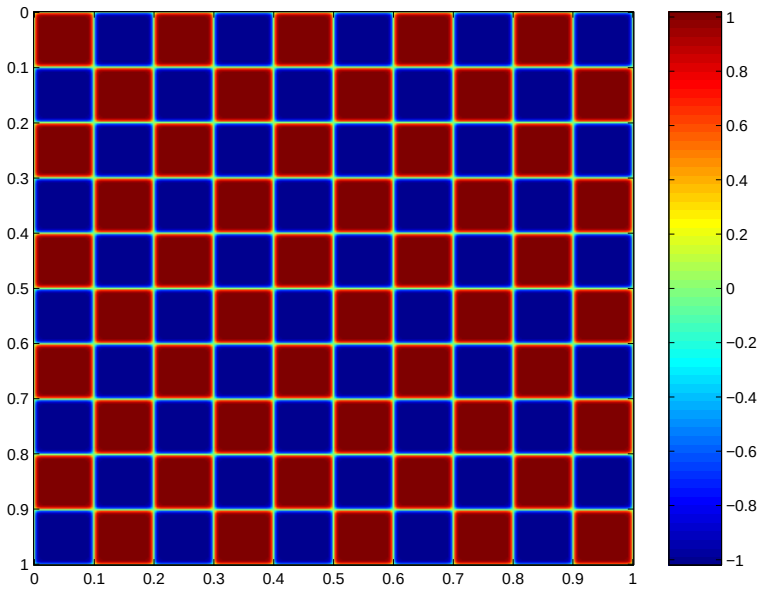

Figure 5.14: Image plot of (9,9)-th state with box potential in 2D, $\varepsilon = 10^{-3}$.

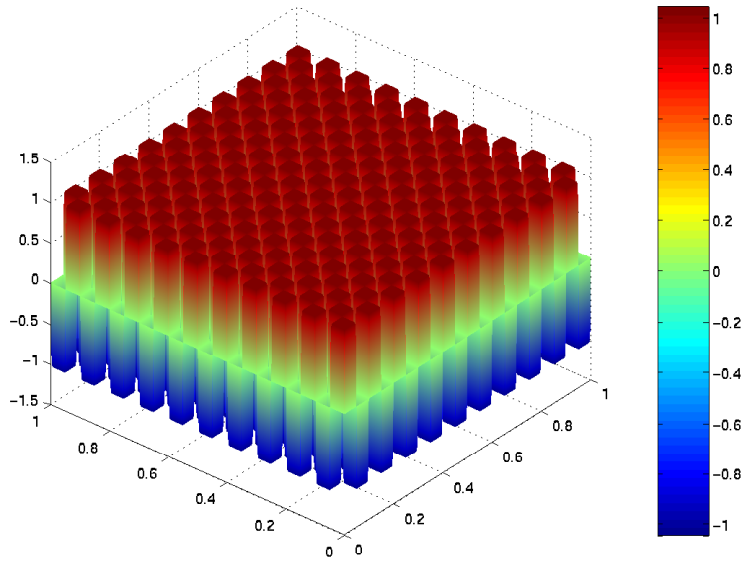

Figure 5.15: Surface plot of (19,19)-th excited state with box potential in 2D, $\varepsilon = 10^{-3}$.

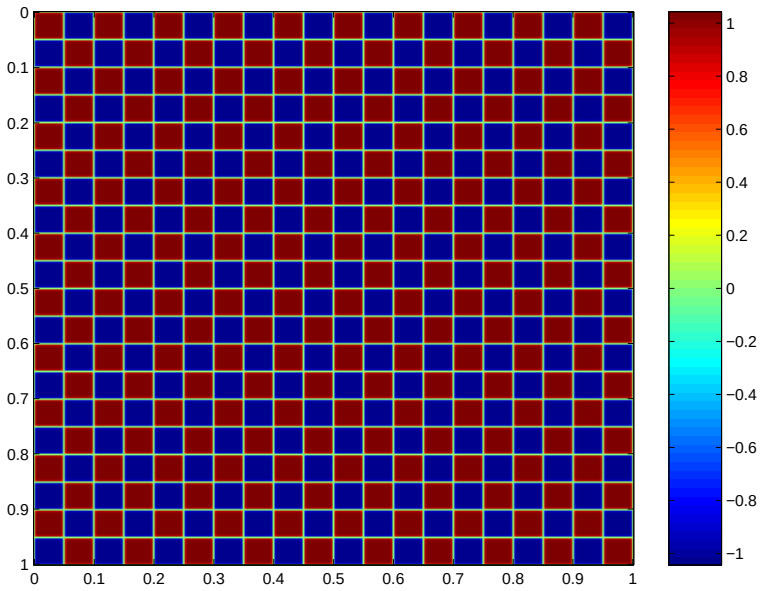

Figure 5.16: Image plot of (19,19)-th excited state with box potential in 2D, $\varepsilon = 10^{-3}$.

ε	0.1	0.01	0.001
E_g	0.8122	0.5262	0.5026
μ_g	1.4437	1.0395	1.0039
$E_{1,1}$	1.2463	0.5532	0.5052
$\mu_{1,1}$	1.9974	1.0797	1.0078
$E_{1,3}$	1.8984	0.5806	0.5077
$\mu_{1,3}$	2.7282	1.1202	1.0117

Table 5.3: Energy and chemical potential of different states of BEC with box potential in 2D for different ε

5.3 Numerical results in 2D for harmonic potential

In this section, we show the ground state and excited states solutions for the BEC in 2D harmonic oscillator potential. The potential for the 2D harmonic oscillator potential is:

$$V(x) \;=\; \frac{x^2+y^2}{2}, \qquad (x,y)\in\mathbb{R}^2.$$

The problem is solved on the domain $\Omega=[-2,2]\times[-2,2]$.

5.3.1 Choice of mesh

Similar to the previous section, the mesh used is based on the idea mentioned previously in section 4.3. Using the same idea, we extend the mesh in both x and y directions. Hence, for a 2D BEC under harmonic potential in the (0,1)th excited state, we will use a uniform mesh in the x-direction as there are no interior or boundary layers. For the y-direction, we choose the mesh as

$$\begin{cases} y_k^* = y_{k-1}^* + h_{y2}, & 0<k\le 64,\\ y_k^* = y_{k-1}^* + h_{y1}, & 64<k\le 192,\\ y_k^* = y_{k-1}^* + h_{y2}, & 192<k\le 256, \end{cases} \tag{5.7}$$

where

$$\begin{aligned} &y_0^* = -2, \qquad y_{256}^* = 2,\\ &y_{64}^* = -\min\left\{1, \varepsilon\ln(256)\right\},\\ &y_{192}^* = 0 - y_{96}^*,\\ &h_{y1} = \frac{|y_{96}^*|}{256}, \quad h_{y2} = \frac{2+y_{96}^*}{128}. \end{aligned} \tag{5.8}$$

5.3.2 Choice of initial data

The choice of initial data used is based on the idea mentioned previously in section 4.4. The initial data used for finding the (j,k)th (j, k can take values 0 or 1) excited state of a 2D BEC under harmonic potential is given as

$$\phi_0(x,y) = x^j y^k \frac{e^{-(x^2+y^2)/2}}{\sqrt{\pi}}. \tag{5.9}$$

5.3.3 Results

For the ground state with harmonic potential, Figures 5.17 and 5.18 show the surface plot and image plot of ground state with harmonic potential with $\varepsilon = 1.56 \times 10^{-3}$, respectively. It is clearly seen that ground state in 2D harmonic potential has no boundary layers in the whole domain $\Omega = [-2,2] \times [-2,2]$, even if ε is very small.

For various excited states in the 2D harmonic potential, Figures 5.19 and 5.20 show the surface plot and image plot of (0,1) excited state with harmonic potential with $\varepsilon = 1.56 \times 10^{-3}$, respectively. Figures 5.21 and 5.22 show the surface plot and image plot of 11-th excited state with harmonic potential with $\varepsilon = 1.56 \times 10^{-3}$, respectively. It is clearly seen that excited states with harmonic potential in 2D do not have boundary layers near the boundary of the domain Ω but have interior layers inside the computed domain Ω.

Table 5.4 shows the energy and chemical potential values for different values of ε in the different states of the BEC in harmonic potentials. The trends are similar to those observed in Table 5.2. We observe that for larger values of ε, the corresponding energy and chemical potentials are also higher. Also, the energy and chemical potential levels in the first excited excited states are higher than the energy and chemical potential levels in the ground state.

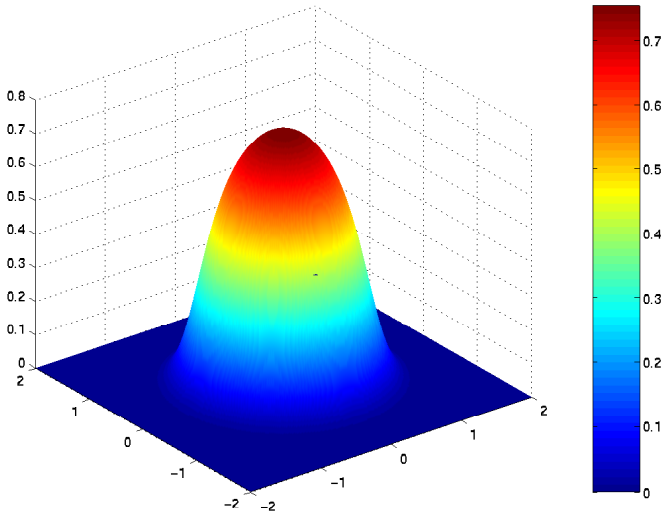

Figure 5.17: Surface plot of 0,0-th state with harmonic potential in 2D, $\varepsilon = 1.56 \times 10^{-3}$.

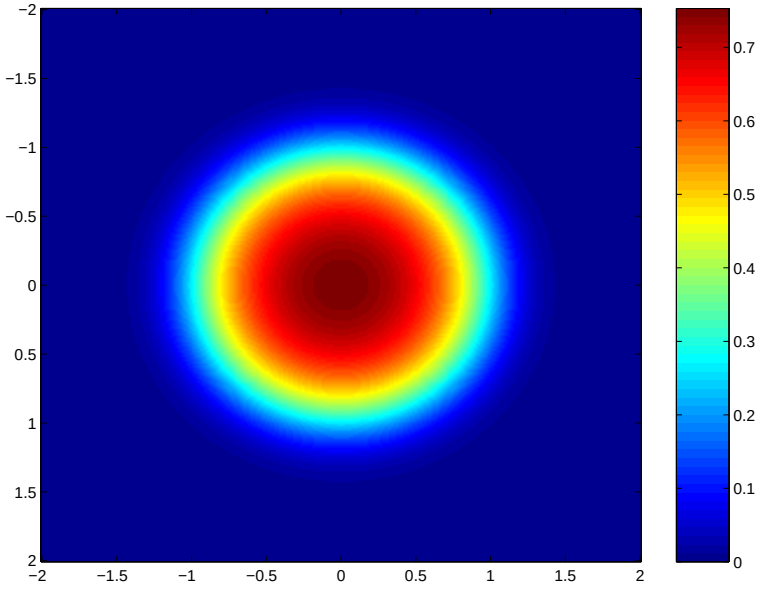

Figure 5.18: Image plot of ground state with harmonic potential in 2D, $\varepsilon = 1.56 \times 10^{-3}$.

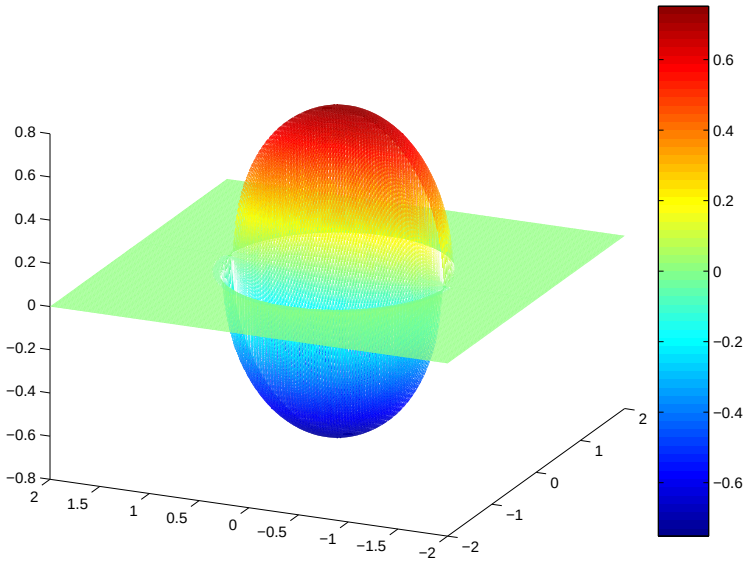

Figure 5.19: Surface plot of (0,1)-th excited state with harmonic potential in 2D, $\varepsilon = 1.56 \times 10^{-3}$.

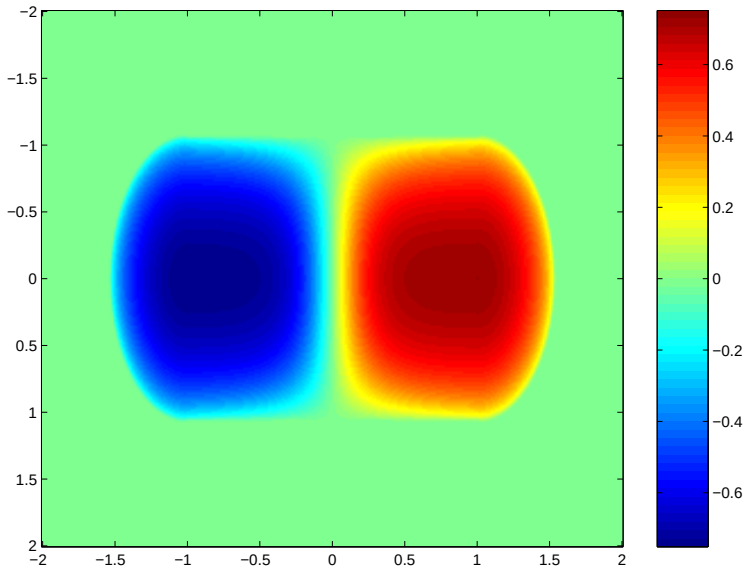

Figure 5.20: Image plot of (0,1)-th excited state with harmonic potential in 2D, $\varepsilon = 1.56 \times 10^{-3}$.

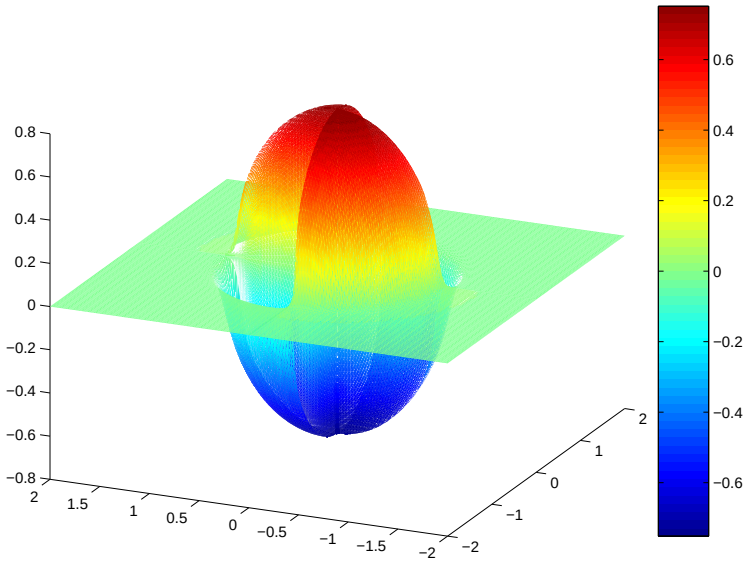

Figure 5.21: Surface plot of (1,1)-th excited state with harmonic potential in 2D, $\varepsilon = 1.56 \times 10^{-3}$.

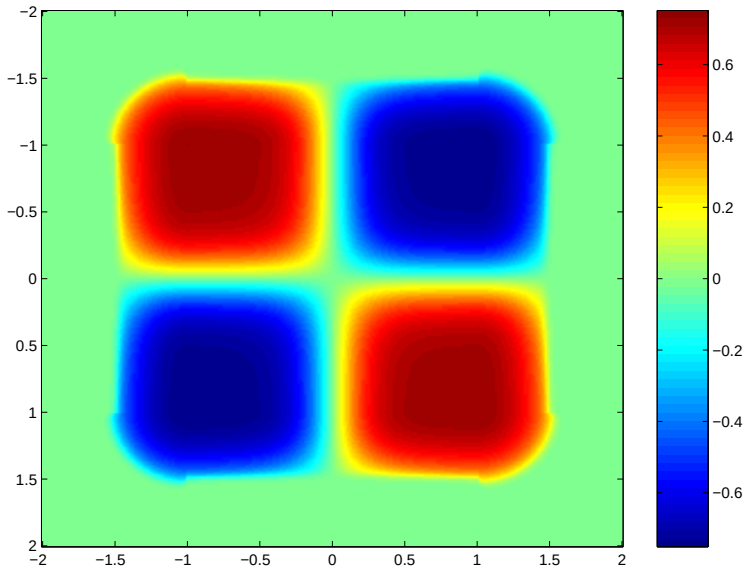

Figure 5.22: Image plot of (1,1)-th excited state with harmonic potential, $\varepsilon = 1.56 \times 10^{-3}$.

ε	0.1×2^{-2}	0.1×2^{-4}	0.1×2^{-6}	0.1×2^{-8}
E_g	0.3777	0.3763	0.3761	0.3761
μ_g	0.5651	0.5642	0.5642	0.5642
$E_{0,1}$	0.3959	0.3807	0.3772	0.3764
$\mu_{0.1}$	0.5831	0.5687	0.5653	0.5645
$E_{1,1}$	0.4148	0.3855	0.3784	0.3767
$\mu_{1,1}$	0.5962	0.5708	0.5655	0.5644

Table 5.4: Energy and chemical potential of different states of BEC with harmonic potential in 2D for different ε.

5.4 Numerical results in 2D for harmonic plus optical lattice potential

In this section, we find the ground state and excited states solutions for the BEC confined in both harmonic trapping potential plus an optical lattice potential. The potential is:

$$V(x) = \frac{x^2 + y^2}{2} + 0.3\sin^2(4\pi x) + 0.3\sin^2(4\pi y), \qquad (x, y) \in \mathbb{R}^2.$$

The problem is solved on the domain $\Omega = [-2, 2] \times [-2, 2]$ and mesh size is 65×65.

The choice of mesh and choice of initial data is exactly the same as the one for harmonic potential shown in section 5.3.1 and 5.3.2.

5.4.1 Results

For the ground state in the 2D harmonic plus optical lattice potential, Figures 5.23 and 5.24 show the surface plot and image plot of ground state with harmonic plus optical lattice potential with $\varepsilon = 0.025$, respectively. It is clearly seen that there are no boundary layers in the whole domain $\Omega = [-2, 2] \times [-2, 2]$.

For various excited states with harmonic plus optical lattice potential, Figures 5.25 and 5.26 show the surface plot and image plot of (0,1)-th excited state with harmonic optical lattice potential with $\varepsilon = 0.025$, respectively. Figures 5.27 and 5.28 show the surface plot and image plot of (1,1)-th excited state with harmonic optical lattice potential with $\varepsilon = 0.025$, respectively. It is clearly seen that there are no boundary layers near the boundary of the domain Ω but there are interior layer inside the computed domain Ω.

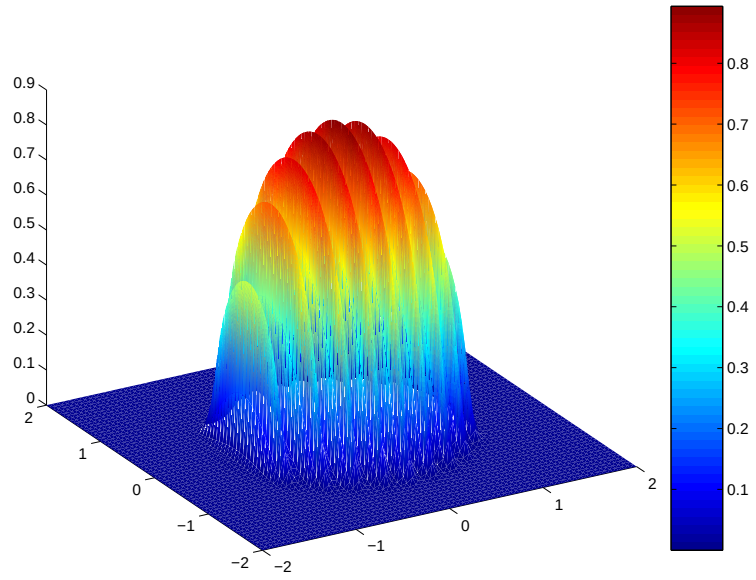

Figure 5.23: Surface plot of ground state with harmonic plus optical lattice potential in 2D, $\varepsilon = 0.025$.

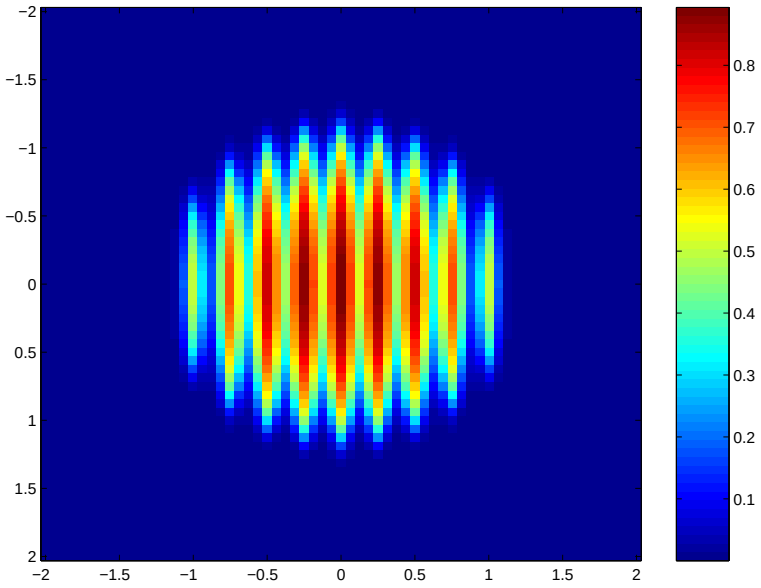

Figure 5.24: Image plot of ground state with harmonic plus optical lattice potential in 2D, $\varepsilon = 0.025$.

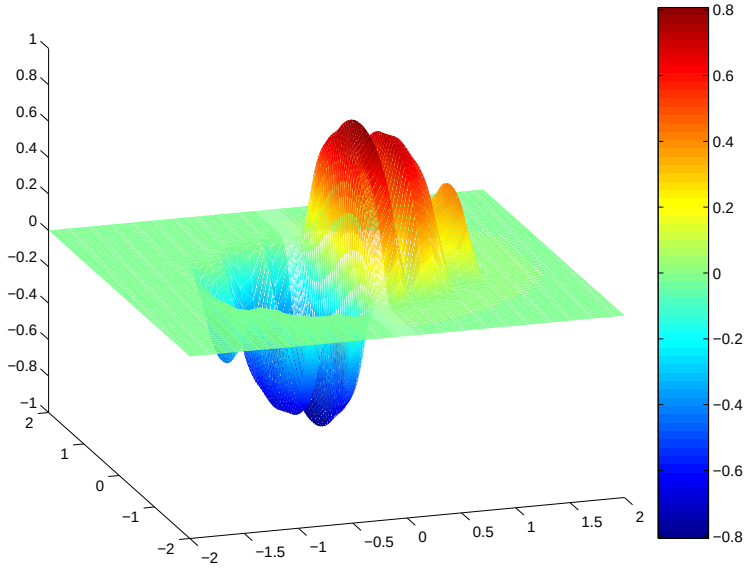

Figure 5.25: Surface plot of (0,1)-th excited state with optical lattice potential, $\varepsilon = 0.025$.

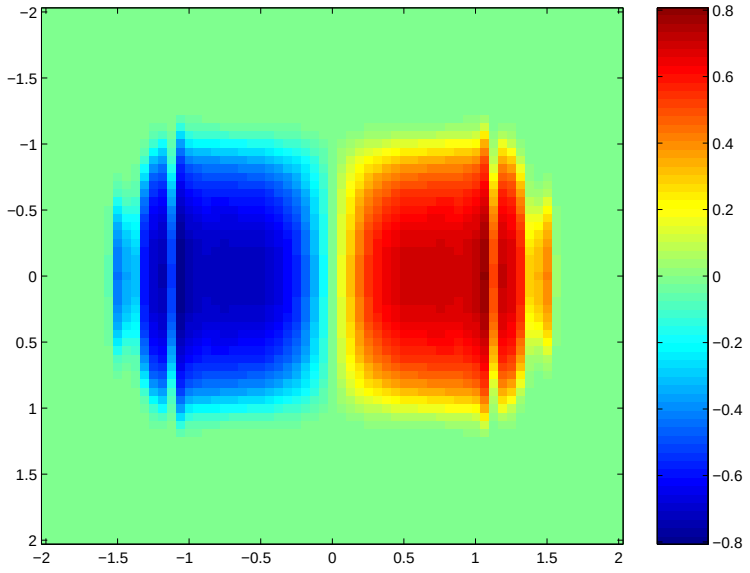

Figure 5.26: Image plot of (0,1)-th excited state with optical lattice potential, $\varepsilon = 0.025$.

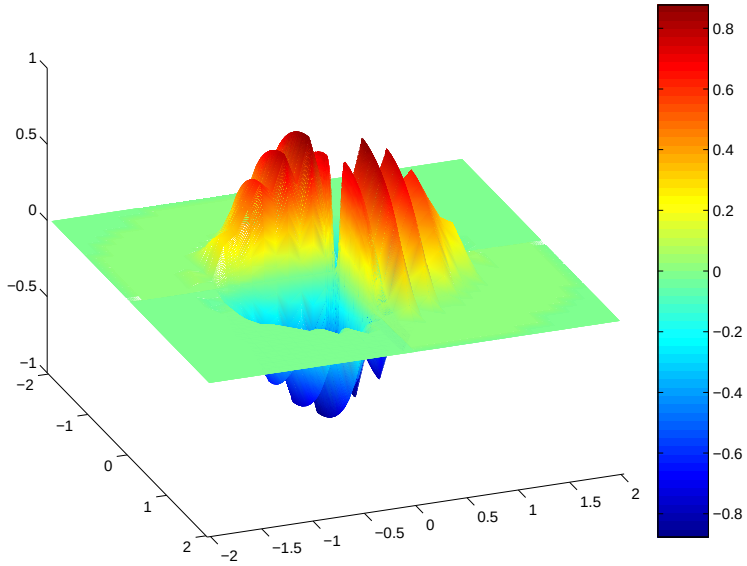

Figure 5.27: Surface plot of (1,1)-th excited state with optical lattice potential, $\varepsilon = 0.025$.

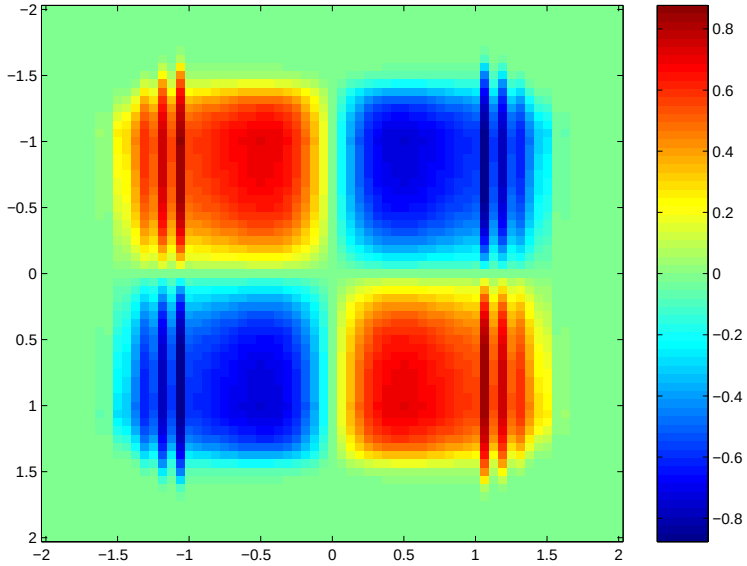

Figure 5.28: Image plot of (1,1)-th excited state with optical lattice potential, $\varepsilon = 0.025$.

Chapter 6

Conclusions

We have presented a new adaptive mesh numerical scheme to discretize the gradient flow for solving the singularly perturbed nonlinear eigenvalue problem with a constraint. This new numerical scheme is based on piecewise uniform mesh.

Our numerical results show that this numerical scheme is uniformly convergent and can accurately and effectively deal with the boundary layers or interior layers in the problem.

When we compare our numerical approximations from the adaptive mesh numerical scheme with the asymptotic approximation of the problem, we find that our numerical results agree with the asymptotic approximations made. We also compare our results from our adaptive mesh numerical scheme with those from the classical unform mesh scheme and find that the adaptive mesh scheme is superior in the reduction of point wise errors in its numerical solution. It achieves this because the proposed adaptive mesh scheme is able to significantly reduce the errors in the boundary layers or interior layers where the largest errors occur. Hence, the numerical errors in the adaptive mesh solution is much smaller than those in the uniform mesh solutions.

Furthermore, we extend our adaptive numerical scheme to two dimensions and

apply the method to solve the ground state or excited states for BEC confined in two-dimensional box potential, two-dimensional harmonic potential and two-dimensional harmonic plus optical lattice potential. Our numerical results found that there are also boundary layers or interior layers in these potentials when $\varepsilon \ll 1$, which in turn implies that there are very complicated phenomena inside the stationary states of BEC when ε goes to zero, i.e. when the BEC is in a semiclassical regime.

For future studies, the error estimate for our adaptive mesh method for singularly perturbed nonlinear eigenvalue problem is an interesting problem that can be further investigated. Also, the adaptive mesh numerical scheme can be extended to discretize the gradient flow in 3D in order to find the ground state or excited states for BEC in a semicalssical regime. Numerical results for the stationary states of BEC in 3D will allow us to further investigate the inherent physics of BEC in a more realistic and accurate fashion.

Bibliography

[1] S. K. Adhikari, Numerical solution of the two-dimensional Gross-Pitaevskii equation for trapped interacting atoms, *Phys. Lett. A*, **265** (2000), pp. 91-96.

[2] M. H. Anderson, J. R. Ensher, M. R. Matthews, C. E. Wieman and E. A. Cornell, Observation of Bose-Einstein Condensation in a Dilute Atomic Vapor, *Science*, **269** (1995), pp. 198-201.

[3] J. R. Anglin and W. Ketterle, Bose-Einstein condensation of atomic gases, *Nature*, **416** (2002), pp. 211-218.

[4] W. Bao and Q. Du, Computing the ground state solution of Bose-Einstein condensates by a normalized gradient flow, *SIAM J. Sci. Comput.*, **25** (2004), pp. 1674-1697.

[5] W. Bao, Ground States and dynamics of multicomponent Bose-Einstein condensates, *Multiscale Model. and Simul.*, **2** (2004), pp. 210-236.

[6] W. Bao and D. Jaksch, An explicit unconditionally stable numerical method for solving damped nonlinear Schrodinger equations with a focusing nonlinearity, *SIAM J. Numer. Anal.*, **41** (2003), pp. 1406-1426

[7] W. Bao, D. Jaksch and P. A. Markowich, Three dimensional simulation of jet formation in collapsing condensates, *J. Phys. B: At. Mol. Opt. Phys.*, **37** (2004), pp. 329-343

[8] W. Bao, F. Lim and Y. Zhang, Energy and chemical potential asymptotics for the ground state of Bose-Einstein condensates in the semiclassical regime, Trans. *Theory Stat. Phys.*, to appear.

[9] W. Bao, H. Wang, and P. A. Markowich, Ground state, symmetric and central vortex state in rotating Bose-Einstein condensate, *Comm. Math. Sci.*, **3** (2005), pp. 57-88

[10] W. Bao and J. Shen, A Fourth-order time-splitting Laguerre-Hermite pseudo-spectral method for Bose-Einstein condensates, *SIAM J. Sci. Comput.* **26** (2005), pp. 2010-2028.

[11] W. Bao and W. Tang, Ground-state solution of Bose-Einstein condensate by directly minimizing the energy function, *J.Comp. Phys.* **187** (2003), pp. 230-254.

[12] Bao and Y. Zhang, Dynamics of the ground state and central vortex states in Bose-Einstein condensation, *Math. Mod. Meth. Appl. Sci.*, **15** (2005), pp. 1863-1896.

[13] S. N. Bose, Plancks Gesetz und Lichtquantenhypothese, *Zeitschift Für Physik A*, **26** (1924) pp. 178-181.

[14] C. C. Bradley, C. A. Sackett and R. G. Hulet, Bose-Einstein Condensation of Lithium: Observation of Limited Condensate Number, *Phys. Rev. Lett.* **78** (1997), pp. 985 - 989.

[15] C. C. Bradley, C. A. Sackett and R. G. Hulet, Evidence of Bose-Einstein Condensation in an Atomic Gas with Attractive Interactions, *Phys. Rev. Lett.*, **75** (1995), pp. 1687-1690.

[16] C.M. Brauner, B. Gay, J. Mathien (Eds.), Singular Perturbations and Boundary Layer Theory, Lecture Notes in Mathematics, Springer, Berlin, 594 (1977).

[17] M. M. Cerimele, M. L. Chiofalo, F. Pistella, S. Succi and M. P. Tosi, Numerical solution of the Gross-Pittaevskii equation using an explicit finite-difference scheme: An application to trapped Bose-Einstein condensates, *Phys. Rev. E* **62 (1)** (2000), pp. 1382-1389.

[18] C. Clavero, F. Lisbona, Uniformly convergent finite difference methods for singularly perturbed problems with turning points, *Numer. Algorithms*, **4** (1993), pp. 339-359.

[19] M. L. Chiofalo, S. Succi, and M. P. Tosi, Ground state of trapped interacting Bose-Einstein condensates by an explicit imaginary-time algorithm, *Phys. Rev. E* **62 (5)** (2000), pp. 7438-7444.

[20] F. Dalfovo and S. Giorgini, Theory of Bose-Einstein condensation in trapped gases, *Rev. Mod. Phys.*, **71** (1999), pp. 463-512.

[21] F. Dalfovo and S. Stringari, Bosons in anisotropic traps: Ground state and vortices, *Phys. Rev. A*, **53** (1996), pp. 2477-2485.

[22] K. B. Davis, M. O. Mewes, M. R. Andrews, N. J. van Druten, D. S. Durfee, D. M. Kurn and W. Ketterle, Bose-Einstein Condensation in a gas of Sodium atoms, *Phys. Rev. Lett.*, **75**, (1995), pp. 3969-3973.

[23] C. M. Dion and E. Cances, Spectral method for the time-dependent Gross-Pitaevskii equation with a harmonic trap, *Phys. Rev. E*, **67** (2003), pp. 046706.

[24] E.P. Doolan, J.J.H. Miller and W.H.A. Schilders, Uniform Numerical Methods for Problems with Initial and Boundary Layers, Boole, Dublin, (1980).

[25] W. Eckhaus, Matched Asymptotic Expansions and Singular Perturbations, North-Holland, Amsterdam, (1973).

[26] M. Edwards and K. Burnett, Numerical solution of the nonlinear Schrödinger equation for small samples of trapped neutral atoms, *Phys. Rev. A*, **51** (1995), pp. 1382-1386.

[27] M. Edwards, R. J. Dodd, C. W. Clark, P. A. Ruprecht and K. Burnett, Properties of a Bose-Einstein condensate in an anisotropic harmonic potential, *Phys. Rev. A*, **53** (1996), pp. R1950-R1953.

[28] J. R. Ensher, D. S. Jin, M. R. Matthews, C. E. Wieman, and E. A. Cornell, Bose-Einstein Condensation in a Dilute Gas: Measurement of Energy and Ground-State Occupation, *Phys. Rev. Lett.*, **77** (1996), pp. 4984-4987.

[29] K. Eriksson, D. Estep, P. Hansbo and C. Johnson, Introduction to adaptive methods for differential equations, *Acta Numerica*, (1995), pp. 105-158.

[30] P.A. Farrell, Uniformly convergent difference schemes for singularly perturbed turning and non-turning point problems, Ph.D. Thesis, Trinity College, Dublin, (1983).

[31] A. Griffin, D. Snoke, and S. Stringaro (Eds.), Bose-Einstein condensation, Cambridge University Press, New York, (1995).

[32] E.P. Gross, Structure of a quantized vortex in boson systems, *Nuovo. Cimento.*, **20** (1961), pp. 454-477.

[33] W. Huang, Y. Ren and R.D. Russell, Moving mesh partial differential equations (MMPDEs) based on the equidistribution principle, *SIAM J. Numer. Anal.*, **31** (1994), pp. 709-730

[34] W. Huang and D. M. Sloan, A simple adaptive grid method in two dimensions, *SIAM J. Sci. Comput.*, **15** (1994), pp. 776-797.

[35] R. B. Kellogg and A. Tsan, Analysis of some difference approximations for a singular perturbation problem without turning points, *Math. Comp.*, **32** (1978), pp. 1025-1039.

[36] J. Kevorkian and J.D. Cole, Perturbation Methods in Applied Mathematics, Springer, New York, (1981).

[37] L. Laudau and E. Lifschitz, Quantum Mechanics: non-relativistic theory, Pergamon Press, New York, (1977).

[38] E. H. Lieb and R. Seiringer, One-dimensional bosons in three-dimensional traps, *Phys. Rev. Lett.*, **91** (2002), pp. 150401.

[39] E. H. Lieb, R. Seiringer and J. Yugvason, Bosons in a trap: a rigorous derivation of the Gross-Pitaevskii energy functional, *Phys. Rev. A*, **61** (2000), pp. 033602.

[40] K. W. Madison, F. Chevy, W. Wohlleben, and J. Dal- ibard, Vortex formation in a stirred Bose-Einstein Condensate, *Phys. Rev. Lett.*, **84** (2000), pp. 806-809.

[41] J. J. H. Miller, E. O'Riordan and G. I. Shishkin, Fitted Numerical Methods for Singular Perturbation Problems, World Scientific (1996).

[42] J. J. H. Miller, E. O'Riordan and G. I. Shishkin, On piecewise-uniform meshes for upwind- and central-difference operators for solving singularly perturbed problems, *IMA J. Numerical Analysis*, **15**(1995), pp. 89-99.

[43] L. P. Pitaevskii, Vortex lines in a imperfect Bose gases, *Zhk. Eksp. Teor. Fiz.*, **40** (1961), pp. 646-649. (Sov. Phys. JETP **13** (1961), pp. 451-454).

[44] L. P. Pitaevskii and S. Stringari, Bose-Einstein condensation, Clarendon Press, New York, (2003).

[45] Y. Qiu and D. M. Sloan, Analysis of difference approximations to a singularly perturbed two-point boundary value problem on an adaptively generated grid, *J. Comput. Appl. Math.*, **101** (1999), pp. 1-25.

[46] H. G. Roos, Layer-adapted grids for singular perturbation problems, *Z. Angew. Math. Mech.*, **78** (1998), pp. 291-309.

[47] H. G. Roos, M. Stynes and L. Tobiska, Numerical Methods for Singularly Pertrubed Differential Equations, Springer-Verlag, Berlin, Heidelberg, New York, (1996).

[48] B. I. Schneider and D.L. Feder, Numerical approach to the ground and excited states of a Bose-Einstein condensated gas confined in a completely anisotropic trap, *Phys. Rev. A*, **59** (1999), pp. 2232-2242.

[49] G. I. Shishkin, Grid approximation of singularly perturbed elliptic and parabolic equations, Second Doctoral Thesis, Keldysh Institute of Applied Mathematics, USSR Academy of Sciences, Moscow, (1990).

[50] A. B. White, On selection of equidistribution meshses for two-point boundary value problems, *SIAM J. Numer. Anal.*, **16** (1979), pp. 472-502.

Name: Chai Ming Huang

Degree: Master of Science

Department: Mathematics

Thesis Title: A Uniformly Convergent Numerical Scheme for Singularly Perturbed Non-Linear Eigenvalue Problem Under Constraints

Abstract

In this thesis, we present a uniformly convergent numerical scheme to solve the singularly perturbed nonlinear eigenvalue problem — the time-independent Gross-Pitaevskii equation in the semiclassical regime, which is used to describe the equilibrium properties of Bose-Einstein Condensate at extremely low temperature. The numerical scheme proposed is based on the piecewise uniform mesh. Through detailed numerical error analysis, the numerical scheme presented is found to be uniformly convergent and is able to treat the interior layers or boundary layers inherent in the solutions of the singularly perturbed nonlinear eigenvalue problem. A comparison of this new numerical scheme based on the piecewise uniform mesh is made against the classical numerical scheme based on uniform mesh and we found that the numerical accuracy is greatly enhanced with the new scheme. We also extended the new numerical scheme to two dimensions and applied it to solve the singular perturbed nonlinear eigenvalue problem in two dimensions.

Keywords:

Bose-Einstein Condensation, Gross-Pitaevskii equation, semiclassical regime, adaptive mesh scheme, ground state, excited states.

A UNIFORMLY CONVERGENT NUMERICAL SCHEME FOR SINGULARLY PERTURBED NON-LINEAR EIGENVALUE PROBLEM UNDER CONSTRAINTS

CHAI MING HUANG

NATIONAL UNIVERSITY OF SINGAPORE

2006

A Uniformly Convergent Numerical Scheme for Singularly Perturbed Non-Linear Eigenvalue Problem Under Constraints

CHAI MING HUANG

2006